1991

Drag on object moving through foam

Chinwha Chung
Iowa State University

INFORMATION TO USERS

This manuscript has been reproduced from the microfilm master. UMI films the text directly from the original or copy submitted. Thus, some thesis and dissertation copies are in typewriter face, while others may be from any type of computer printer.

The quality of this reproduction is dependent upon the quality of the copy submitted. Broken or indistinct print, colored or poor quality illustrations and photographs, print bleedthrough, substandard margins, and improper alignment can adversely affect reproduction.

In the unlikely event that the author did not send UMI a complete manuscript and there are missing pages, these will be noted. Also, if unauthorized copyright material had to be removed, a note will indicate the deletion.

Oversize materials (e.g., maps, drawings, charts) are reproduced by sectioning the original, beginning at the upper left-hand corner and continuing from left to right in equal sections with small overlaps. Each original is also photographed in one exposure and is included in reduced form at the back of the book.

Photographs included in the original manuscript have been reproduced xerographically in this copy. Higher quality 6" x 9" black and white photographic prints are available for any photographs or illustrations appearing in this copy for an additional charge. Contact UMI directly to order.

U·M·I

University Microfilms International
A Bell & Howell Information Company
300 North Zeeb Road, Ann Arbor, MI 48106-1346 USA
313/761-4700 800/521-0600

Order Number 9207240

Drag on object moving through foam

Chung, Chinwha, Ph.D.

Iowa State University, 1991

U·M·I
300 N. Zeeb Rd.
Ann Arbor, MI 48106

Drag on object moving through foam

by

Chinwha Chung

A Dissertation Submitted to the

Graduate Faculty in Partial Fulfillment of the

Requirements for the Degree of

DOCTOR OF PHILOSOPHY

Department: Aerospace Engineering and Engineering Mechanics
Major: Engineering Mechanics

Approved:

Signature was redacted for privacy.

In Charge of Major Work

Signature was redacted for privacy.

For the Major Department

Signature was redacted for privacy.

For the Graduate College

Members of the Committee:

Signature was redacted for privacy.

Iowa State University
Ames, Iowa
1991

TABLE OF CONTENTS

LIST OF TABLES

LIST OF FIGURES

ACKNOWLEDGEMENTS

I wish to express my special thanks to Dr. Bruce R. Munson, my advisor, for his excellent guidance and encouragement during my study. Appreciation also extends to Dr. Colver, Dr. Mitra, Dr. Sturges, and Dr. Tannehill who, while serving as committee members, have each contributed in their own way to the completion of my Ph. D. program.

I would like to thank every professors and staff members in the Department of Aerospace Engineering and Engineering Mechanics for providing high quality education, financial support, and enjoyable envirnment throughout my stay. A special appreciation extends to Mr. Thomas J. Elliott for his technical assistance during my experiments.

I wish to thank my wife, Insook, for her understanding, patience, and encouragement. Also, I express my sincere thanks to my mother and parents-in-law for their endless love and continuous encouragement. Without their support, successful completion of my study would have been very difficult.

CHAPTER 1. INTRODUCTION

Foams are the materials consisting of open or closed cell matrix structures, which may be in a liquid or solid phase, separated by a gas phase between the matrices. Foams can be categorized into two major groups as characterized by the matrix phase materials: solid foams and liquid foams. Solid foam can be grouped again as an open cell foam or a closed cell foam by the shape of its matrix structures. With closed cell materials, the gas is dispersed in the form of discrete gas bubbles and the matrix forms a continuous phase. In open cell solid foams, the voids coalesce so that both the solid and the fluid phases are continuous. Figures 1.1 and 1.2 show sketches and photos of each type of foam. Foamed plastics are examples of solid foam, among which sponge and styrofoam are examples of open cell foam and closed cell foam, respectively. Examples of liquid foams are beer foam, shaving cream, soap foam, etc.

The applications of foam are growing due to foam's unique mechanical properties. Most solid foams have unusually low densities, high strength-to-weight ratio, and many are excellent acoustical, thermal, and electrical insulators. Foams have other advantages, such as good wave transmission, resistance to abrasion, and vibration damping. In addition to the general properties of foam, liquid foams have a few more interesting characteristics that differentiate them from ordinary Newtonian fluids. These characteristics include the fact they may slip on the contacting solid surface

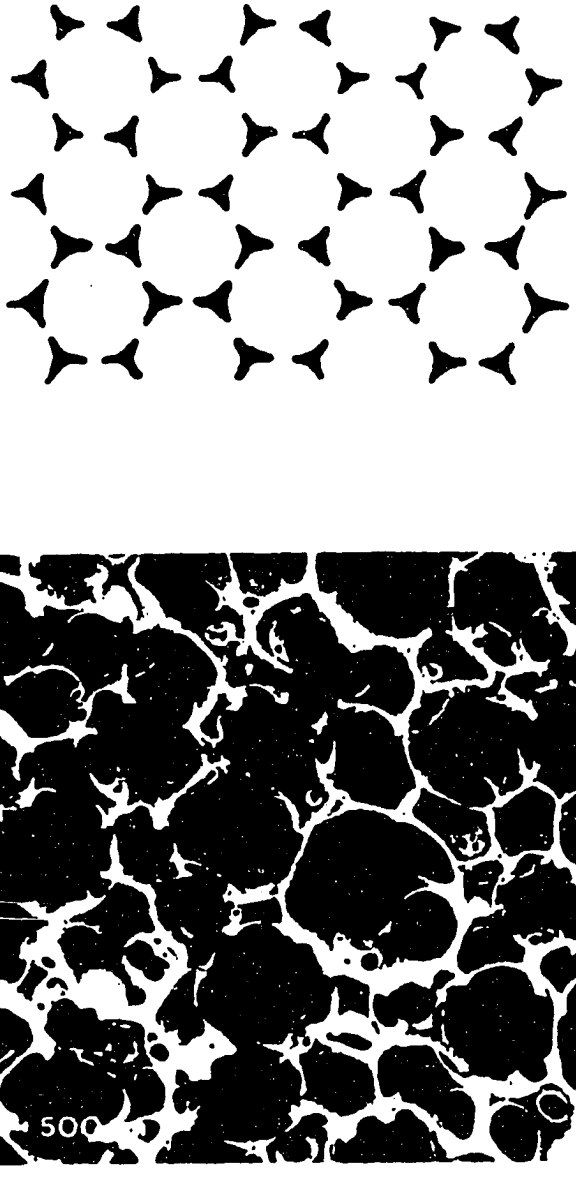

Figure 1.1: Open cell foam: (a) Two-dimensional structure representation (b) Micrograph of a sample

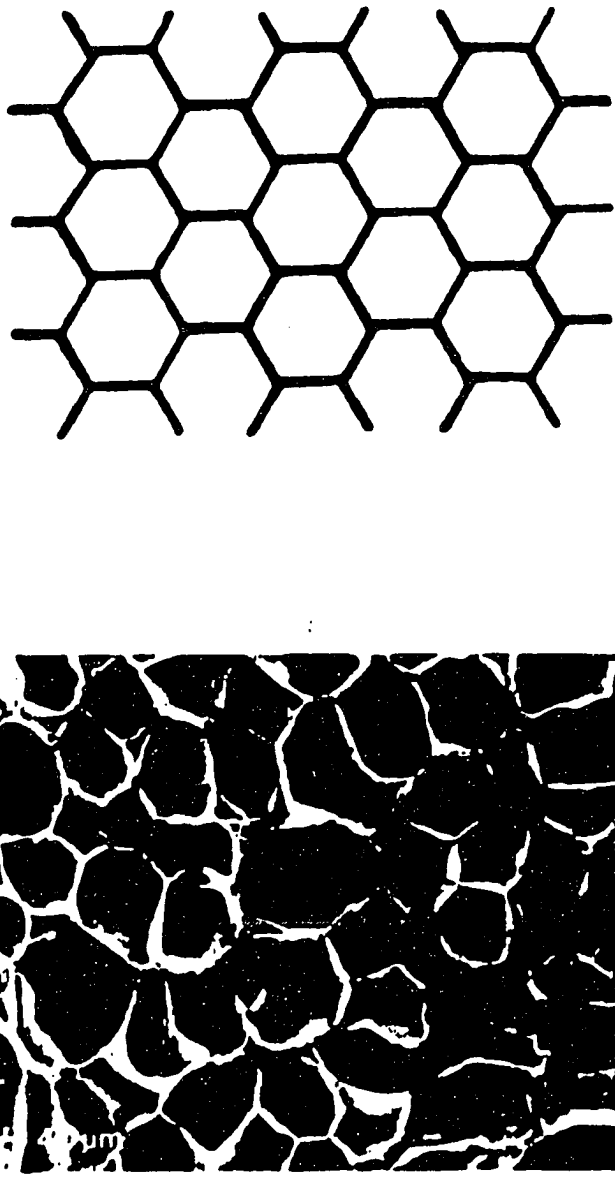

Figure 1.2: Closed cell foam: (a) Two-dimensional structure representation (b) Micrograph of a sample

along which they flow, they may pick up particles in the liquid phase, and their rheological properties are non-Newtonian, e.g., the shear stress is not linearly related to the rate of strain. Liquid foams of various types are of use in a wide variety of industrial applications, including fire fighting, manufacturing processes, and the oil and gas industry.

The demand of understanding liquid foam flow is increasing with the growing application of foam material. Even in the manufacturing process of solid foams, the understanding of liquid foam is required because the foam material is often injected into a mold and/or curing oven as a liquid phase. The prediction and control of liquid foam properties in this pre-process stage are desirable for the designing and manufacturing of the proposed product.

While a considerable amount of effort has been devoted to the understanding of the structure, makeup, and physical properties of solid foams and liquid foams, relatively little experimental effort has been devoted to the understanding of the fluid mechanics of foam flows, except for the flow of foam in pipes and through porous material. Therefore, the purpose of this research is to present experimental data concerning the nature of foam flow obtained by measuring drag forces on various objects with various surface conditions as they move through foam.

The term "foam" in this thesis will be limited specifically to liquid foams, which are fluid type materials consisting of numerous gas bubbles separated by thin liquid films such that the volume of the liquid phase is considerably smaller than the volume of the gas phase. The experiments were conducted to determine the drag force on an object placed in a uniform stream of foam. From these experiments, the drag force was shown to be a function of body shape, size, surface roughness, foam velocity, and

the foam properties.

The experiments conducted for this research were conducted in a manner similar to those done on the measuring of the aerodynamic drag on objects in wind tunnels, e.g., the object to be investigated was fixed in a uniform stream of fluid (foam), and the drag force was measured by a means of force balance. Rather than using a conventional foam generator which uses air blowing into the foaming liquid to produce the foam, an agitation (beating) method was used for this research. In this way, a consistently uniform and steady-state foam flow covering a wide range of foam properties was generated.

On a macroscopic scale, i.e., the length scale of the object moving through the foam is much larger than the typical size of the bubbles, foam behaves in ways quite similar to a Bingham plastic material. In other words, there is a highly nonlinear shear thinning relationship between the drag and the velocity, including the existence of an apparent yield force to initiate motion of the object.

Since foam is considered to have a yield force which is a Bingham plastic property, there may be a yielded envelope region around the object moving through the foam [1]. In the region where the shear stress is less than the yield stress, the material behaves as a rigid solid. On the other hand, in the region where the shear stress exceeds the yield stress, the material flows. Therefore, the flow and solid regions are separated by a distinct yield surface. For the case of moving objects in Bingham material, the region inside the yield surface is called yielded envelope region.

Since foam is opaque, direct visualization of the yield surface is not easy. In this study, the drag force variance for the object near a wall (the wall effect) was investigated to detect the possible existence of a yield surface. The comparison of

these results to those of the Newtonian case strongly suggest the existence of a yield surface.

As many previous reserchers have pointed out, one of the interesting features of foam flow is its slip phenomenon on solid surfaces. To investigate the dependence of drag force on the slip phenomenon, both smooth and rough surfaced models were used. It was found that the drag was a function of the surface roughness, and the variance was confined to the magnitude of the yield force of the foam tested. As a general result, the drag force increased with increasing liquid phase viscosity or increasing liquid volume fraction, defined as foam quality in this thesis.

To better understand, the results of this experimental study, the contents are organized as follows. The literature review of previous experimental and theoretical studies is discussed in Chapter 2. A description of the experimental set-up, foam properties measurement, and specimens tested in this study are described in Chapter 3. The experimental set-up is categorized into four groups. These four groups are test section, foam velocity control, drag force measurement, and data collecting. The devices used to measure foam drainage rate, foam quality, viscosity and surface tension of the liquid, as well as a description of the smooth surface and rough surface models tested are mentioned.

Experimental procedures are explained in Chapter 4. First, the procedures for most of the experiments run are organized on a step-by-step basis: preparation of foamy liquid (soap-water solution), preparation of steady-state foam flow, and drag force measurement on specimens. Then, procedures for investigating the wall effect and storing the experimental data are introduced. Theory which relates to this experimental research is discussed in Chapter 5. Previous experimental and theoretical

studies are discussed in detail to explain slip phenomenon in foam flow, yield stress, effective viscosity of foam, and wall effect.

Results and discussions are described in Chapter 6. Section 6.1 includes results on sixteen different smooth surface specimens tested in seven different foams. The result of an attempt to index the bubble size by introducing drainage rate concept are discussed in section 6.2. The test results to investigate the possible existence of a yield surface is in Section 6.3. In Section 6.4, our experimental results are compared with the existing foam theory. The test results on both rough surface models and comparison with Bingham theory are discussed in Section 6.5. The test on dispersed foam to investigate the relationship between viscosity and quality is discussed in Section 6.6.

CHAPTER 2. LITERATURE REVIEW

The early stage of foam research was based on chemistry concepts such as chemical structures of foaming agents and their stability. Foam's natural tendency is to minimize surface energy by reducing surface area, and the bubble size increases with time. Instability of foam due to drainage, regional concentration of surfactant, and related chemical mechanisms lead to film rupture and result in bubble coalescence. Cheng and Natan [57] reviewed such foam degradation mechanisms.

Recently, chemical engineering researchers extended their knowledge in rheology to the foam field. The systematic study of foam flow requires knowledge of numerous scientific disciplines because liquid films control foam characteristics. Physicochemical principles related to the soap films are fundamental to foam rheology.

The major features of foam flow, which differ from ordinary Newtonian fluid flow, are the slip phenomenon at the moving wall, the effective viscosity which is larger than liquid phase viscosity, and the Bingham-plastic characteristics.

The slip boundary condition arises from a macroscopic point of view considering a conceptual model of the wall liquid film region. Since the slip phenomenon is naturally demonstrated by experimental study, many previous experimental efforts have been devoted to quantify the slip velocity and to develop wall slip correction techniques following the basic background of early studies on dilute gas bubble sus-

pensions and foam structures. These are discussed in Sections 2.1 and 2.2. The details of these previous studies on slip phenomenon will be introduced in Section 2.3.

"Apparent viscosity" and "effective viscosity" are the terminologies used to distinguish foam viscosity from foam agent liquid viscosity. Apparent viscosity refers to the experimentally measured viscosity without the slip velocity correction. On the other hand, effective viscosity refers to the viscosity of a foam field when slip velocity is eliminated. There is evidence [46] that apparent viscosity is lower than effective viscosity. Most of the theoretical studies deal with effective viscosity. The background of previous works on apparent viscosity and effective viscosity will be discussed in Section 2.4.

2.1. Dilute Gas Bubble Suspensions

Most materials that are called foams consist of gas bubbles separated by thin liquid (or solid) films. That is, the quality, ϕ, defined as the gas volume divided by the foam volume, is not significantly less than one. Gas-bubble suspensions are another extreme in volume fraction of a gas-liquid mixture. In rheological concept, dilute gas-bubble suspensions are analogous to the dilute emulsions of neutrally buoyant drops of one liquid within another immiscible liquid when the volume fraction of the dispersed phase is very small.

Dilute gas suspensions, unlike foams, can be analyzed by considering single drops by using mathematical techniques available for solving the Stokes equations. Under small deformation, Taylor [39] has shown that the effective viscosity, μ_e, of a dilute

emulsion is

$$\mu_e = \mu\{1 + \phi_d[\frac{5\lambda + 2}{2(\lambda + 1)}]\} \tag{2.1}$$

where μ is the continuous-phase viscosity, $\lambda = \mu^*/\mu$ is the viscosity ratio (μ^* is the viscosity of the dispersed phase), and ϕ_d is the volume fraction of the dispersed phase (which is assumed small).

Reviewing the theories that apply to dilute emulsions and gas-bubble suspensions, Kraynik [19] pointed out the following difference between the rheology of foams and dilute gas–bubble suspensions: for dilute emulsions, non-Newtonian effects arise from interactions between droplets and the external liquid phase. By contrast, the shape of bubbles in static foam is largely determined by neighboring bubbles, and non-Newtonian behavior occurs even when viscous forces are absent.

Schowalter et al. [34] extended Taylor's theory to show that the spherical drop in dilute emulsions deforms and the shape depends on capillary number, $Ca = \mu a\dot{\gamma}/\sigma$, where σ is the interfacial tension, a is the drop radius, and $\dot{\gamma}$ is the deformation rate. The capillary number is a relative measure of viscous forces that tend to distort the drop and interfacial tension, which favors sphericity. Later, Taylor [40] analyzed bubble expansion in unbounded fluids to determine the dilatational (effective) viscosity μ' of dilute gas-bubble suspensions. Recently, the interfacial dilatational viscosity, κ, has been obtained by Edwards [11]. The equation for μ' is

$$\mu' = \mu[\frac{4}{3\phi_d}(1 + \frac{\kappa}{\mu a}) - 1.733] \tag{2.2}$$

Prud'homme and Bird [30] employed a "cell" model and found the last term of Eq. (2.2) to be −1 instead of −1.733.

2.2. Foam Structure

Plateau [25] observed that three films on a planar surface always meet at equal dihedral angle of 120°. The film junction region, now called Plateau borders, forms the edges of polyhedral gas bubbles (see Figure 2.1). The Plateau border is the bubble film junction region such that, in 3-dimensional foam, four bubble edges meet at an equal angle of $\cos^{-1}(-1/3) \simeq 109.47^{\circ}$

Around this Plateau border, four bubbles form a tetrahedron shape and four corners have tri-dimensional figures. Due to the surface tension of each bubble, all the bubble edges at the corner have a small radius of curvature. Therefore, a finite amount of liquid will be naturally present at the Plateau border.

Kelvin [17] determined that this honeycomb shape is the ideal foam structure where a space is partitioned into identical cells of equal volume and minimal surface area. This identical shapes of monodisperse foam structure is currently the model for theorists, despite Metzke's observation [21] that such an ideal cell does not exist in actual bubbles.

2.3. Slip at the Wall

The slip phenomenon refers to a situation where a velocity discrepancy occurs between the solid wall and fluid phase; the fluid phase velocity is lower than that of the solid due to a certain velocity discontinuity. In such cases, the layer of fluid next to the solid surface has a finite tangential velocity. The term "slip flow" is appropriate for this kind of flow.

Kraynik [19] pointed out, however, that the slip is merely a convenient macroscale

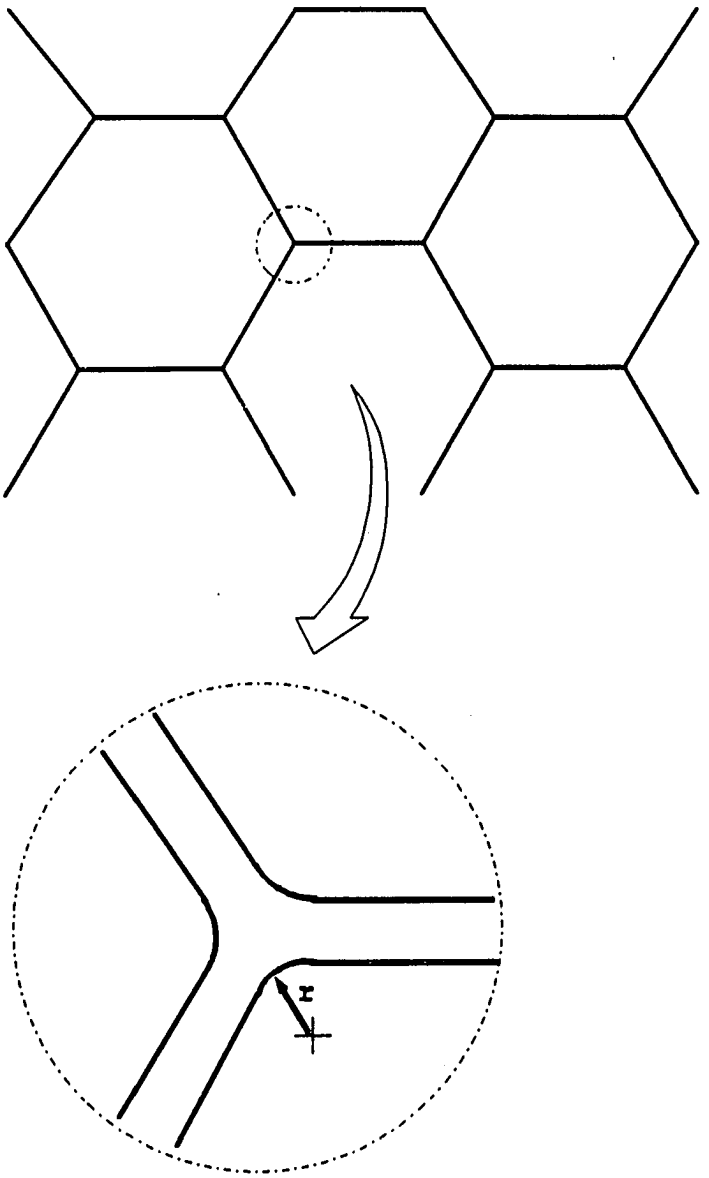

Figure 2.1: Two-dimensional representation of the Plateau border

description of the wall boundary condition, whose cell-level mechanism depends upon the existence of a thin fluid layer that does not itself slip, but wets the wall and lubricates the foam flow.

As mentioned previously, in the macroscopic view (i.e., characteristic length of the object is much greater than the diameter of the foam cell), foam flow shows a similar "apparent slip" phenomenon on the solid boundaries. Since early theoretical attempts to correct the slippage in a non-Newtonian flow by Reiner [33] and Mooney [22], numerous efforts have been devoted to model this interesting phenomenon.

Reiner considered a finite thickness of lubricating layer next to the wall, in which the velocity gradient is much larger than in the other region. The flow in the lubricating layer shows a linear velocity profile according to the fluidity concept. The term "fluidity" is an experimentally defined coefficient as a function of shear stress, which relates the wall slip velocity and shear stress. If the slip velocity is given by $U_s = h_e \tau_w / \mu$, where h_e is the effective thickness of liquid layer and the τ_w is the wall shear stress, then the wall fluidity is simply $\psi_w = h_e / \mu$. The outer flow can be distinguished from the lubricating layer by the different velocity gradient. Figure 2.2 shows this model, in which there is a distinct functional discontinuity between the two regions.

For the case of foam flow, as a proposed Bingham material, the outer flow region could be divided once again into two regions, a yielded region (fluid region) and an unyielded region (solid region). The yielded region is the region where foam yield strength is exceeded. The unyielded region is the region where the shear stress is less than the yield stress and the stream lines are not affected by the object. For example, in pipe flow, the unyielded region shows a plug type flow. Since the thickness of the

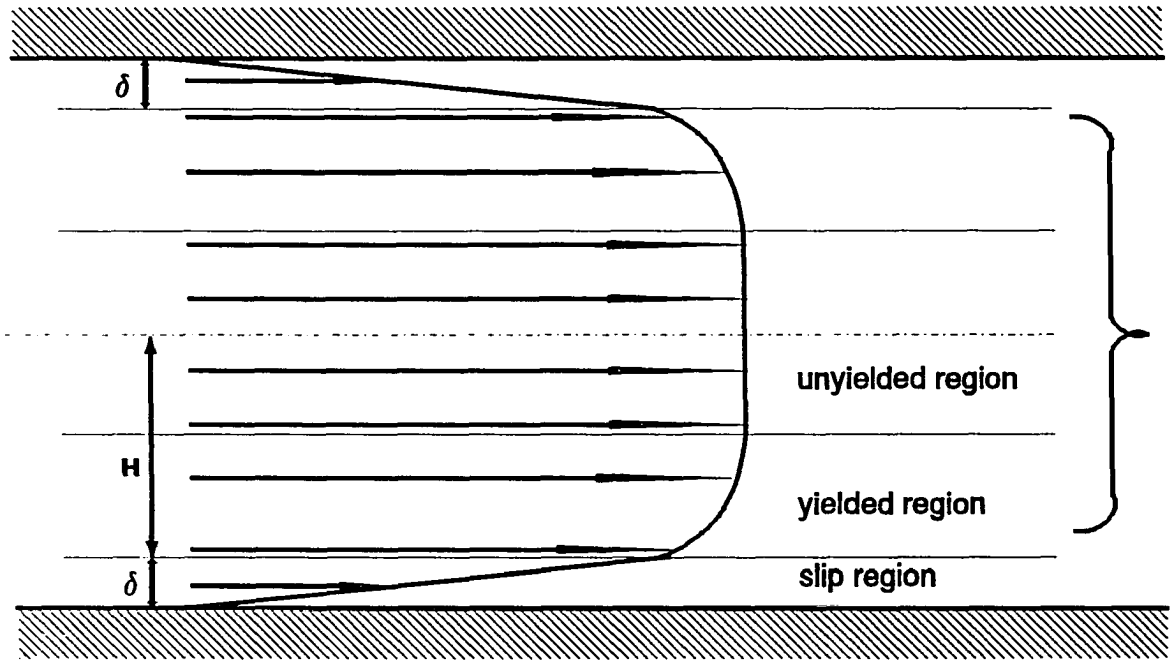

Figure 2.2: The conceptual two-dimensional foam flow model

lubricating layer region is negligible on a length scale compared to outer regions for the case of foam flow, (i.e., $\delta \ll$ H) most researchers treat the phenomenon as a wall slip from a macroscopic point of view rather than considering it as another region that has a different velocity gradient.

Wenzel et al. [45] performed an experiment using a transparent pipe test section with a 2.75 inches diameter to detect the wall slip velocity. Because a transparent pipe was used, the wall slip velocity could be determined by tracing the movement of a bubble at the wall with time. This slip velocity is plotted as a function of the average velocity (volume flow rate divided by cross-sectional area) for two different ranges of bubble diameter, d (Figure 2.3). Since the boundary liquid layer is analyzed as a laminar Newtonian film, and a slip velocity U_s is assumed to exist at the inner surface. Then

$$\tau_w \propto \frac{U_s}{\delta} \tag{2.3}$$

where τ_w = wall shear stress and δ = the thickness of the layer. Figure 2.4 indicates that the pressure loss and, therefore, τ_w, increase with increasing average velocity. However, Figure 2.3 shows that for small bubble foam, an apparent maximum slip velocity is attained. This implies that δ decreases with increasing average velocity, since τ_w increases with average velocity. Since δ was not measured, this was not verified experimentally.

Later, with experiments using a concentric cylinder viscometer, Wenzel's [46] results contradicted his previous hypothesis, where the wall liquid layer is considered to decrease with increasing velocity. If the wall boundary region of the fluid is assumed to be Newtonian, then

$$\tau_w = \mu \partial U / \partial y = \mu U_s / \delta \tag{2.4}$$

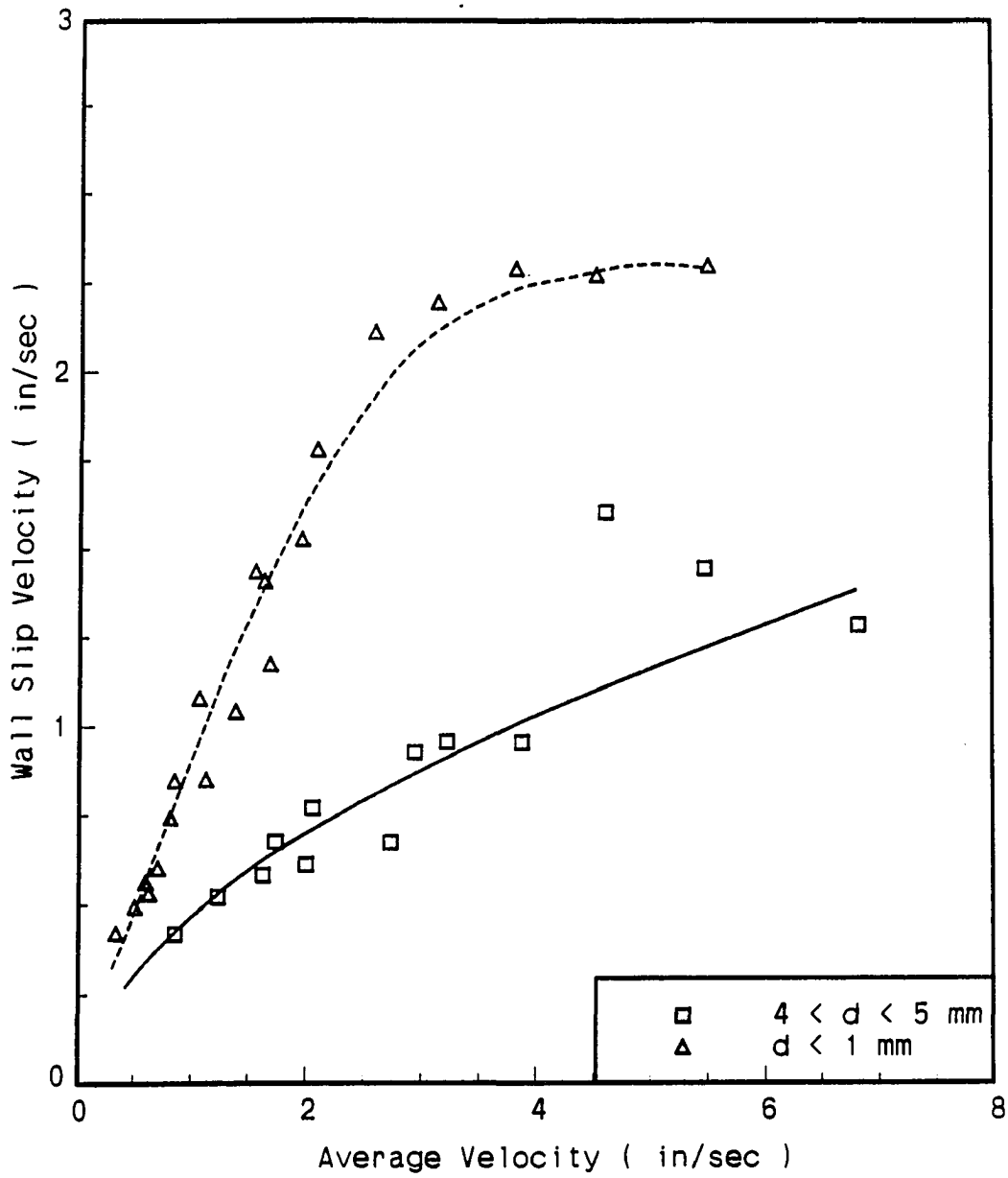

Figure 2.3: Variation of wall slip velocity for 2.75 in. diameter smooth pipe. From Wenzel et al. [45]

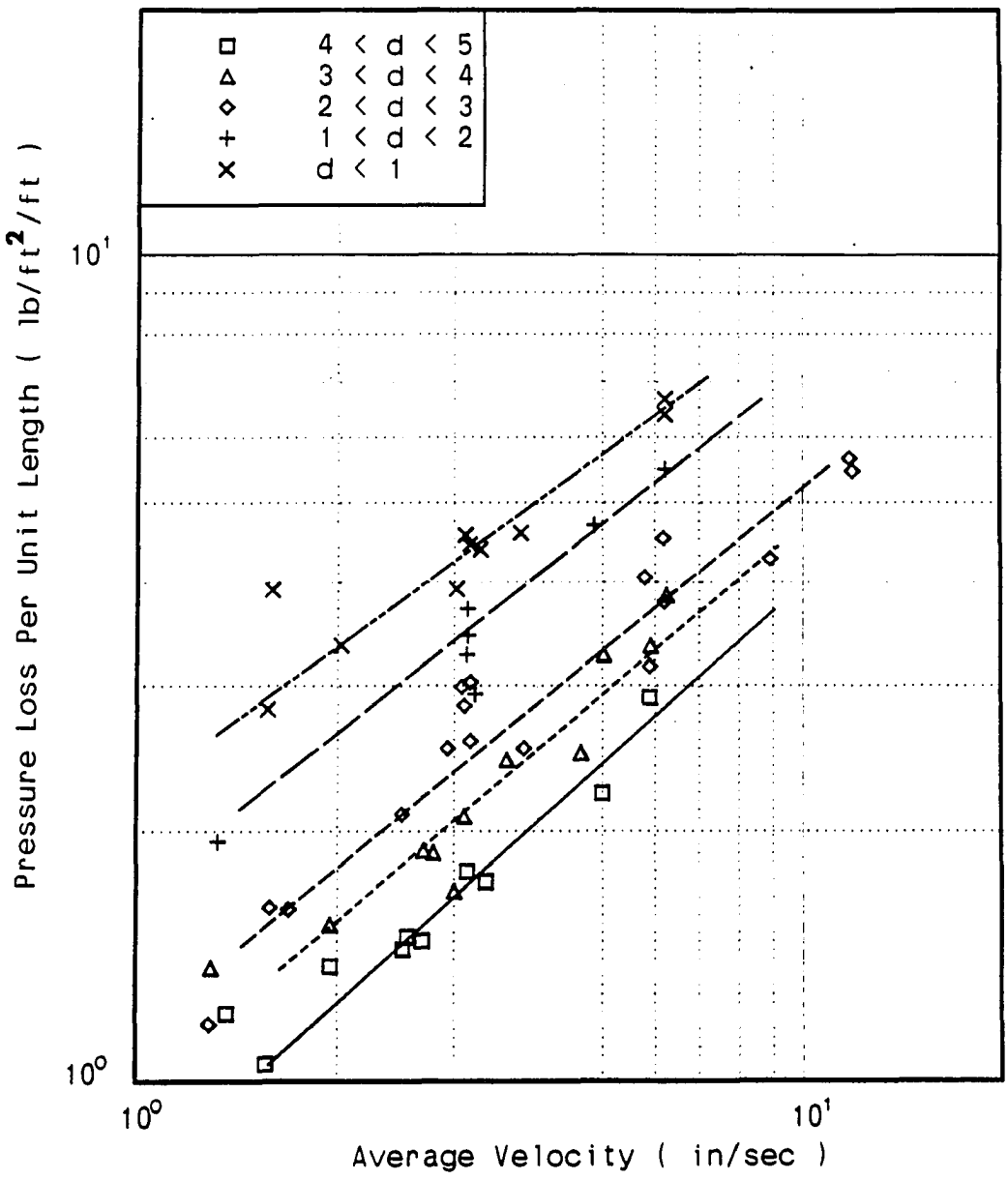

Figure 2.4: Variation of pressure loss with average velocity. From Wenzel et al. [45]

where U_s is the slip velocity and δ is the thickness of the liquid film layer on the wall. Now, if δ is assumed to be a function of U_s according to

$$\delta = \alpha\, U_s^{1-\beta} \tag{2.5}$$

then

$$\tau_w = \mu \frac{U_s}{\alpha U_s^{1-\beta}} = \mu U_s^{\beta}/\alpha = C U_s^{\beta} \tag{2.6}$$

With the values of C and β attained from curve fitting, α can be calculated. The result is

$$\delta = \alpha\, U_s^{0.62} \tag{2.7}$$

with $\alpha = 3.7 \times 10^{-4}$ being a dimensional constant between U_s (in./sec) and δ (in.). That is, the liquid layer thickness increases as a function of wall velocity. Also, δ turned out to be of the same order of magnitude as the thickness of a liquid film between bubbles of the same foam.

Similar recent experimental work using essentially the same method has been performed by Lemlich [41]. He argued that the "apparent slip," which is the sliding phenomenon due to fluidity of the liquid film layer at the wall, should be distinguished quantitavely from the actual slip (real slip). Lemlich ran the foam through horizontal commercial acrylic and galvanized steel pipes. He showed that in the acrylic pipe the foam flows almost entirely by slip, with a very close approach to plug flow as confirmed by dye injection. When the fluid particle on the wall slides instead of rotates (the "not wetted" case), the actual slip boundary condition will hold. He suspected that the plug flow case might happen due to actual slip when the wall is not wetted (or is at best poorly wetted), since the pipe was acrylic. Or perhaps the wall shear stress did not exceed the yield stress of the foam. Therefore, the foam

totally slides on the liquid layer without deformation, or the combination of both. The linear relationship Lemlich found between shear stress and shear strain in this case could suggest what really happened in the boundary region of foam flow. Since the straight line passes through the origin, the non-slip condition on a solid boundary in the microscopic view should be valid.

Extrapolation of the smooth wall shear stress versus wall velocity data to zero velocity indicated a small, but finite, yield stress. This phenomenon was observed for flow in smooth tubes by several investigators [39, 27], although a detailed analysis has not been made. Experimental evidence [36] shows that the wall fluidity vanishes below the finite value of wall shear stress (called the slip yield stress). If the shear stress is in the range between the slip yield stress and the foam yield stress, the foam is transported entirely by plug flow. This plug flow has also been reported by several investigators[2, 18].

Lemlich's results agree with those of Wenzel et al., based on experimental observations which showed that the liquid film thickness, δ, at the wall increases as velocity increases. As seen in Figure 2.5, film thickness has an asymptotic limiting value at higher speeds. A plausible explanation for the increase of film thickness with the foam velocity is suggested by Lemlich as follows. The layer of bubbles immediately adjacent to the wall is subjected to shear as the foam moves along. As a result of this shear, the liquid from nearby Plateau border regions, which act as small reservoirs, is dragged out at the wall. As the velocity increases, the shear force on the layer of the bubbles increases, thus dragging more liquid up to a certain limiting value until the reservoirs are depleted.

Lemlich also used a galvanized steel pipe for the rough boundary condition. The

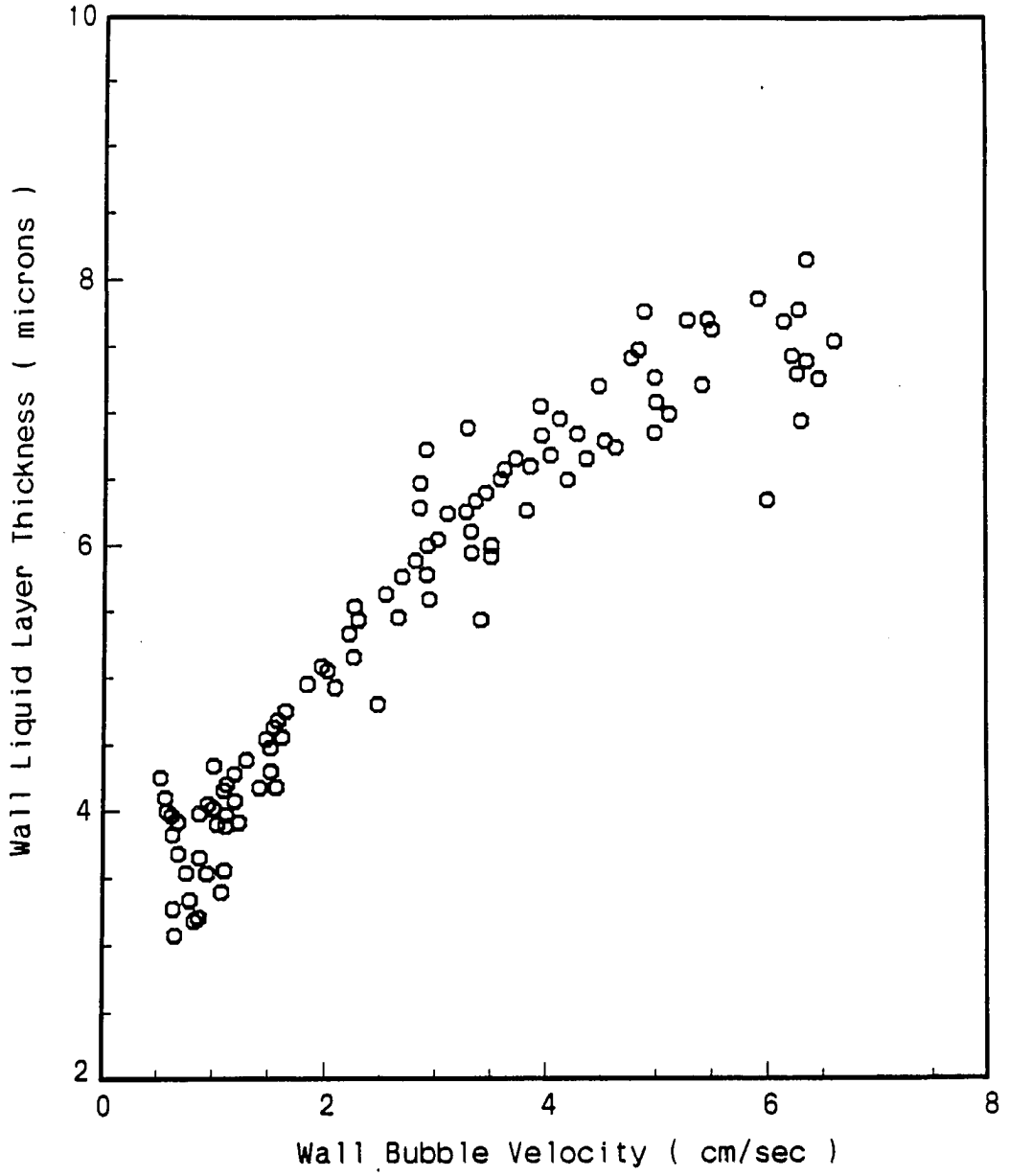

Figure 2.5: Liquid film thickness at the wall vs. visually measured wall bubble velocity for particle-free foam flowing through acrylic pipe of 4.44 cm i.d. From Lemlich [41]

roughness of the inside of the pipe was much larger in length scale than that of the liquid layer at the wall. In analyzing the data, he found no slip at the wall, and consequently, pseudoplastic behavior existed in the foam field.

Reasonable analysis of this slip phenomenon can be found very recently [14, 47, 15, 27, 26, 29]. Because of the difficulty of measuring the actual boundary film layer (liquid layer) thickness, Princen [27] suggested the use of an effective thickness, h_e. From his analysis using a concentric-cylinder viscometer with slip-layers at the inner and outer cylinder walls, Princen defined the fluidity as the ratio of effective thickness and viscosity of the boundary layer, h_e/μ, and espressed the functional relationship between fluidity of the liquid boundary layer and wall shear stress, τ_w. The wall shear stress, τ_w, is measured by the viscometer until reaching foam yield stress, τ_o. The fluidity was found to be zero below a small but finite slip yield stress, $(\tau_w)_o$, and rapidly increased with τ.

The classical method to account for the slip phenomenon, due to the thin liquid layer having a large velocity gradient, was first presented by Mooney [22]. The improvement of this method, which is similar to Princen's idea mentioned above, was recently reported by Yoshimura et al. [47]. Using two measurements on rotating cylinder geometries with different gaps but equal ratios of radii, Yoshimura et al. present an analysis of flow with wall slip. Then, they show how to correct the experimental data for the slip, and how to calculate viscosities and wall slip velocities.

The wall slip correction techniques developed for viscometry devices have been verified by experiments, using non-decaying slip materials such as a clay suspension and oil-in-water suspension. The decaying process is a combination of the drainage of the continuous liquid phase and the rupture of individually surrounded bubbles. For

the neutrally buoyant drop or particle suspension case, neither drainage nor rupture occur. For the case of foam, however, there has been difficulty for the application of these methods due to the decay problem that occurs during testing.

2.4. Yield Stress and Viscosity Function

Foam, considered as a Bingham material, has a yield stress. Early evidence of yield-stress phenomena in foams can be found in experimental studies [6, 20]. The experimental attempt to measure foam flow charateristics has started rather recently. Mooney's [22] measurment of the pressure drop for foam flow in tubes of different diameter may be the first. His experimental method was adopted and extended by Wenzel et al. [45].

Wenzel et al. [45] performed experiments to determine the relationship between the pressure drop and the average foam velocity for foam flow in smooth pipes. He found that the data points lie on straight lines on the logarithmic plot (see Figure 2.4). Such lines have the relationship, $\Delta P/L = KU^n$, in which $\Delta P/L$ = the pressure loss per unit length of pipe, U is the average velocity, n is the slope of the line, and K is constant. As seen from Figure 2.4, the effect of bubble size is apparent for this flow in the velocity range tested. In general, the parameter fitting schemes require prior knowledge of the explicit functional relationship. The above experimental studies do not provide systematic generalization due to a lack of important variables such as surface tension, foam quality change, and viscosity of the foaming agent solution.

Later, Wenzel [46] investigated the effect of the foam yield stress, effective viscosity and apparent viscosity, including the foam expansion factor, $\Psi \equiv V_f/V_l$, where V_f is foam volume and V_l is liquid volume. He noticed that earlier studies used

smooth walled concentric cylinder viscometers, and few distinguished between the two basic flow mechanisms which can exist: the shearing of the foam matrix and the sliding of the matrix along a smooth boundary.

In order to determine the shear stress in the absence of wall slip, Wenzel employed a cone and plate viscometer with radially placed high vanes. Also he used a concentric cylinder viscometer to study the wall slip phenomenon. The inner cylinder was vaned to prevent slip which could, therefore, only occur on the smooth outer cylinder wall. He used a soap-solution with a surface tension of 25 dynes/cm at room temperature and a viscosity about 12 percent greater than distilled water. Wenzel ran the experiment with an average shear rate from 0.18 s^{-1} to 1.35 s^{-1}. The data were fit to a general equation of the power type:

$$\tau = \tau_O + K\dot{\gamma}^N \tag{2.8}$$

where τ is the effective shear stress, τ_O is the yield stress of foam matrix, $\dot{\gamma}$ is the shear rate, and K and N are constants.

From the plot (Figure 2.6), Wenzel found a strong correlation between τ_O and the inverse of the average bubble diameter, $1/d$. He also found, however, no meaningful relationship between the expansion factor and the yield stress, which indicate that yielding is primarily a surface phenomenon, depending on the number of films per unit volume rather than film thickness. The effective viscosity calculated turned out to decrease with increasing shear rate. No relationship was found between the effective viscosity and the bubble diameter, which indicates that the flow mechanism is different from the yield mechanism. The other observation is that under higher shear rates with large bubble foams, there was a tendancy for the bubbles to reform into more stable smaller ones.

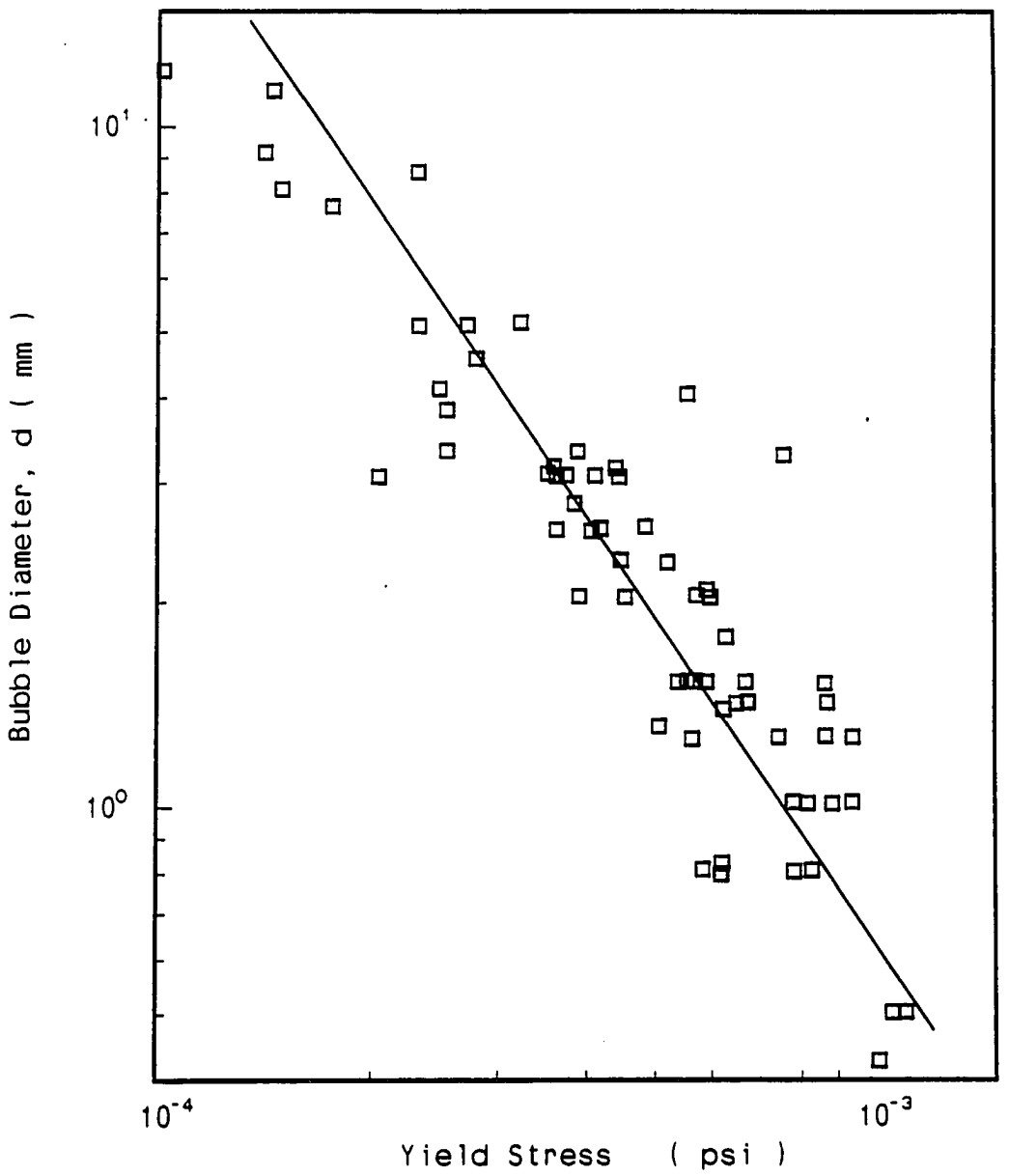

Figure 2.6: Variation of yield stress with bubble diameter. From Wenzel [45]

In similar recent experimental work, Lemlich [41] used almost the same method. He ran the foam through horizontal commercial acrylic and galvanized steel pipes. Lemlich noticed that researchers appeared to be divided as to whether foam is better described as pseudoplastic or Bingham plastic. As mentioned earlier, if the fluid requires a finite yield stress before it begins to flow, the fluid is Bingham-plastic material. A pseudoplastic refers to the shear thinning characteristics with no yield stress, which decreases resistance with increasing stress.

Lemlich found that in acrylic pipes, the wall shear depends only on the volumetric flow rate of foam, not on the average bubble diameter. This lack of effect of bubble diameter contrasts with the findings of Wenzel et al. [46]. Due to the limitations of the experimental set-up, the range of foam quality was limited (ϕ ranged from 0.88 to 0.99 for most runs). Lemlich found the variation of foam quality did not seem to have much of an affect on the foam flow.

Lemlich used galvanized steel pipe for the rough boundary condition. The roughness of the inside of the pipe was much larger in length scale than the liquid layer at the wall. Lemlich found no slip at the wall of gavanized steel pipe, and a pseudoplastic behavior of the foam field. His finding of the lack of a yield stress contradicts other studies.

Khan and Armstrong [13, 14, 15, 16] is one of the research groups who started a set of theoretical analysis based on a two-dimensional microscopic foam structure. They idealized the foam cells to be monodisperse, two-dimensional hexagons, so that the foam can be visualized as a collection of infinitely long cylinders with hexagonal cross-section (see Figure 2.1). Khan and Armstrong set the general mathematical expression for the stress tensor which gives the total stress in terms of the shape of

the cell orientation, interfacial tension, and the rate of deformation in the liquid.

They also modeled the reformation process of the bubble in foam by investigating the stress-strain relationship. With increasing strain, a critical strain, γ_O, is reached when the bubbles meet their stable limit; they then slide instantly along the liquid film and reform. The stress corresponding to this critical strain (yield strain) is the suggestion of the foam yield stress, τ_O. Khan and Armstrong defined different cell orientations for foam under deformation in certain directions. By assuming idealized hexagonal, monodisperse foam cells with dry foam (ϕ is about 1), they obtained the results that the stress-strain relationship is independent of initial cell orientation. However, the critical strain varied with orientation, and therefore, the yield stress was a function of orientation. The yield stress, τ_O, was directly proportional to the liquid surface tension and inversely proportional to cell size [13].

Later, Kahn and Armstrong extended their theoretical investigation to include the effects of viscous and interfacial forces present in the foam film for both small and large deformations [14]. They found that the yield stress, critical yield strain, and the stress-strain relation are independent of the size distribution about a constant mean cell size and are coincident with foam consisting of monodisperse, regular hexagonal cells. Khan and Armstrong introduced the modified capillary number, $Ca' = (\sqrt{3/2})(1 - \sqrt{\phi}) \times \sqrt{\phi}(\mu\dot{\gamma}a/\sigma)$, as a ratio of the viscous to the interfacial forces, where μ is the liquid phase viscosity, ϕ is foam quality, $\dot{\gamma}$ is deformation rate, a is average bubble radius, and σ is interfacial surface tension. The introduction of the liquid viscosity into the model produced a strong deviation from their previous results [13] in both the stress field and the cell deformation for Ca' larger than 0.01. The viscous effects were independent of initial cell orientation.

Weaire et al. [44] calculated stress-strain curves for a number of samples of two-dimensional disordered foams by using a computer simulation. Compared to the idealized hexagonal foams, the disordered foam comprised bubbles with arbitrary sizes and shapes to simulate more natural-like foam. They found the elastic constant, defined in terms of stresses and modulus of elasticity for computational convenience, takes a value close to that of ideal hexagonal foam with the same mean cell area. Similarly, the yield stresses show only slight variation among reasonable disordered structures. Their finding on the elastic constant closely agrees with Princen's and Kahn and Armstrong's explicit calculations, namely, that the elastic constant does not depend on orientation. This curious finding remains unexplained.

Kraynik [19] pointed out that merely calling foam highly viscous is an understatement, because foam possesses a yield stress, τ_o, below which the deformation rate is zero and, therefore, the viscosity is infinite. When the shear stress, τ, exceeds the yield stress, the shear-rate-dependent viscosity $\mu_{f(\dot{\gamma})}$ can be represented by

$$\mu_{f(\dot{\gamma})} = \tau_o/\dot{\gamma} + \mu_p(\dot{\gamma}) \qquad (\tau > \tau_o) \tag{2.9}$$

where $\mu_p(\dot{\gamma})$ is a constitutive function that depends upon shear rate. The Bingham fluid model, with μ_p constant, is the most familiar form of Eq. (2.9). Foam–viscosity data are sometimes fit to the familiar power law $\mu_f = m\dot{\gamma}^{n-1}$, where m and n are constant parameters. When n is significantly greater than zero, viscous contributions beyond the yield stress are indicated. Thondavadl and Lemlich [41] report $n = 0.61$. for the foam they tested.

Kraynik also noticed that effective yield stress can be defined theoretically, while it can not be easily measured. It is considered to be a convenient empiricism for representing the viscosity function over the shear-rate range of an experiment because

many yield-stress values reported for foam, by using various viscometers, are just intercept parameters obtained by fitting steady-flow data. They are not a direct measurement of an effective yield stress. While recognizing the inadequacy of experiment to prove the existence of a yield stress, Kraynik asserts that foam does have a yield stress based upon reasonable experimental evidence and the predictions of micromechanical models. Later, Kraynik [18] reported that the yield stress decreases with increasing liquid contents.

Reinelt and Kraynik [31] investigated the film level viscous flow on a microscopic model developed by considering small deformations of an idealized material with two-dimensional, spacially periodic cell structure. From this analysis, they found that the viscous contribution to the effective viscosity is $O(Ca^{2/3})$ and depends on the foam orientation but not its liquid content. The viscosity function for simple shear and planar extension exhibits the same power-law dependance on strain rate and shows no evidence of a yield stress.

Kahn and Armstrong [15] performed an experiment on foam (ϕ ranged 0.92 to 0.97) to measure the effective viscosity and yield stress using a parallel spectrometer. They applied sand paper to both plate surfaces to eliminate the slip phenomenon. From the plot in terms of viscosity versus shear rate, they observed that the viscosity of foam approaches an infinite value at a non-zero stress, which corresponds to the yield stress. The value of the foam effective viscosity, which is significantly higher than the liquid viscosity, is an increasing function of quality (gas volume fraction) ϕ. The yield stress was also found to increase with ϕ. Comparing the experimental data for $\phi = 0.97$ to their two-dimensional model theory prediction when $\phi = 1$, Khan and Armstrong found the model to give the correct trend of the functional

relationship between viscosity and shear rate, but to overpredict the data by a factor of six. They could not run the experiment at a higher shear rate because of foam structure breakdown due to rupture in this region.

The shear-rate dependence of viscosity (effective viscosity) has been studied theoretically and experimentally by several investigators [8, 42, 38, 5] by using a viscometer. Princen [26, 27] introduced the fluidity to correct for wall slip and ran the experiment using a concentric-cylinder viscometer and highly concentrated emulsions which are analogous to the foam at some extent. Yoshmura et al. [47] used the same emulsions but different experimental techniques and measured yield stress values consistent with Princen. Princen's and Yoshmura's use of the similarity between concentrated emulsions and foams are considered excellent at low deformation rates. For the case of foam, however, direct application of these viscometric methods has a practical limit due to foam's stability and compressibility.

Schwarts and Princen [35] extended their two-dimensional theory for the viscosity of foams and concentrated emulsions. They considered, in detail, the viscous dissipation in the film between the bubbles as the system is subjected to a periodic uniaxial strain that does not exceed the elastic limit (or yield point). These ideas, when combined with the structural constraints that exist within a foam, lead to an expression for the effective viscosity of these complex fluids. They found that the contribution of viscous dissipation, relative to the elastic work done in deforming a foam, can be quite significant and this dissipation gives rise to a fundamentally non-Newtonian contribution to the effective viscosity. The effective viscosity exceeds the viscosity of the continuous phase by a factor proportional to $(\sigma/\mu a\dot{\gamma})^{1/3}$.

CHAPTER 3. EXPERIMENTAL APPARATUS

3.1. Experimental Set-up

The experimental apparatus was designed to provide a means to measure the drag force on objects placed within flowing foam (see Figure 3.1). The foam flow was confined inside a rotating tank, which had a channel along the outer wall. The foam in the channel was continually agitated to maintain constant foam properties throughout the testing. The tank was rotated by a variable speed motor, controlled by a speed controller.

A tachometer attached to the motor was used to measure the angular velocity of the rotating tank. The tachometer output dc voltage, which was proportional to the angular velocity of the tank, and thus the foam velocity was read by a digital multimeter and recorded on the x-axis of a plotter. A micro switch was attached next to the motor shaft which has a key hole, so the micro switch could turn off and on once per turn. This on-off signal was read by a counter and converted to a time period in the counter. The calibrated relationship between this period and the rotating speed of the tank was used to check the validity of the dc tachometer output.

The drag force on various objects was detected by a strain-gauge force transducer. The transducer signal was passed through a Wheatstone-bridge in the strain-

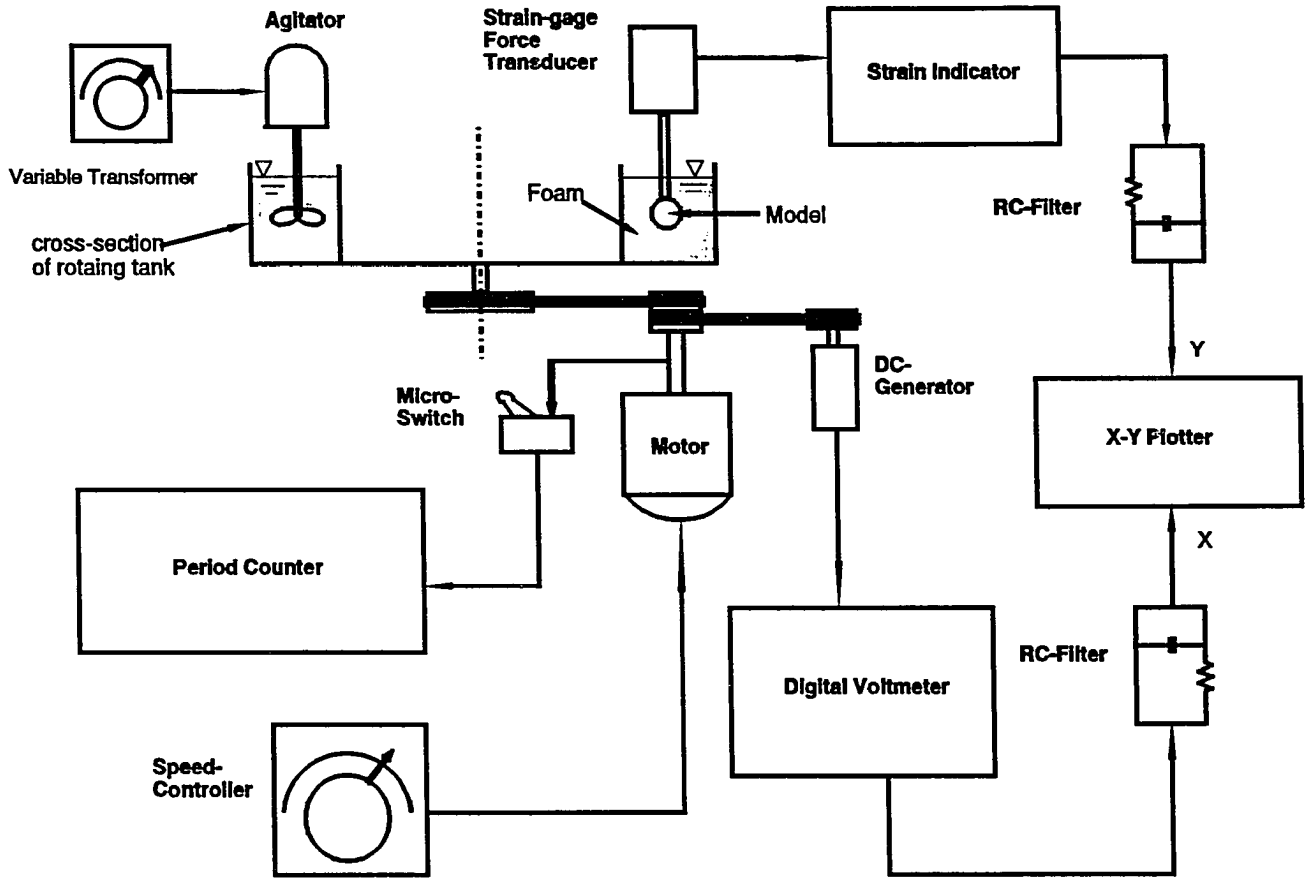

Figure 3.1: Schematic diagram of experimental set-up

indicator and recorded on the y-axis on the plotter. Thus, it was possible to directly record graphs of drag as a function of velocity.

The experimental set-up can be grouped into four major parts by their functions: test section, foam flow velocity control, drag force measurement, and data recording.

3.1.1. Test section

As shown in Figure 3.2, a rotating tank, having an open channel formed by two concentric walls, was used as the means to provide a uniform steady-state foam flow. The tank was made of Plexiglass to visually observe the foam. Such observation helped ensure that the foam generated was homogeneous throughout (i.e., no foam decay at the bottom).

The diameter of the outer tank wall was 1.143 m, the inner diameter was 0.902 m, and the height was 0.108 m. Constant foam properties were maintained by means of a variable speed agitator (a mixer on the end of a rotating shaft) located at the center of the channel, opposite the force transducer. The agitator was made by Palo Lab, Inc., type V-10. A variable autotransformer made by Staco Energy Product Co., type 2PF1010, was used to control the agitator speed.

3.1.2. Foam velocity control

The rotating tank was connected to a gear reducer that was rotated by a variable speed motor made by Electro-Craft Co. (EC). The motor was controlled by an EC speed control, model E650M. The foam velocity, U, was obtained from $U = \omega R$, where R is the radius from the center of the tank to the test object and ω is the angular velocity of the tank. For most of the tests, the model was centered within

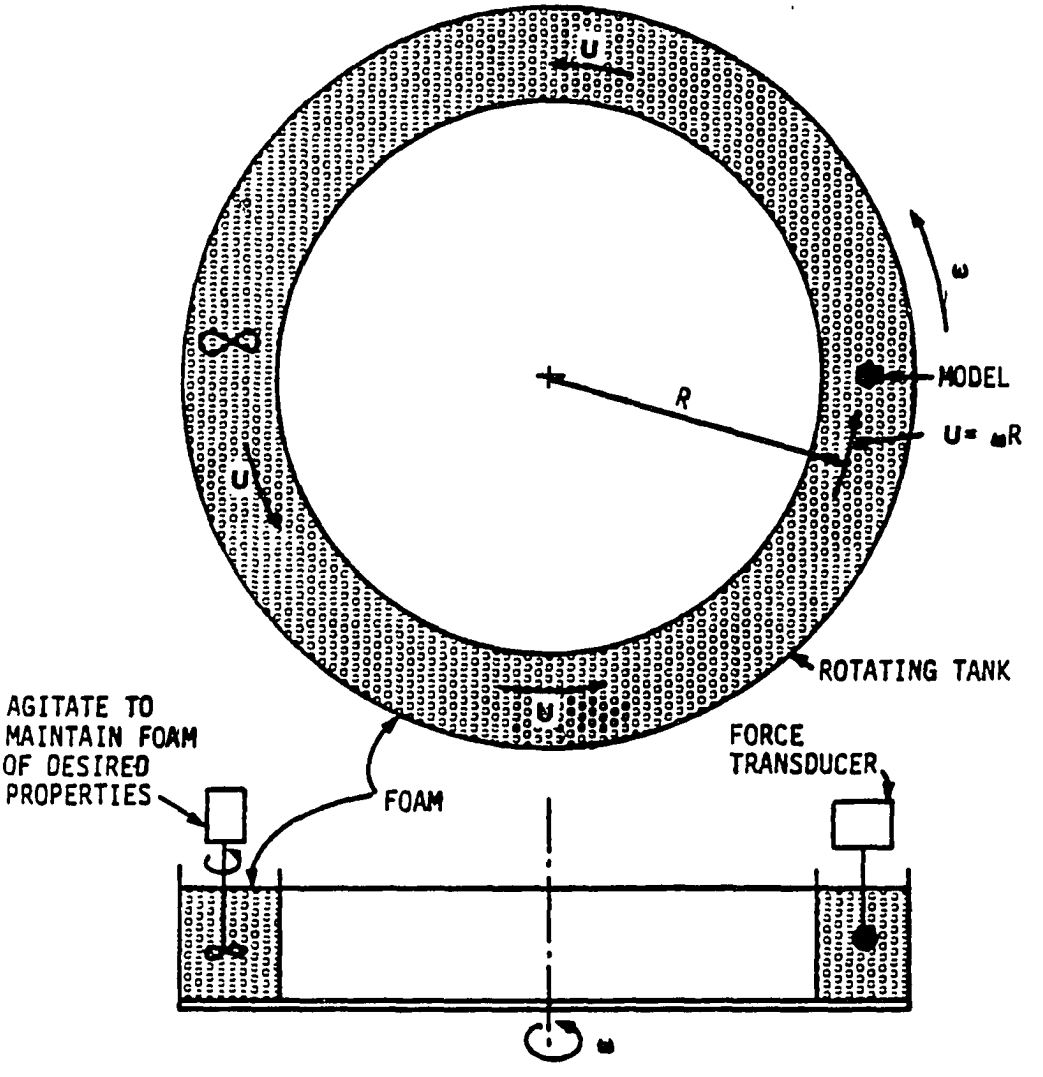

Figure 3.2: Schematic representation of test section

the $(1.143m - 0.902m)/2 = 0.12m$ foam channel with $R = 0.962\ m$. The angular velocity was obtained from a precision dc tachometer (voltage generator) attached to the variable speed motor that rotated the tank.

The dc tachometer was made by Horowe Servo Control, Inc., model 1211-003, and the rate of generating voltage was 20.8 $volt/1000\ rpm$, with 8000 rpm maximum. Its linear characteristic was checked through a calibration procedure. Although the tachometer had unstable nonlinear output under 10 rpm, this angular velocity was equivalent to a foam velocity 0.0024 m/sec or less, which was very slow and negligible. The output was read by a Keithley Digital Multimeter, model 195. The electric noise in the tachometer signal was attenuated by an RC-filter before being fed to the plotter.

3.1.3. Drag force measurement

The drag force, F_D, on the objects tested was measured by a dual cantilever beam force transducer using strain-gauges, full bridged for high resolution. The sketch of the force transducer is shown in Figure 3.3. The transducer was carefully designed to provide the desired resolution and accuracy for the data range covered.

To prevent the transducer from rusting, stainless steel (18-8) with a thickness of 0.381 mm and a width of 12.7 mm was selected and used for the cantilever beams. The beam length, 250 mm, was optimized with the thickness and width within design criteria, which was aimed for the maximum possible resolution with small deflection.

Prior to the present study, there were no drag data for objects moving through foam. Hence, there was no way to estimate the magnitude of the expected drag force in order to design the force transducer properly. Thus, a set of preliminary

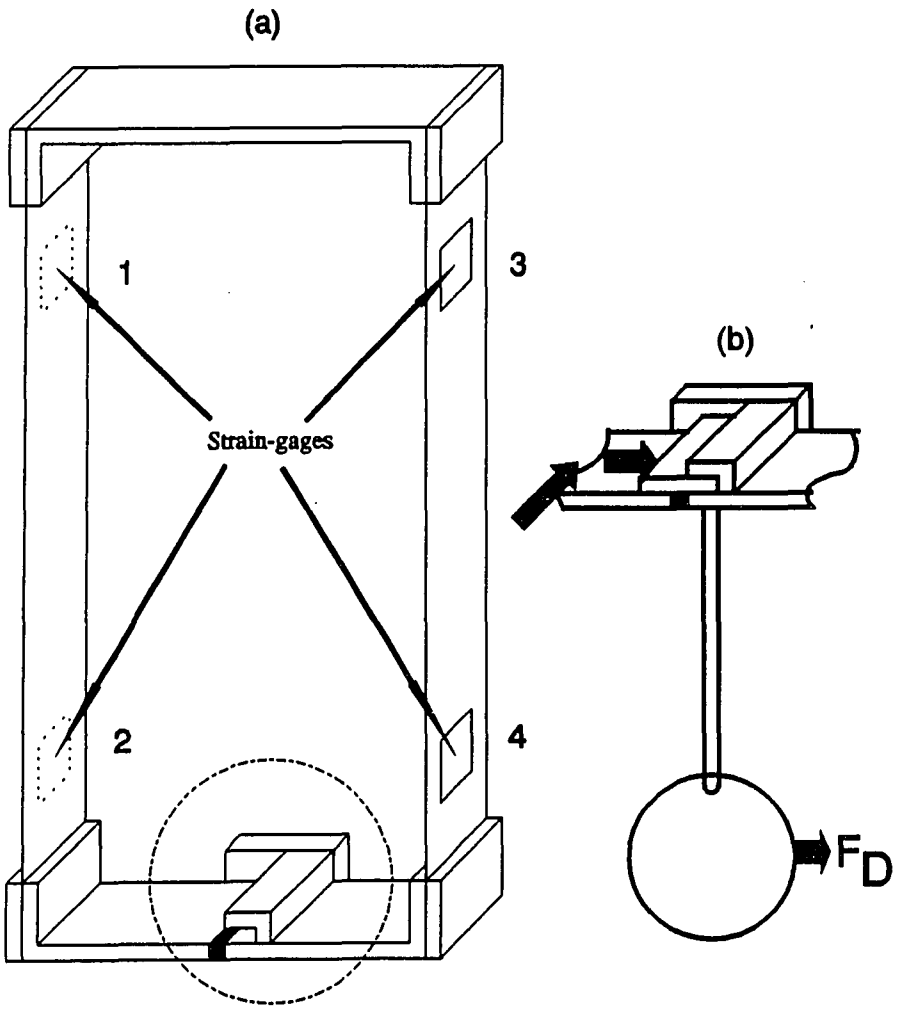

Figure 3.3: (a) Sketch of dual cantilever beam force transducer (b) The illustration of installation of model to the transducer slot

experiments using a torsion bar force transducer was run to determine the possible maximum drag force, which turned out to be about 0.4 Newton.

If 0.5 N drag is acting on the object, 0.25 N force F is delivered to each end of the cantilever beam. The constraint equation for one of the cantilever beams where both ends have a fixed boundary condition is

$$F = \frac{12EI\delta}{L^3} = \frac{Ebt^3\delta}{L^3} \tag{3.1}$$

where E is the modulus of elasticity, b and t are the width and thickness of the beam, δ is the deflection, and L is the length of the beam. For the set-up, the Eq. (3.1) becomes

$$0.25N = \frac{(190 \times 10^9 N/m^2)(12.7 \times 10^{-3} m)(0.318 \times 10^{-3} m)^3 \delta}{(0.25m)^3}$$

or

$$\delta = 0.025m = 2.5cm$$

The moment, M, due to the force at the end of a cantilever beam is

$$M = \frac{FL}{2} = 3.125 \times 10^{-2} Nm$$

Since the strain gauge is attached 2.5 cm from the beam end, the moment, M_ϵ, at that position is $M_\epsilon = 2.5 \times 10^{-2} Nm$. With M_ϵ, the strain is

$$\epsilon = \frac{M_\epsilon C}{EI} = \frac{6\ M_\epsilon}{Ebt^2} \tag{3.2}$$

or

$$\epsilon = \frac{6(2.5 \times 10^{-2} Nm)}{(190 \times 10^9 N/m^2)(12.7 \times 10^{-3} m)(0.381 \times 10^{-3} m)^2} \simeq 430\mu$$

This maximum strain is under the allowable strain limit 6000 μ of the strain gauge.

Now, the actual strains in the strain gauges are

$$\epsilon_1 = +\frac{M_\epsilon C}{EI} + \epsilon_{axial}$$

$$\epsilon_2 = -\frac{M_\epsilon C}{EI} + \epsilon_{axial}$$

$$\epsilon_3 = +\frac{M_\epsilon C}{EI} + \epsilon_{axial}$$

$$\epsilon_4 = -\frac{M_\epsilon C}{EI} + \epsilon_{axial}$$

Since the strain gauges are full bridged, the output strain ϵ' is

$$\epsilon' = \epsilon_1 - \epsilon_2 + \epsilon_3 - \epsilon_4$$

so that the axial strains cancel (i.e., the weight of the model does not affect the output strain), and the total output strain is

$$\epsilon_{max} = 4\epsilon \simeq 4(430\mu) = 1720\mu$$

The strain gauges were selected for the output range and base metal for the self temperature compensation. Strain gauge model EA-06-240LZ-120 option E, made by the Measurements Group. Inc., was selected and used for force transducer. The strain indicator, model $P-3500$ by the Measurements Group. Inc., was used as the output device.

3.1.4. Recording data

For the experiments conducted, the drag force and velocity were plotted on a Hewlett Packard $X-Y$ Recorder, Model 7044A, giving F_D versus U graphs. The

cumulated plot was digitized by using a Tektronix digitizer made by Summagraphics, model ID-TAB-1111, which was connected to Tektronix 4113A terminal. The digitized data were stored as data files in a VAX computer for future use.

3.2. Foam Property Measurement Devices

A wide variety of materials can be used to generate foams. The terminology "foaminess" or "foaming ability" is used to describe how well the material produces foam. Experimentally, for example, this means that agitation may produce a larger volume of foam on liquid A than on liquid B. Usually, foaming solutions (or foaming liquids) refer to the solutions which have foaming ability. This equivalence exists because it is generally agreed that pure liquids do not foam. Examples of foaming solutions that have a strong foaming ability are soap solutions which are salts of fatty acids having a high molecular weight, alkyl sulfates, sulfonates ethylene oxide adducts, cationic surfactants, etc.

For the purpose of this study, a stable high expansion foam was desirable to ensure that the drag force measurements were obtained in a uniform steady-state flow. Commercially available soap solutions were found to be very stable with excellent foaming ability. In this experiment, a commercially available liquid detergent (Joy) was used. This provided an inexpensive, consistent, stable foam, and was harmless to contact. Depending on the soap solution-to-water ratio, the resulting foam can vary widely in its physical properties, i.e., long lasting, heavy, strong, etc. These physical properties can be quantified by measuring bubble size, volume expansion rate, liquid viscosity, and surface tension.

3.2.1. Drainage rate measurement device

The bubble size (or cell size) is one of the components which defines foam characteristics. In actual foam, the bubbles have a random size distribution. Thus, the concept of average bubble size (mean bubble diameter) is used for practical purposes. Usually, the length divided by the number of bubbles in a known length gives the average bubble diameter.

Since the measurement of average bubble diameter is not easy in a dynamic (flowing) situation, the concept of drainage rate was proposed as an attempt for indexing the average bubble size in this study (see Section 6.2). Drainage involves thinning of the liquid films that separate the foam cells. Because of gravitational effects and surface tension variation in stationary liquid foam, the liquid in the films, which separate the gas bubbles, drains through the capillary liquid film path. Figure 3.4 is a sketch of the device used to measure the drainage rate, which was made by joining two different sizes of glass tubes. The larger upper cylinder is a foam sample (200 ml) reservoir, and the smaller lower part is used to deposit the cumulated liquid drained from the upper part. The upper cylinder is about 12 cm high with an inner diameter of 6.6 cm, and the lower tube was about 28 cm high with an inner diameter of 1.14 cm. The size of the lower cylinder was designed to collect the amount of the collapsed liquid volume from a 200 ml foam sample in the upper cylinder.

3.2.2. Quality (gas fraction) measurement device

Another foam property that is important in characterizing a foam is its quality. The quality is defined as the volume fraction of the gas phase volume contained in that foam. The terminologies such as gas fraction or gas expansion rate are used for

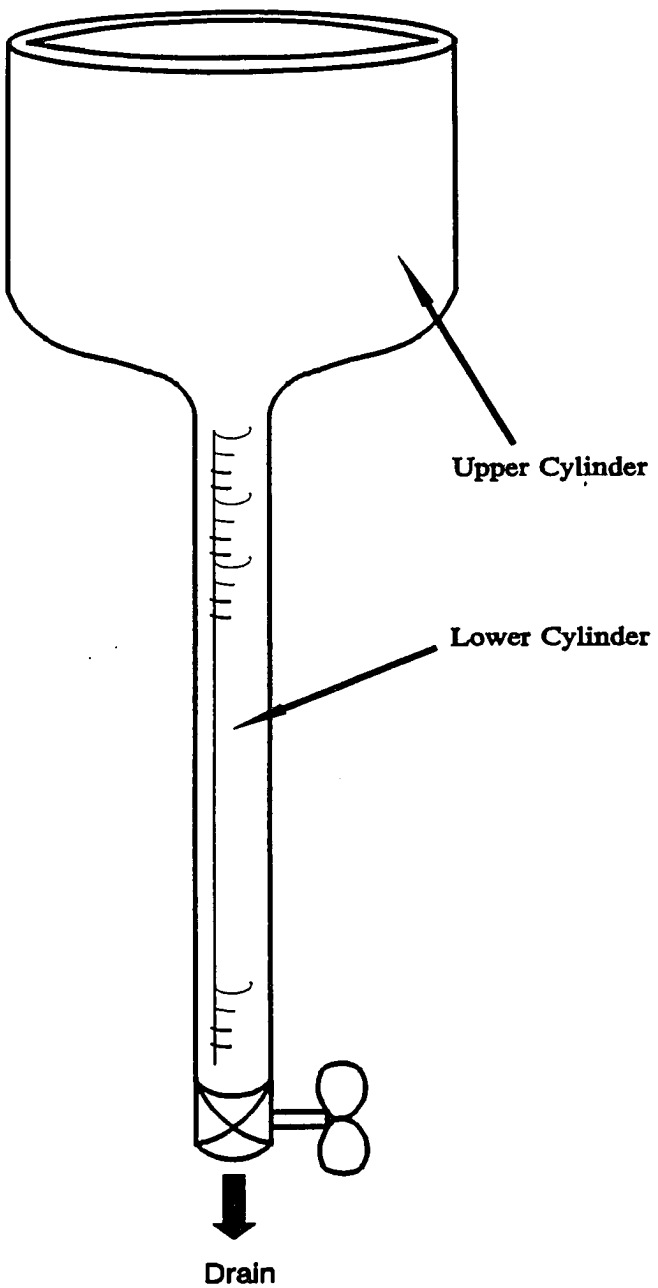

Figure 3.4: Open cylinder device for measuring foam drainage rate

the same purpose.

Therefore, quality can be calculated by measuring the volume of liquid from the collapsed foam after completing the drainage rate measurement. A 50 *ml* graduated cylinder was used to measure the drained liquid volume.

3.2.3. Viscosity measurement devices

As a foam flows, velocity gradients are generated within the liquid films that separate the individual bubbles. Thus, the viscosity of the liquid may be an important parameter affecting the drag force. Capillary tube viscometers made by Cannon Instrument Co., Cannon-Fenske Routine type, were used to measure the kinematic viscosity of the liquid. To cover the viscosity range involved, four different sizes of viscometers were used; these are nominal sizes 75, 100, 150, and 200 covering ranges from 1.6 to 8, 3 to 15, 7 to 35, and 20 to 100 centistokes, respectively. The normal size 350 capillary viscometer, which covers from 100 to 500 centistokes, was used to measure the viscosity of the pure Joy solution.

For the measurement of the effective viscosity of the low quality foam (gas bubble suspensions), a concentric cylinder viscometer made by Arther H. Thomas Co. was used.

3.2.4. Surface tension measurement device

Another very important parameter affecting the generation and flow of foam is the interfacial surface tension between the liquid and gas components of the foam. A surface ring-tensiometer made by Central Scientific Co. was used to measure surface tension of the soap-water solution for the foams in this study.

3.3. Specimens

The drag on objects is expected to be a function of the geometric properties of the object, i.e., size, shape, and surface composition. To determine this dependence, a fairly comprehensive set of specimens was constructed and tested. They were attached to the force transducer by means of a thin support stem, which was a hollowed stainless steel needle of diameter 1.52 mm and length 75 mm. These specimens can be grouped by their surface conditions: smooth-surfaced models and rough-surfaced models. In addition to these models, a bare stem was tested to measure the partial drag portion on the immersed stem part.

3.3.1. Smooth surface models

Eighteen smooth-surfaced (Plexiglass or painted wood) spheres, disks, flat plates and ellipsoids were tested in foams of different properties. The spheres were 19.1 mm, 25.4 mm and 38.1 mm in diameter. All of the disks and ellipsoids were 25.4 mm in diameter normal to the flow direction to make it easy to compare the effect of geometry.

The smooth-surfaced models tested in this study are listed in detail in Table 3.1, and a photograph of some of these models is shown in Figure 3.5. The experimental data obtained for these smooth surfaced objects show the functional relationships between drag force, geometry, velocity, and foam properties.

3.3.2. Rough surface models

Several different sphere sizes and flat plates oriented parallel to the flow were used to investigate the effect of surface roughness. The rough surfaces were created by

Table 3.1: Smooth surface models

Models	Shape Description	Model no.	$l(mm)$
Sphere	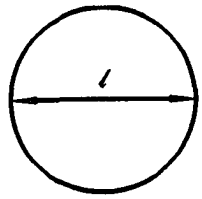	2	19.1
		3	25.4
		4	38.1
Disk	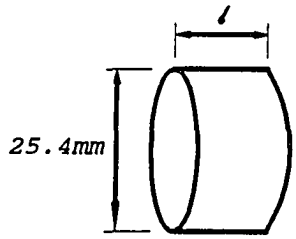	5	2
		6	5
		7	12
		8	25
Ellipsoid	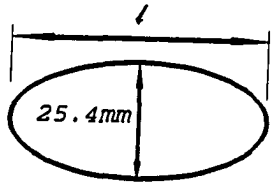	9	8.89
		10	15.31
		11	20.07
		12	24.13
		13	30.42
		14	36.91
		15	51.88
		16	103.76
Plate	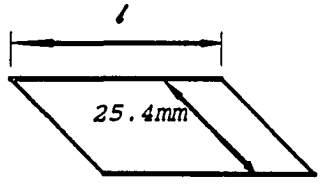	17	50.8
		18	76.2
		19	101.6

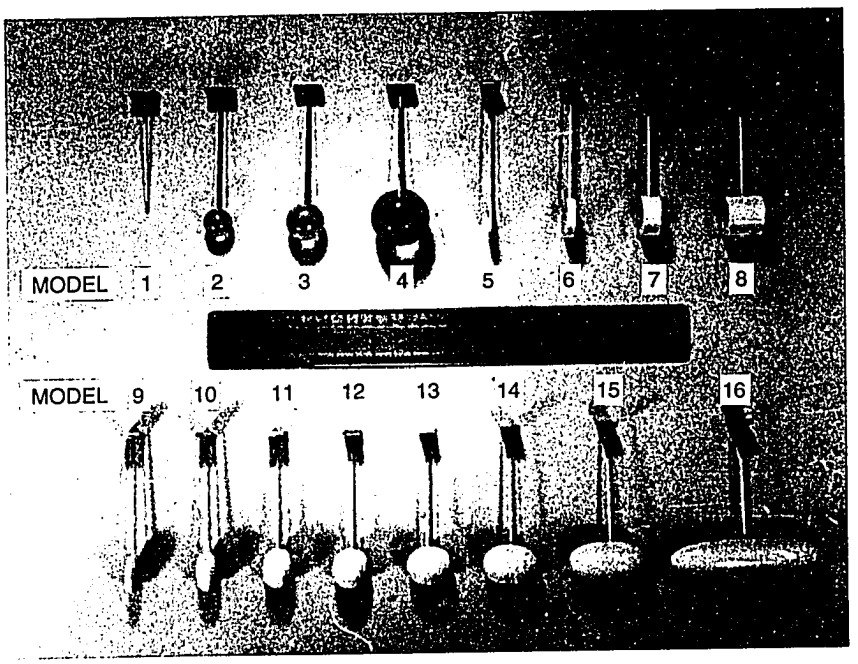

Figure 3.5: A photograph of the smooth surfaced models for this study

applying glass particles of different sizes to the models. Silicon coated glass particles were used to avoid possible dissolving problems in the foam.

Five different ranges of particle sizes were prepared in the range of 44 to 589 μm. These ranges were 44 μm to 74 μm, 74 μm to 149 μm, 149 μm to 250 μm, 250 μm to 420 μm, and 420 μm to 589 μm. Three different sizes of spheres and two different lengths of flat plates are used as models. These include 19.1 mm, 25.4 mm and 38.1 mm diameter spheres, and 50.8 mm and 101.6 mm length plates. Figure 3.6 is a photograph of samples of rough surface specimens.

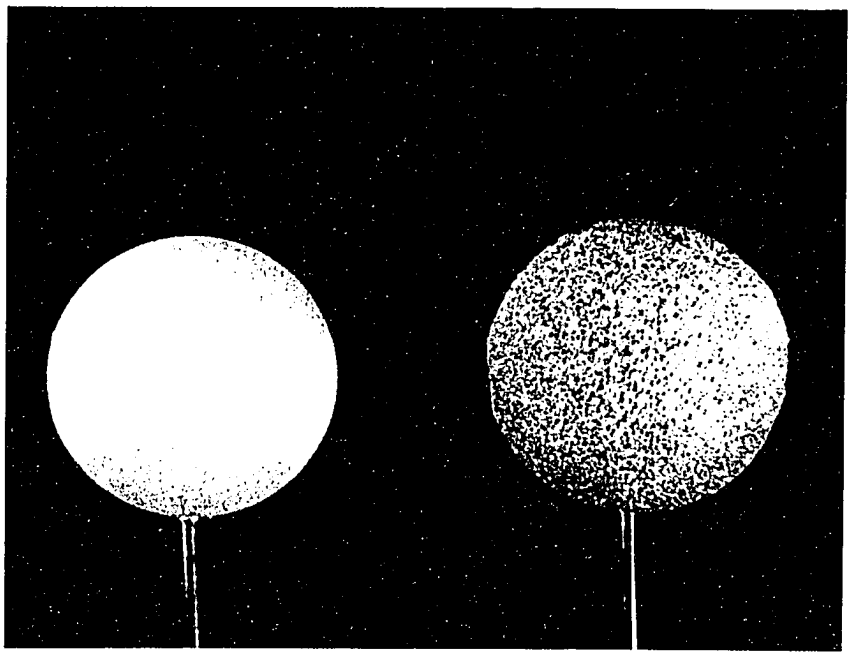

Figure 3.6: A photograph of samples of 38.1 mm dia. rough surfaced sphere. Roughness for left is 44–74 μm, and right is 420–589 μm

CHAPTER 4. PROCEDURES

4.1. Preparation of the Soap-water Solution

The foam was produced by the mechanical agitation (beating) of a soap-water solution. The viscosity of the liquid used to make the foam (an important property affecting the drag force) was adjusted by altering the soap-to-water ratio. An agitator was used to mix 4 to 8 liters of water and 0.45 to 1.2 liters of Joy in the rotating tank. Then the tank and agitator were stopped to let the foam decay to ensure the uniform mixture of soap-water solution.

4.2. Preparation of the Steady-state Foam Flow

Since the drag force is highly sensitive to viscosity, the temperature was maintained at about $20^{\circ}C$ throughout the experiment in order to maintain a constant viscosity. Before taking any drag force measurements, the apparatus (rotating tank and agitator) was run for about one hour to reach a steady-state foam flow. Upon reaching steady-state, a sample (200 ml) was taken from the foam and the drainage rate was recorded. After the sample foam had completely collapsed, the quality, viscosity, and surface tension were measured (see Section 4.3).

Before the drag force measurement, with no specimen attached to the force transducer, the null of the strain indicator was adjusted. Then, the highest expected

drag force for that specific foam was measured by loading the 101.6 mm-long ellipsoid model to the force transducer and running the tank at the highest foam velocity, about 0.4 m/sec. The y-axis of the plotter scale was adjusted to this working range.

4.3. Foam Property Measurement

After the steady-state was reached, 200 ml sample foam was taken out for a series of foam property measurements: drainage rate, foam quality, liquid viscosity, and surface tension.

4.3.1 Drainage rate measurement

The method of drainage rate measurement is simple. A 200 ml foam sample was taken from the tank and left alone in the larger upper cylinder of the drainage device (see Section 3.2.1). The drained liquid volume was measured with elapsed time. If the volume V of liquid exuded is measured for several time intervals, the drainage rate, dV/dt, can be found; t is time. The drainage rate can be rescaled by plotting V/V_O against t, where V_O is the initial volume of the liquid in the foam.

4.3.2. Foam quality measurement

After recording the drainage rate, the foam quality was calculated by measuring the liquid volume obtained from the completely collapsed sample foam. For example, if the original 200 ml sample of foam collapsed into 50 ml of liquid, its quality is $\phi = 0.75$.

For the experiments involving the drag as a function of velocity using smooth wall specimens reported in this study, the quality ranged from 0.81 to 0.88. The quality

ranged from 0.73 to 0.81 for the experiments performed to investigate the relationship between drag, velocity, and quality. For the dispersed gas bubble experiments, the quality varied from 0.0 to 0.64. For the rough surface model, the quality was 0.8.

4.3.3. Liquid viscosity measurement

After the measurement of foam quality, the liquid viscosity of the collapsed liquid was measured. The viscosity was determined by measuring the time it takes for a given quantity of liquid to flow through a capillary tube viscometer.

Before measuring the viscosity, the capillary tube was cleaned out with the same soap-water solution to be measured. Four different sizes of viscometer were used to cover the viscous range tested. In some cases, the viscosity of the liquid was in the range covered by either of two nominal sizes (application overlap region). In these cases, both viscometers were used to compare the readings. For example, both nominal size 75 and 100 viscometers were used for the kinematic viscosity about 5 centistokes, the range of either viscometer. The results obtained were very close to each other.

For experiment on smooth specimens, viscosity ranged from $1.12 \times 10^{-3} Ns/m^2$ to $20.4 \times 10^{-3} Ns/m^2$. The viscosity ranged from $4 \times 10^{-3} Ns/m^2$ to $24 \times 10^{-3} Ns/m^2$ for the experiments to investigate the relationship between drag, velocity and quality. For the dispersed gas bubble experiments, the viscosity was $210.6 \times 10^{-3} Ns/m^2$. For the rough surface model, the viscosity was $7.1 \times 10^{-3} Ns/m^2$.

4.3.4. Surface tension measurement

With the same liquid, the surface tension was measured by using a ring surface tensiometer. Surface tension was determined by measuring the force needed to pull a circular wire ring free from the surface of the liquid. Three readings were collected on the soap-water solution, and those readings were very close to each other. The surface tension range varied from 0.059 N/m to 0.077 N/m in this study.

4.4. Drag Force Measurement on Specimens

By interchanging the specimens and varying the foam flow velocity, the drag force as a function of velocity was plotted on scaled graph paper on the $x-y$ plotter for a variety of shapes. For each model the drag force was measured by starting at the highest velocity (approximately 0.4 m/sec), reducing the velocity to zero and returning to the highest velocity. This was done to provide a recheck on the measurements.

The specimens were exchanged at the highest velocity and the same process was repeated. This procedure was used to reduce the possibility of non-uniform foam due to foam decay when the tank is stationary. Another advantage of proceeding from high velocity to low velocity was the ease of detecting the yield point immediately upon reaching velocity zero.

This experimentally measured yield point could differ somewhat from the true yield point (effective yield point), which is theoretically defined for the foam field. The experimental yield point (apparent yield point) may be lower than the effective yield point due to the slip condition of the foam flow.

After the completion of the drag experiments for one foam, another foam sample

(200 ml) was taken out and its properties were rechecked.

4.5. Investigating Wall Effect

Since the foam is considered to have some properties of a Bingham plastic material, a confined yielded region around the moving model might exist, with the remainder of the flow unyielded (rigid body motion). To verify the existence of this yield region, tests were conducted with a 19.1 mm diameter sphere positioned at different locations between the tank wall and the center of the foam channel. The sphere was located at various distances from the wall at the same depth in the foam flow. This was done by attaching the force transducer to a precision sliding device. The experiments were performed for seven different foam velocities.

4.6. Storing Experimental Data

After the data were written on the $x - y$ plotter paper (see Figure 4.1), the Tektronix digitizer was used to collect the data and store the data file in a VAX computer. By giving proper scales to both axis through the digitizer driver, the plot unit system was converted to the S.I. unit system.

These converted data were written as a data file and stored in the VAX computer storage. This made it easier to fit the curve to the data points and to reproduce the output combination for certain comparison purposes. The collected data were modified in the computer by subtracting the drag portion on the bare stem.

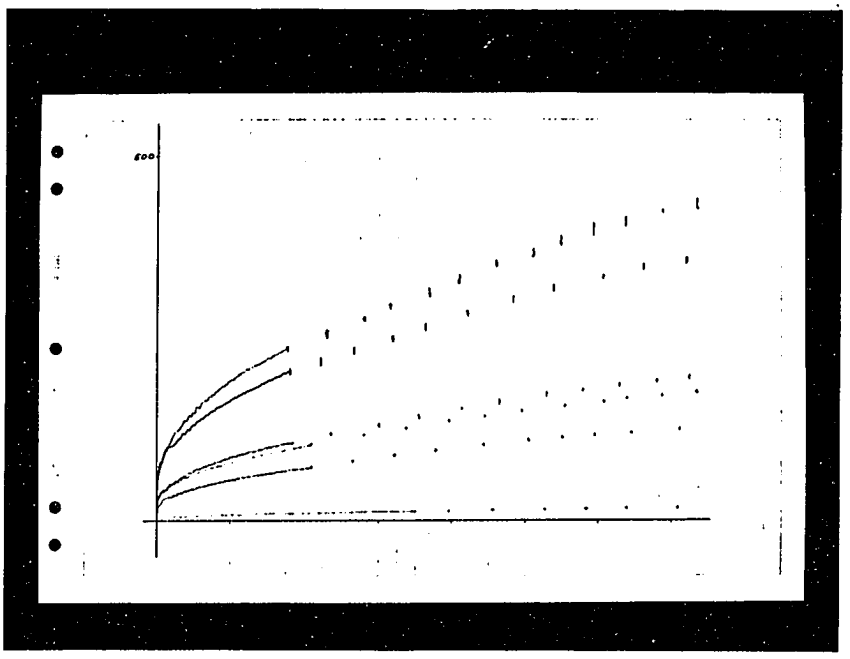

Figure 4.1: A photograph of a sample output on x-y plotter

4.7. Effective Viscosity Measurement on Dispersed Gas Bubble Suspensions

The pure Joy solution was used to investigate the relationship between the effective viscosity and the foam quality in the low quality range. Due to its high viscosity, the pure Joy solution has the ability to maintain bubbles in a liquid phase for a certain amount of time. The viscosity of the pure Joy solution was determined to be $210.6 \times 10^{-3} Ns/m^2$ by using a nominal size 350 capillary tube viscometer. The surface tension of the pure Joy solution was measured as 0.0627 N/m. For comparison purposes, the corresponding values for water are $1.12 \times 10^{-3} Ns/m^2$ and 0.0734 N/m, respectively.

The low quality foam (or dispersed gas suspension) was produced by the mechanical agitation of the liquid coupled with air blowing into a large beaker. The combination of air blowing and agitation provided a wide range of low quality foam. The resulting quality range was from $\phi = 0.0$ (i.e., pure liquid) to 0.632.

The sample foams were run in the concentric cylinder viscometer, and the drive weight–angular velocity data (proportional to shear stress–rate of strain) were recorded. To prevent foam decaying problems, quick measurements were done at low deformation rate on each foam sample.

CHAPTER 5. THEORY

The theory presented in this chapter was developed by previous investigators. Due to lack of comparable foam flow experimental data, importing an approximate theory which is somewhat related to this study is useful for the purpose on analyzing our results. The theory introduced in Section 5.1 was developed in conjunction with experiments of highly concentrated emulsions by Princen [27]. Analogous to foam, this theory is considered adaptive to high quality foam flow in low deformation rate, where compressibility is negligible.

Next, despite prevailing suspicions, foam has been considered as a Bingham-plastic material by many previous investigators. As mentioned earlier, being dissimilar to the Newtonian laminar flow, the flow pattern around the object in Bingham material is altered from uniform flow only within a limited range. To verify the fact, a thoughtful investigation on foam as a proposed Bingham material would be of interest. For this purpose, some derivation from the study on spheres moving in Bingham material by Beris et al.[1] will be introduced in Section 5.2.

5.1. Highly Concentrated Emulsions

An emulsion is a system consisting of a liquid dispersed, using tiny droplets, in another immiscible liquid. As a counterpart of dilute emulsions mentioned in Section

2.1, highly concentrated emulsions refer to emulsions with the volume fraction of the dispersed phase comparable to that of foam. It was shown by Princen [27] that the yield stress, τ_o, of foams and highly concentrated emulsions is given by

$$\tau_o = 1.277(\sigma/a_{32})\phi^{1/3}F_{max}(\phi) \quad (0.74 < \phi < 1) \tag{5.1}$$

where σ is the interfacial tension, $F_{max}(\phi)$ is the mean dimensionless contribution to the yield stress per drop, and a_{32} is the surface-volume mean drop radius. $F_{max}(\phi)$, determined experimentally from measurements of τ_o in a concentric-cylinder viscometer, was found to increase sharply with ϕ. The simple dependence of τ_o on σ has been verified. The dependence of τ_o on a_{32}, however, was found to be more complex, probably as a result of the finite thickness of the aqueous films separating the droplets of the emulsion.

Recently, Princen and Kiss [29] revised their previous work [27]. In this new study, the yield stress is given by

$$\tau_o = \sigma\phi^{1/3}Y(\phi)/a_{32} \text{ for } \phi > 0.74 \tag{5.2}$$

where $Y(\phi)$ is a function whose value was experimentally found to be significantly lower than obtained in the previous study [27]. Within the range of ϕ considered in the recent study, $Y(\phi)$ is accurately represented by

$$Y(\phi) = -0.080 - 0.114log(1-\phi) \tag{5.3}$$

up to the deformation rate, $\dot{\gamma}$, of about 40 s^{-1}.

When $\tau > \tau_o$, the stress and effective shear viscosity of all emulsions are described by

$$\tau = \tau_o + 32(\phi - 0.73)\frac{\sigma}{a_{32}}Ca^{1/2} \tag{5.4}$$

and

$$\mu_e = \tau_o/\dot{\gamma} + 32(\varphi - 0.73)\mu Ca^{1/2} \tag{5.5}$$

where $Ca = \mu a_{32}\dot{\gamma}/\sigma$. This result is applicable when $Ca < 10^{-4}$.

The viscous term deviates from Princen and Kiss' previous model in the value of the exponent of Ca (i.e., 1/2 vs. 1/3). This latest model is in much better qualitative agreement with experiment than other recent models (Kraynik's [18] and Armstrong's [14]), at least for their system investigated.

5.2. Flow Past a Sphere in a Bingham Plastic

Beris et al. [1] adopted the Bingham plastic constitutive equation [40] for a viscoplastic material to simulate creeping motion of rigid a sphere through a Bingham plastic, assuming no slip, by using the finite element/Newton method. They predicted large differences between Bingham-plastic and Newtonian fluid flows in the flow pattern around the sphere and in the drag coefficient, which depend on the dimensionless value of the critical yield stress, Y_g. Below Y_g, the material acts as a solid. The different portions of the flow domain and the yield surfaces attached to the sphere and surrounding the fluid are shown in Figure 5.1.

The two dimensionless numbers used are the Bingham number, N_B, which measures the ratio of the strength of the yield stress to the viscous stress, and the Stokes (i.e., negligible inertia) drag coefficient C_s. These groups are defined as

$$N_B \equiv \frac{2\tau_o R_o}{\eta_o U} \tag{5.6}$$

$$C_s \equiv \frac{F_D}{6\pi\eta_o U R_o} \tag{5.7}$$

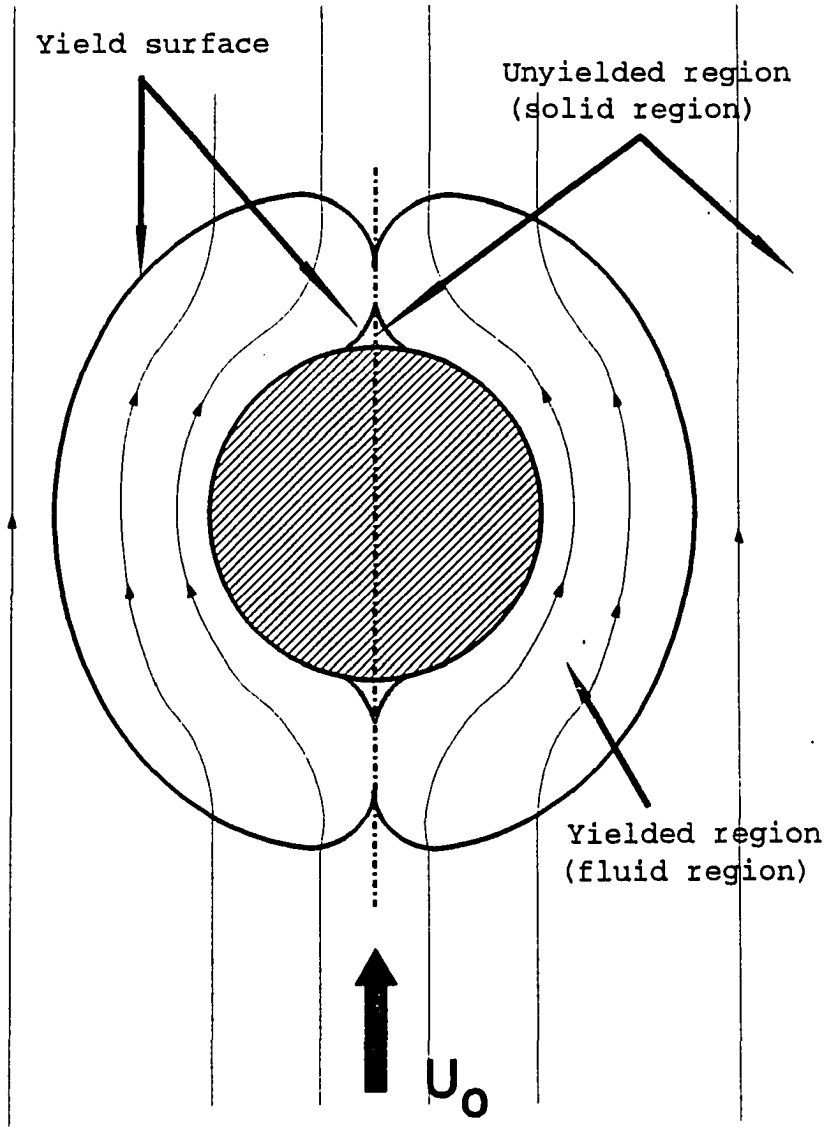

Figure 5.1: Plastic and solid regions for the flow surrounding a solid sphere falling in a Bingham plastic material. From Beris et al. [1]

Table 5.1: Solution parameters for selected values of Y_g. From Beris et al. [1]

Y_g	N_B	C_s
0.0	0.0	1.0
0.001	0.007	1.17
0.01	0.108	1.74
0.036	0.747	3.46
0.06	2.299	6.39
0.088	8.047	15.24
0.1	14.91	24.85
0.11	27.36	41.45
0.12	59.59	82.77
0.13	197.5	253.2
0.133	340.7	426.9
0.135	544.6	672.3

where F_D is the external force acting on the sphere, η_o the plastic viscosity, τ_o the yield stress, R_o the sphere radius and U the velocity, respectively.

The third dimensionless parameter, Y_g, called the dimensionless yield stress parameter, can be formed as

$$Y_g = 2\tau_o\pi \ R_o^2/F_D \tag{5.8}$$

which is related to N_B and C_s by

$$N_B \equiv 6C_sY_g \tag{5.9}$$

The calculated results for N_B, C_s and Y_g are in Table 5.1, and the plot C_s versus Y_g is in Figure 5.2.

For comparison to our experimental results, these equations are modified in the form of $F_D = f(U)$. From the work by Beris et al., the sphere will move only when Y_g is below 0.143. Otherwise, there is not enough force to overcome the yield-stress

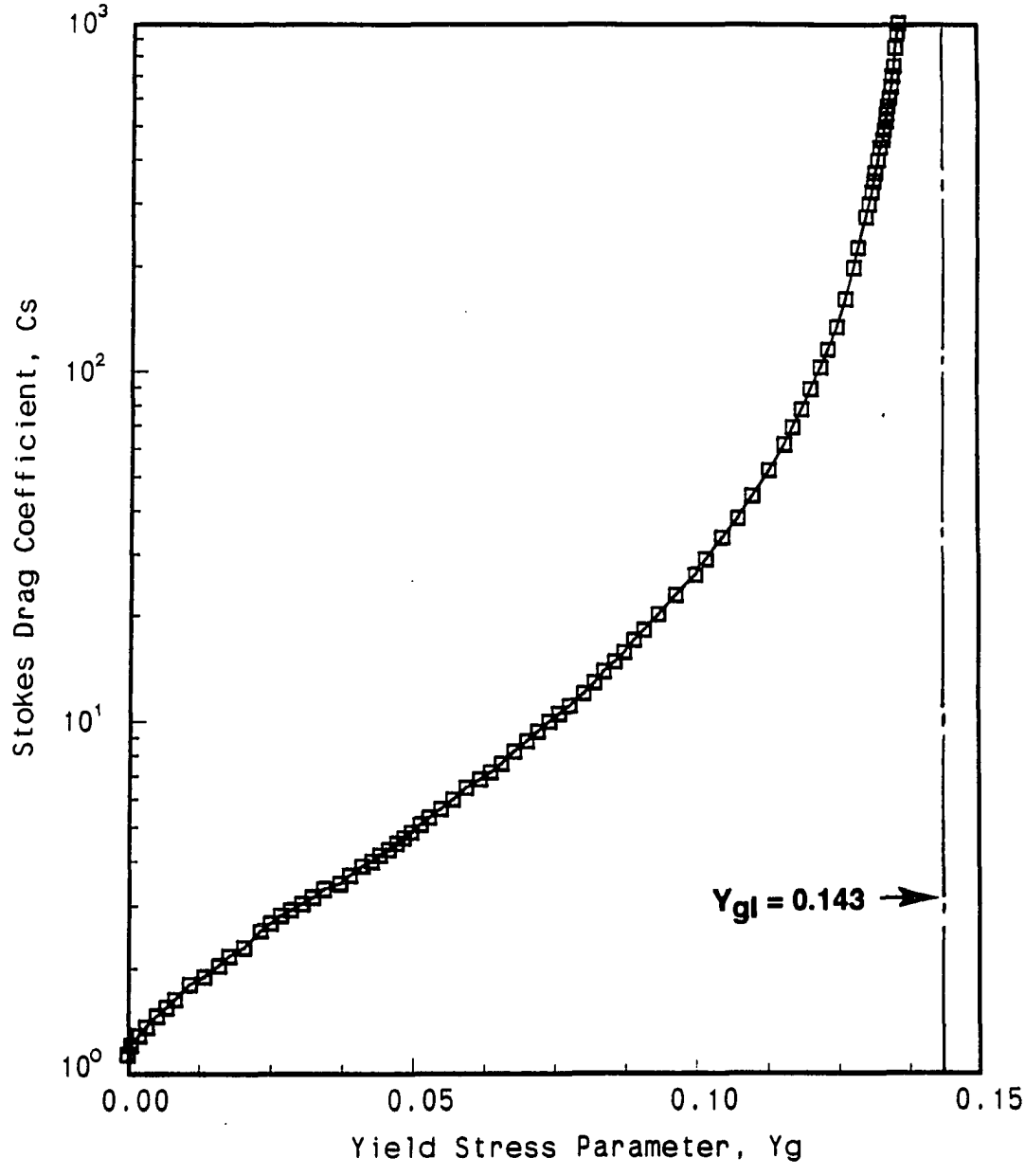

Figure 5.2: Dependence of the Stokes drag coefficient on the yield-stress parameter Y_g. From Beris et al. [1]

drag force. Let this limiting value be denoted Y_{gl} and corresponding limiting external force F_l so that

$$F_l = \frac{2\tau_o \pi R_o^2}{Y_{gl}} \tag{5.10}$$

If the external force F_D is less than F_l , there will be no motion of the sphere. Rearranging Eq. (5.7) gives

$$F_D = 6\pi\eta_o U R_o C_s \tag{5.11}$$

or

$$U = \frac{F_D}{6\pi\eta_o R_o C_s} = \frac{F_D}{6\pi\eta_o R_o(\frac{N_B}{6Y_g})} \tag{5.12}$$

and

$$\frac{F_D}{F_l} = \frac{Y_{gl}}{Y_g} = \frac{0.143}{Y_g} \tag{5.13}$$

From Eqs. (5.6) and (5.9),

$$U = \frac{\tau_o R_o}{3\eta_o C_s Y_g} = \frac{2\tau_o R_o}{\eta_o(6C_s Y_g)} \tag{5.14}$$

Substitution Eq. (5.9) to (5.14) yields

$$U = \frac{2\tau_o R_o}{\eta_o N_B} \tag{5.15}$$

or

$$U = \frac{U_o}{C_s Y_g} \text{ where } U_o \equiv \frac{\tau_o R_o}{3\eta_o} \tag{5.16}$$

Applying the scaling scheme from the boundary layer analysis, Beris et al. approximates

$$C_s \simeq \frac{\alpha Y_g}{(\beta - Y_g)^2} \tag{5.17}$$

where $\alpha = 1.031$, and $\beta = 0.143$ as Y_g approaches β.

Then Eq. (5.16) becomes

$$\frac{U}{U_o} = \frac{1}{C_s Y_g} \simeq \frac{(\beta - Y_g)^2}{\alpha Y_g^2} \tag{5.18}$$

as Y_g approaches β.

From Eq. (5.13),

$$Y_g = \frac{\beta}{(\frac{F_D}{F_l})} \tag{5.19}$$

$$\frac{U}{U_o} = \frac{[(\frac{F_D}{F_l}) - 1]^2}{\alpha} \tag{5.20}$$

or

$$\frac{F_D}{F_l} = \sqrt{\alpha \frac{U}{U_o}} + 1 \tag{5.21}$$

As $\frac{U}{U_o}$ approaches zero,

$$\frac{F_D}{F_l} = 1 + 1.015\sqrt{\frac{U}{U_o}} \tag{5.22}$$

The plot of Eq. (5.22) is given in Figure 5.3.

Based on a perturbation analysis, Beris et al. show that the drag coefficient can be written as

$$C_s = 1 + a_3 N_B^{\frac{1}{2}} + a_4 N_B + \textit{higher} \text{ order terms} \tag{5.23}$$

or

$$C_s = 1 + 1.874\sqrt{N_B} + 1.152 N_B \tag{5.24}$$

This approximate result is accurate to within 2.5 % of the finite element results for the entire range of N_B.

Using Eqs. (5.6) and (5.7), Eq. (5.24) can be rewritten as

$$F_D = (6\pi\eta_o R_o)U + (43.4\tau_o R_o^2) + (49.9\sqrt{\eta_o R_o^3 \tau_o})\sqrt{U} \tag{5.25}$$

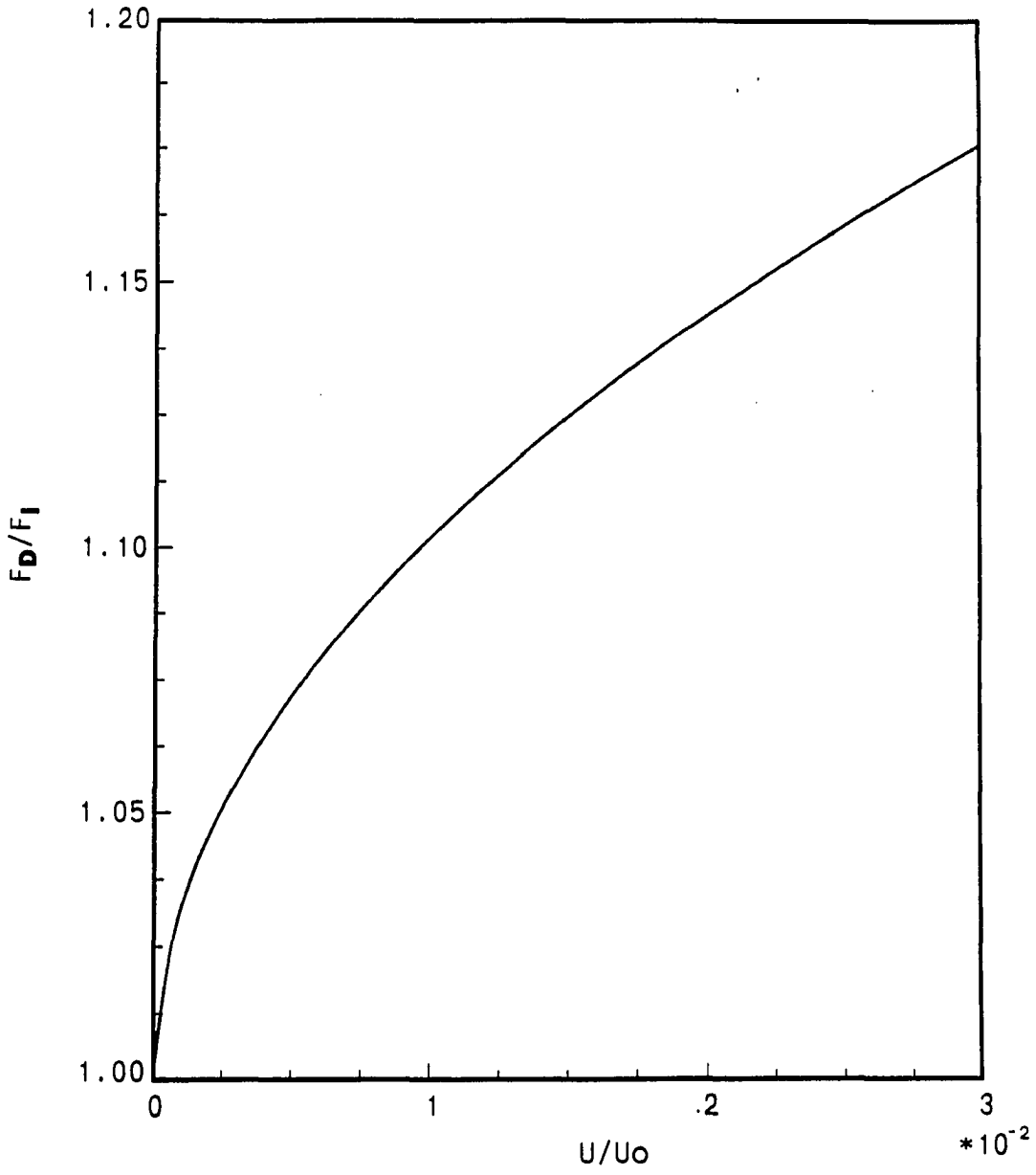

Figure 5.3: Dimensionless drag-velocity curve for Bingham material as dimensionless velocity approaches zero

The first term of Eq. (5.25) is that portion of the drag that corresponds to Newtonian creeping flow around the sphere, the second term is the yield force resulting from the finite yield stress of the Bingham plastic and the last term gives the shear thinning effect.

5.3. Wall Effect

By using both boundary element and finite element methods for the creeping motion of shear thinning fluids past a sphere in the presence of a wall, Tanner et al. [9, 37] found that the shear thinning characteristic can reduce the drag coefficient of the sphere remarkably compared to that of the case in the absence of fluid shear thinning.

The study done by Beris et al. [1] on Bingham material showed the enveloped yielded region around the sphere and unyielded outer region where the uniform incoming streamlines were not affected. Since foam is considered to be a Bingham material, there may be an envelope region around the specimen in which there is a shearing motion, surrounded by an unyielded region.

Since foam is opaque, however, visualization of the flow is not easy. Investigation of the wall effect, as described in Section 4.5, could be an indirect way to detect this region. The foam has a low density, and therefore it has a negligible inertia. In addition, each bubble, which is comparable to the fluid particle, is confined by the others. Due to these conditions, turbulent-like flow was not observed in the range of foam flow tested. Therefore, the wall effect for a sphere at a low Reynolds number, or creeping flow, in Newtonian fluid would be of interest for comparison purposes.

The motion of a sphere parallel to a single plane wall and parallel to two external

plane walls was treated by Faxen [12]. For the case of a sphere falling at the position $b = 3l$ (Figure 5.4), Faxen obtained the following resistance formula:

$$F_D = \frac{6\pi\mu R_o U}{1 - 0.6526(R_o/l) + 0.1475(R_o/l)^3 - 0.131(R_o/l)^4 - O(a/l)^5} \tag{5.26}$$

A sphere located such that $b = 3l$ will rotate about an axis which is perpendicular to the direction of the fall and parallel to the walls. The direction of rotation is opposite to that which would occur if the sphere touched the nearest wall.

For the special case where the sphere lies centered between the two plane walls, Faxen obtained

$$F_D = \frac{6\pi\mu R_o U}{1 - 1.004(R_o/l) + 0.418(R_o/l)^3 + 0.21(R_o/l)^4 - 0.169(R_o/l)^5} \tag{5.27}$$

where $2l$ is the distance between the walls.

Faxen also determined the wall effect for a sphere and single plane wall,

$$F_D = \frac{6\pi\mu R_o U}{1 - (9/16)(R_o/l) + (1/8)(R_o/l)^3 - (45/256)(R_o/l)^4 - (1/16)(R_o/l)^5} \tag{5.28}$$

One might be tempted to assume that the limiting cases for two walls could be built up in a simple fashion from the solution for a single plane wall and a sphere, as suggested by Oseen [24], by separately adding the effects. This leads to the formula

$$F_D = \frac{6\pi\mu R_o U}{1 - (9R_o/16)[(1/l_1) + (1/l_2)]} \tag{5.29}$$

where l_1 and l_2 are the distances of the middle of the sphere from each wall. Thus, this procedure results in $\frac{3}{4}(R_o/l)$ for the lead term of the wall correction in Eq. (5.26), rather than the correct value of 0.6526 (R_o/l). Similarly, we would obtain $\frac{9}{8}(R_o/l)$ for the lead correction term in Eq. (5.27) instead of 1.004 (R_o/l).

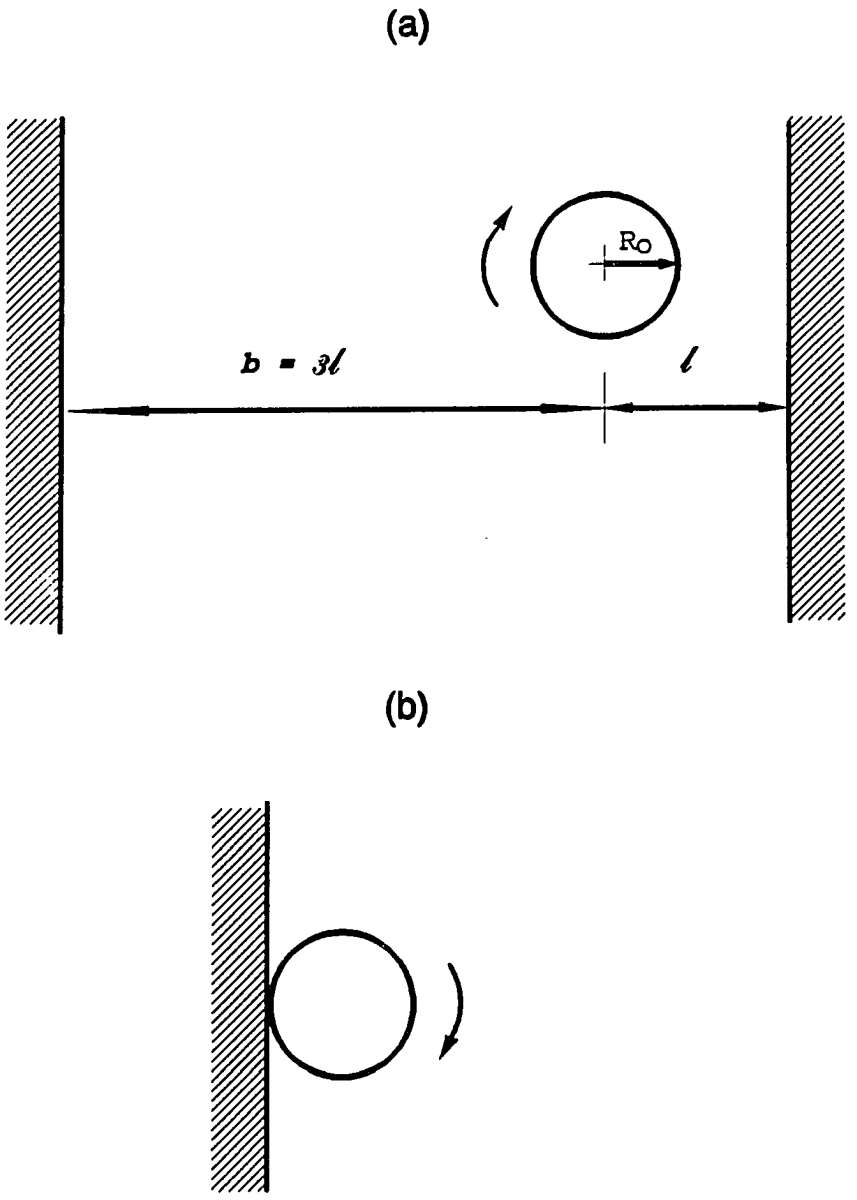

Figure 5.4: Direction of rotation of a free falling spheres

The above equations are for free falling spheres which experience rotation of the sphere. Wakiya [43] investigated the resistance of a sphere which is held fixed. The results suggest that the difference occurs in the second wall-correction term, which is order of $(R_O/l)^3$. If we neglect the difference for our case, we can compare our experimental result to Eq. (5.29) for practical purposes. The comparison of wall effect between this Newtonian creeping flow case and foam flow case will be followed in Section 6.3.

CHAPTER 6. RESULTS

It has been suggested that experiments designed to measure the drag on objects in foam would be very difficult to perform. However, the foam generated by the foam machine developed for this study was uniform, and the steady-state flow was successfully achieved. The output plots of drag versus velocity were well defined, and consequently, favorable results were gathered. Therefore, the experiments proposed for this study were successfully performed and analyzed.

The overall drag results on smooth surfaced models for various foams are discussed in Section 6.1. In Section 6.1, the general observation for the drag-viscosity-quality relationship, and shape dependency are presented. A discussion on an attempt to index the average bubble size by varying the drainage rate is discussed in Section 6.2. In Section 6.3, the wall effect investigation to verify Bingham characteristics for foam is analyzed and compared with the Newtonian creeping flow case. The comparison of experimental results of this study with approximate theory for highly concentrated emulsions is discussed in Section 6.4. The drag results on rough surfaced models are presented in Section 6.5. Finally, experimental results on dispersed gas bubble suspension to explore the effective viscosity-quality relationship is presented in Section 6.6.

Table 6.1: The foam used for smooth specimen tests

Foam ID	Viscosity, μ $\times 10^{-3}(Ns/m^2)$	Quality, ϕ	Surface tension, σ (N/m)
SCFA	1.37	0.83	0.055
SCFB	1.12	0.82	0.059
SCFC	1.24	0.81	0.063
SCFD	13.0	0.88	0.065
SCFE	7.22	0.82	0.077
SCFF	17.1	0.82	0.072
SCFG	15.1	0.81	0.070

6.1. Smooth Surfaced Models

The experimental data on eighteen different smooth surfaced models (see Table 3.1) are plotted, and the results are fit to the power law function. The observations were made among drag, viscosity, and quality. These are presented in Section 6.1.1. In Section 6.1.2, shape dependency of flat plates, disks, and ellipsoids is discussed.

6.1.1. General observations

Some of the properties of the foams used in the drag force test for the smooth surface specimens are tabulated in Table 6.1. Of the seven foams listed, each had a quality in the relatively narrow range of 0.81 to 0.88. On the other hand, the viscosity varied from 1.12×10^{-3} to $17.1 \times 10^{-3} Ns/m^2$, and the surface tension was in the range of 0.055 to 0.077 N/m. The drag force results are presented in Figures 6.1 through 6.19. As expected, drag force depends on the speed, size, shape, and roughness of the object, and the viscosity and quality of the foam. A thorough discussion of the results is presented below.

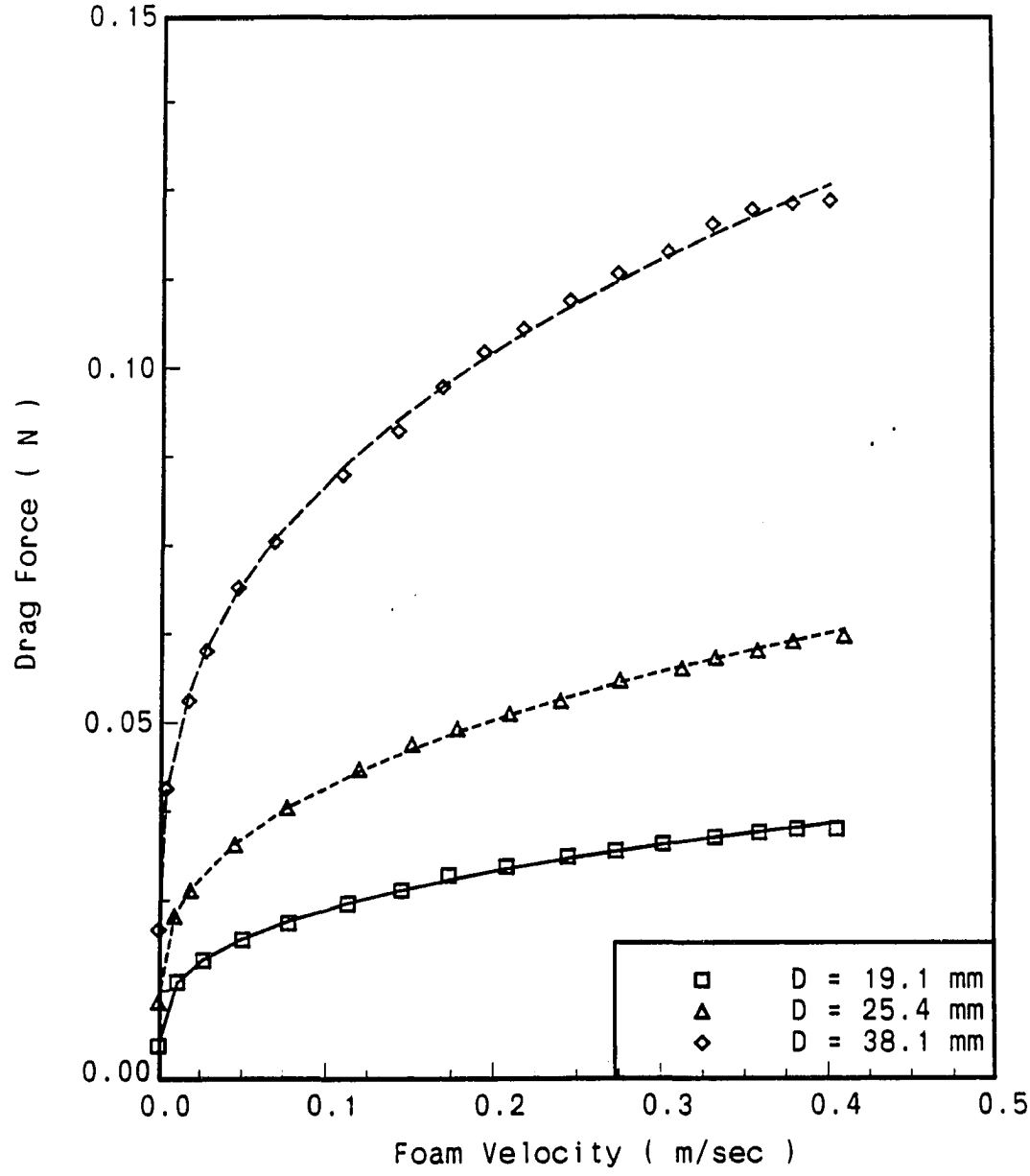

Figure 6.1: Drag force on smooth spheres for foam ID = SCFA

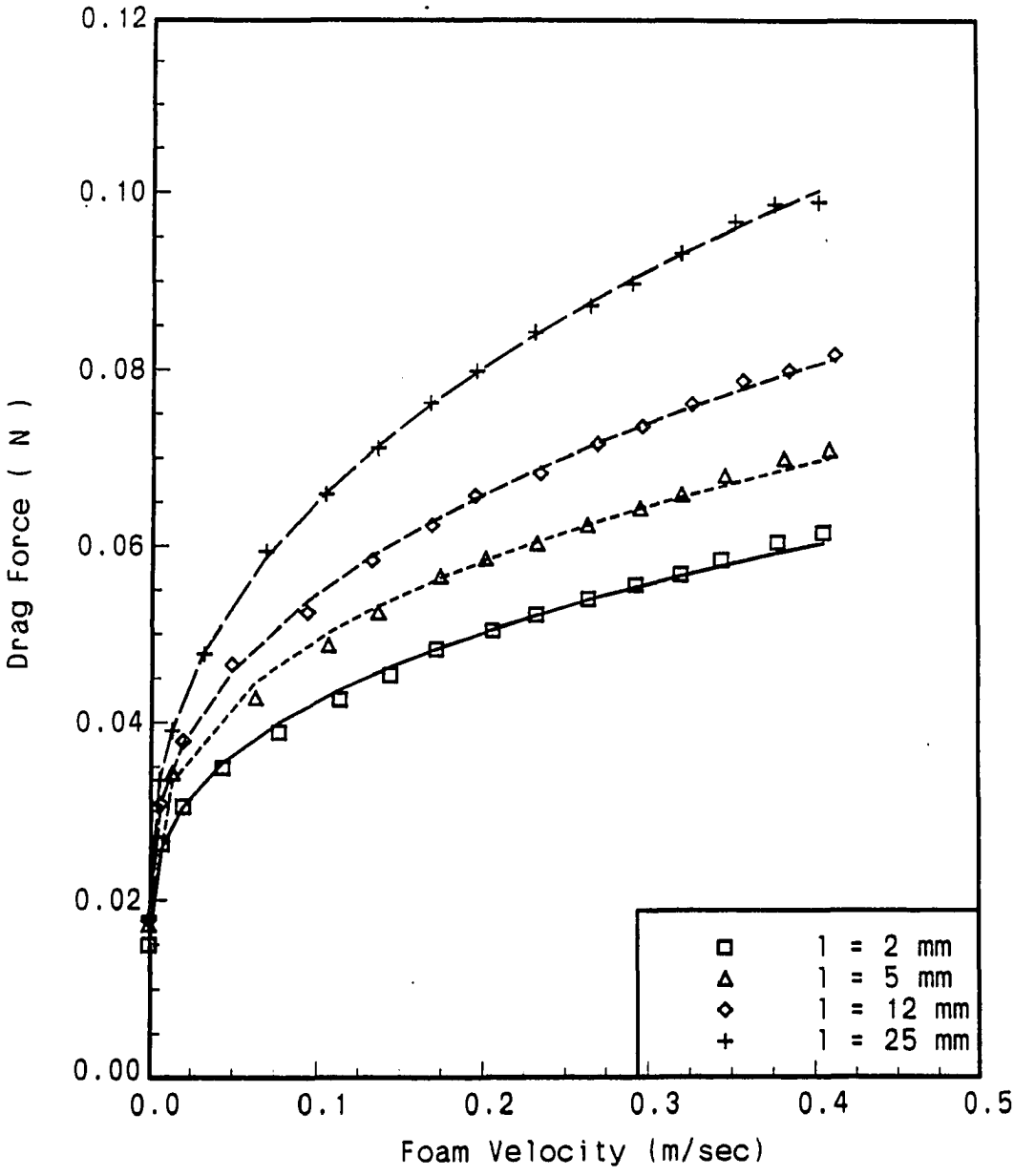

Figure 6.2: Drag force on disks for foam ID = SCFA

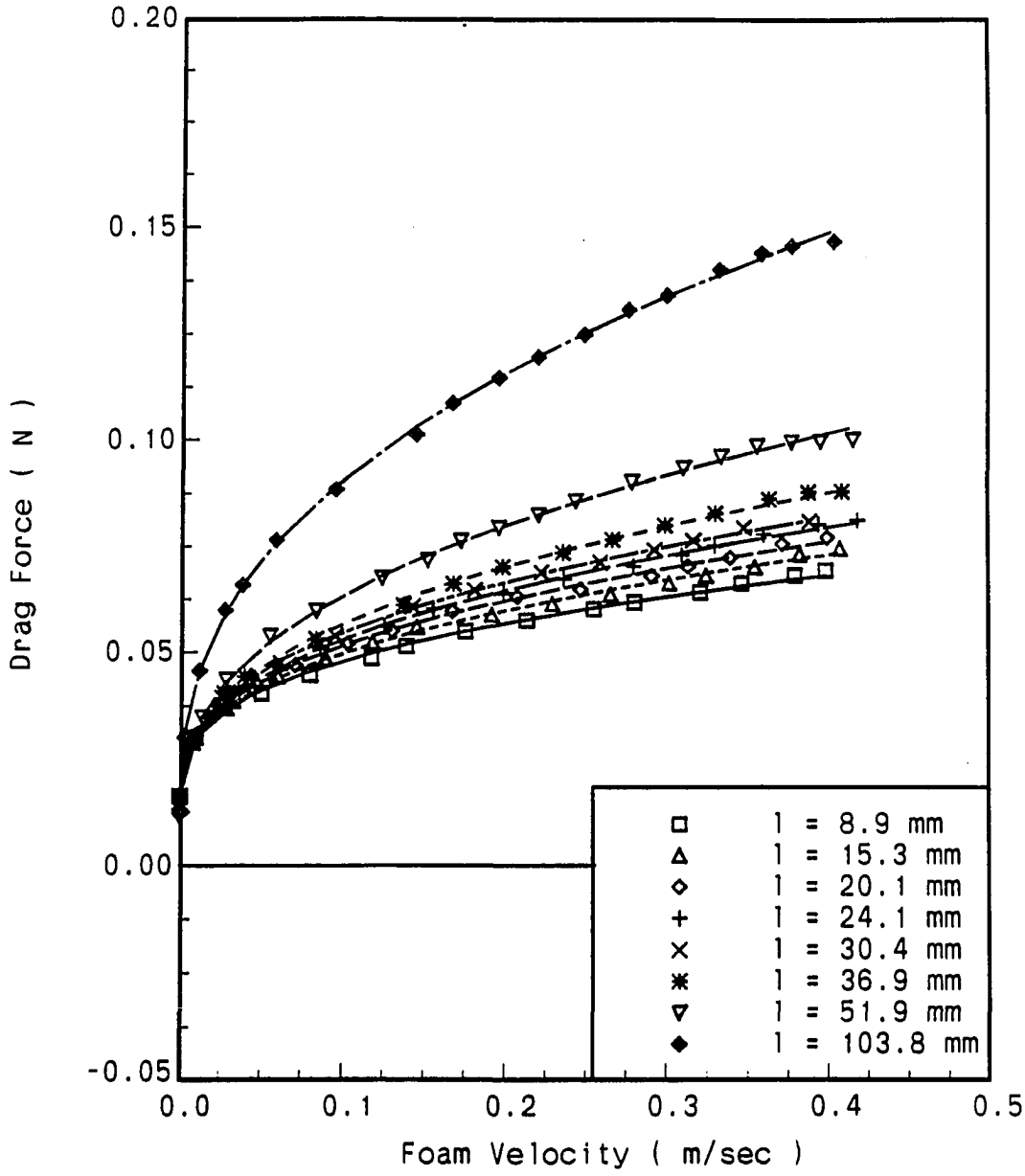

Figure 6.3: Drag force on ellipsoids for foam ID = SCFA

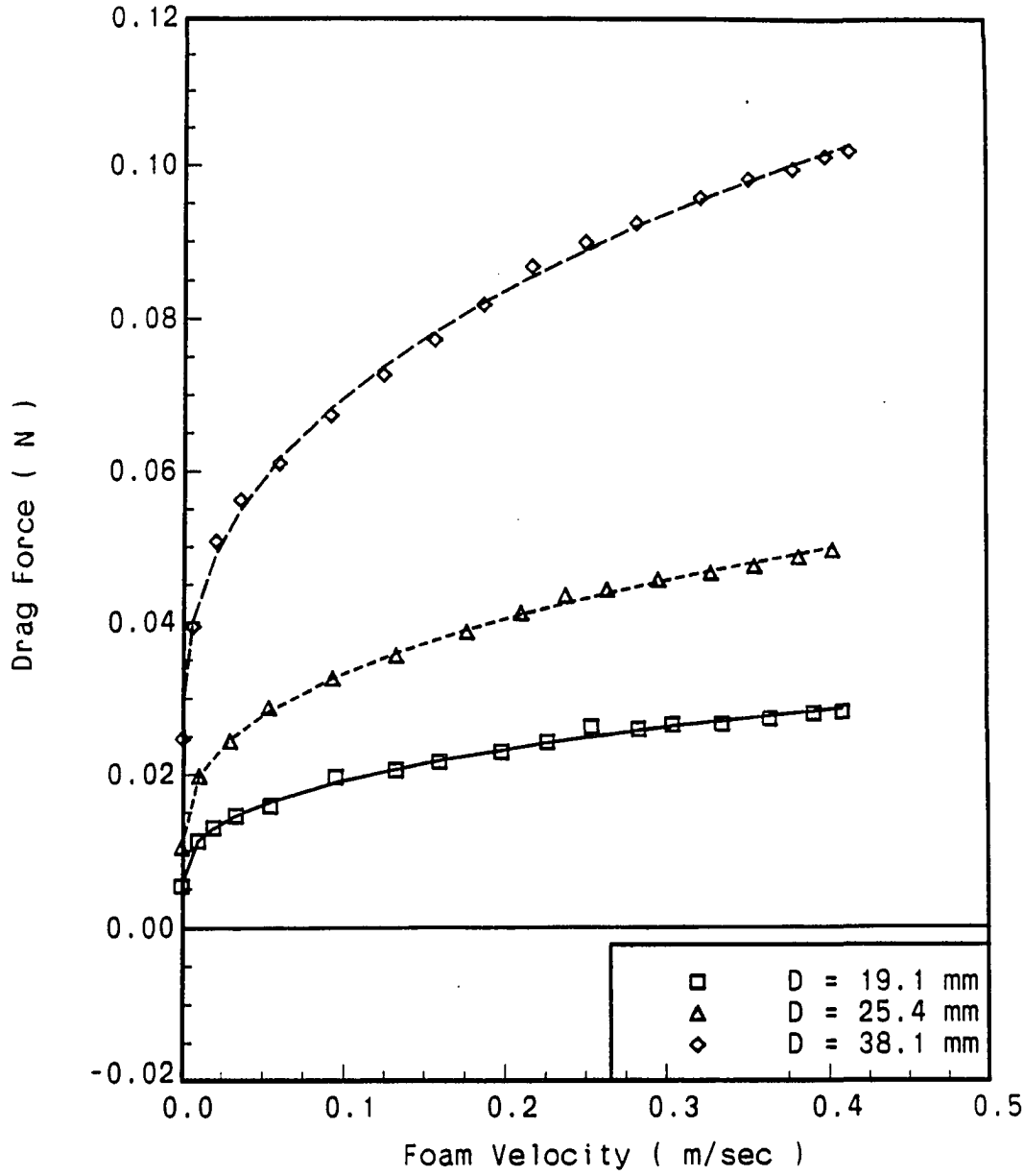

Figure 6.4: Drag force on spheres for foam ID = SCFB

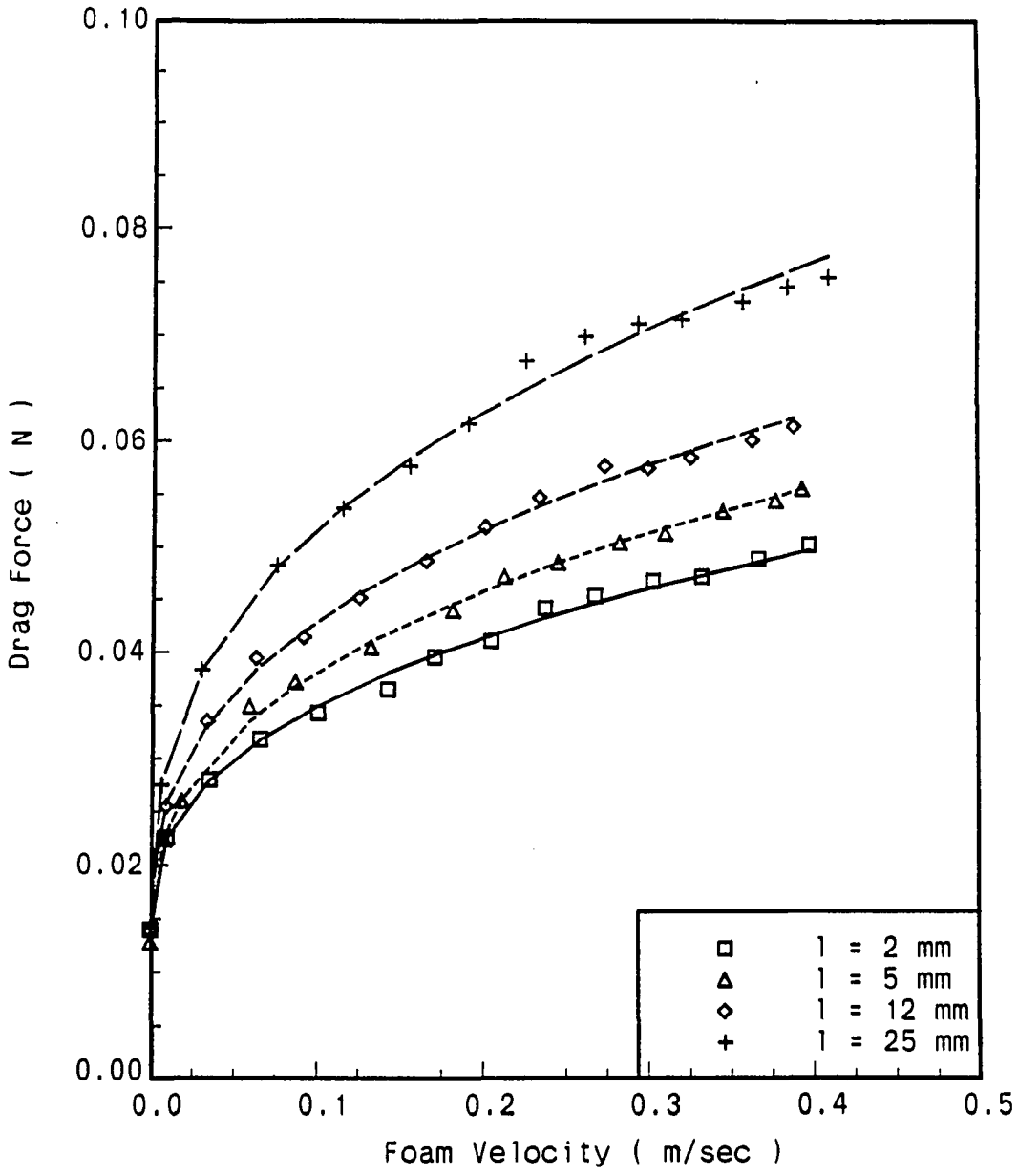

Figure 6.5: Drag force on disks for foam ID = SCFB

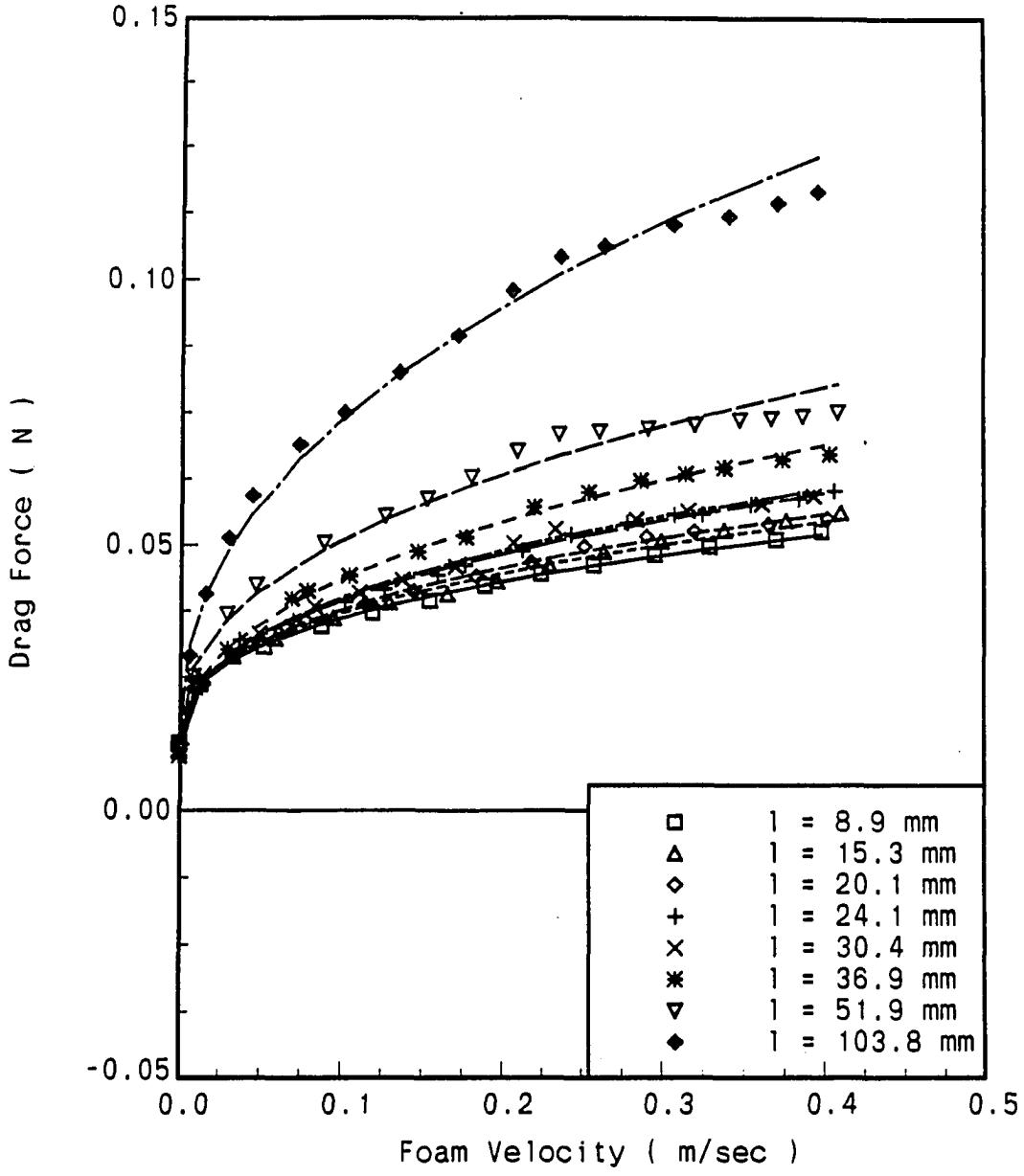

Figure 6.6: Drag force on ellipsoids for foam ID = SCFB

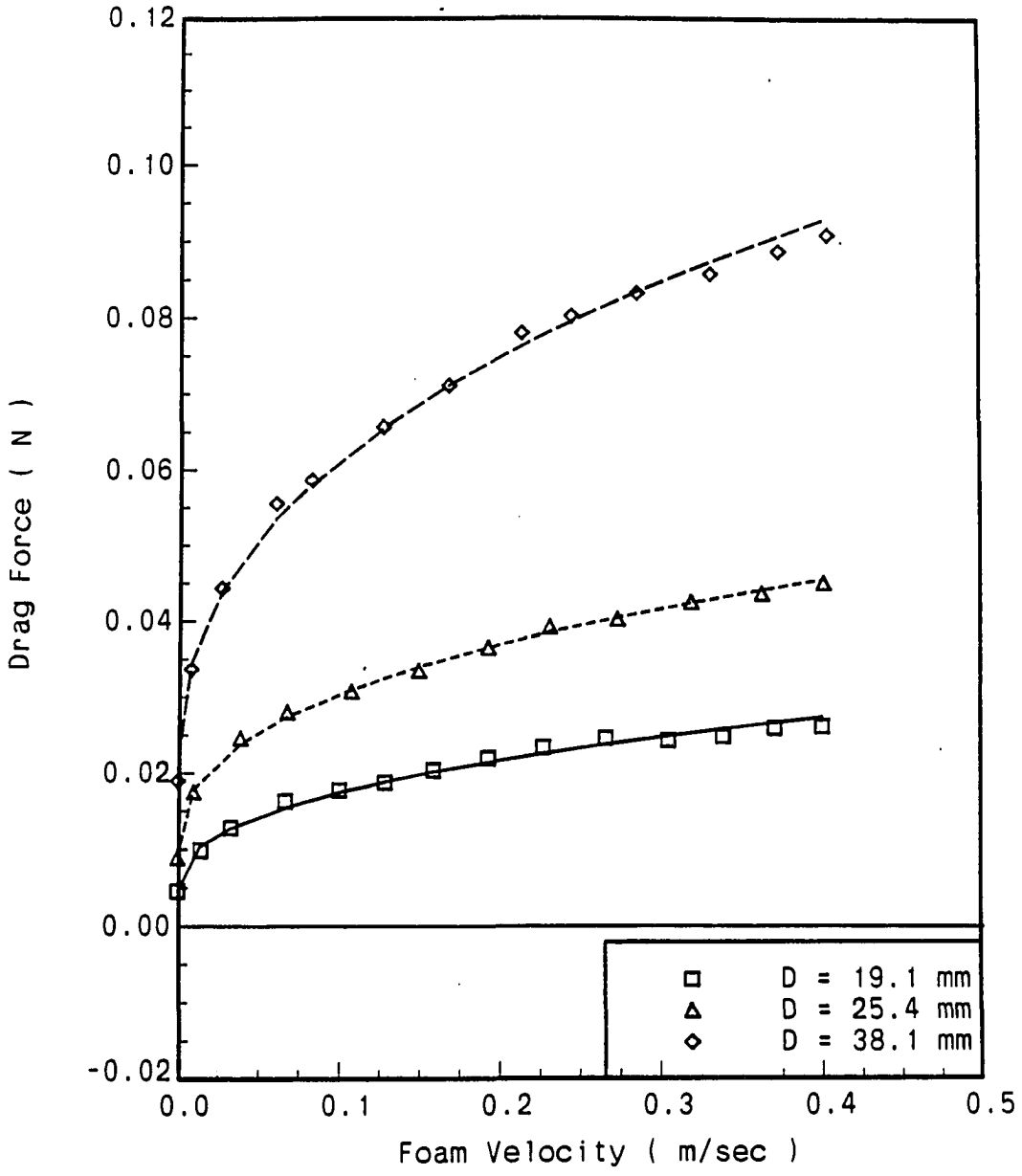

Figure 6.7: Drag force on spheres for foam ID = SCFC

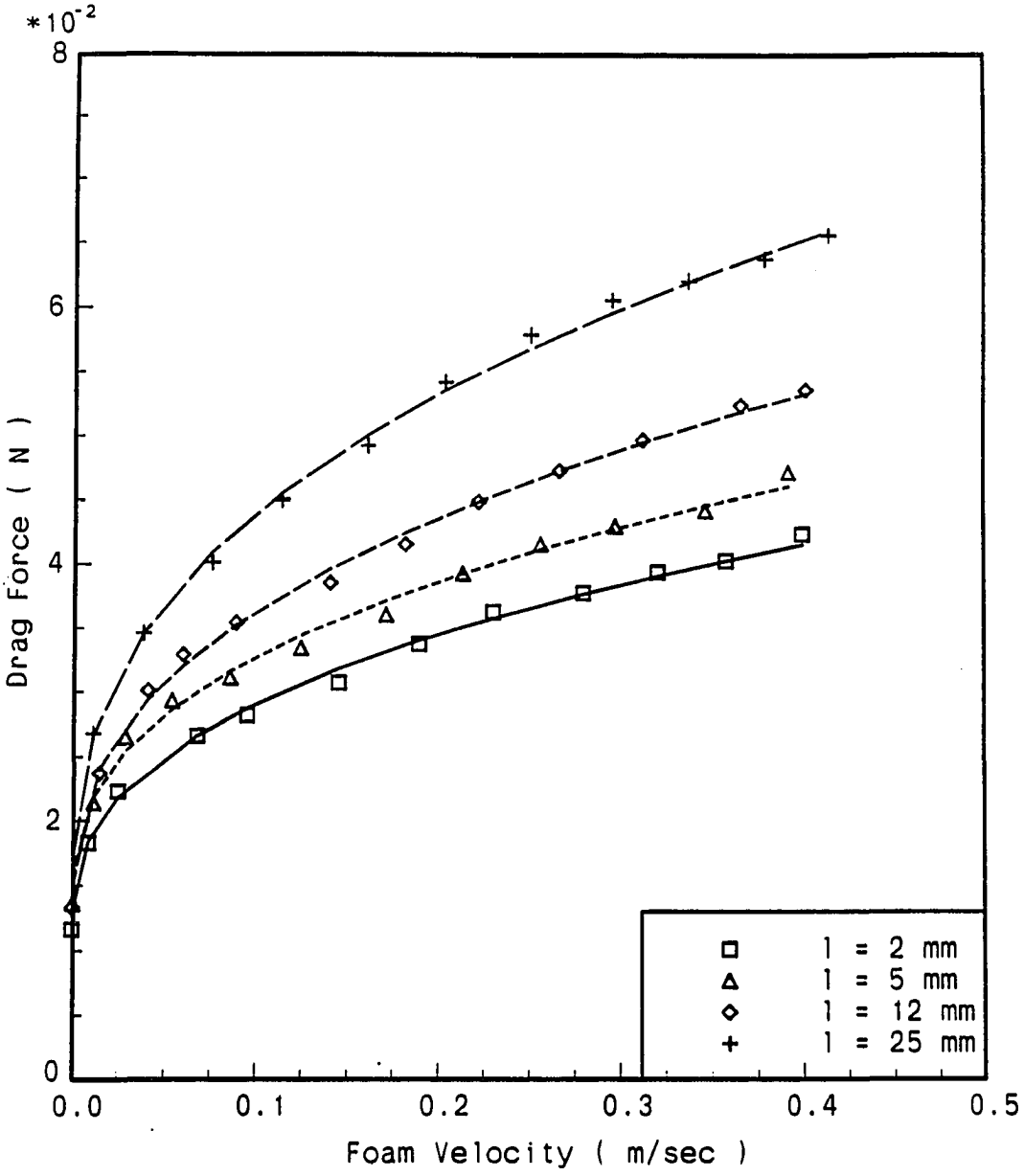

Figure 6.8: Drag force on disks for foam ID = SCFC

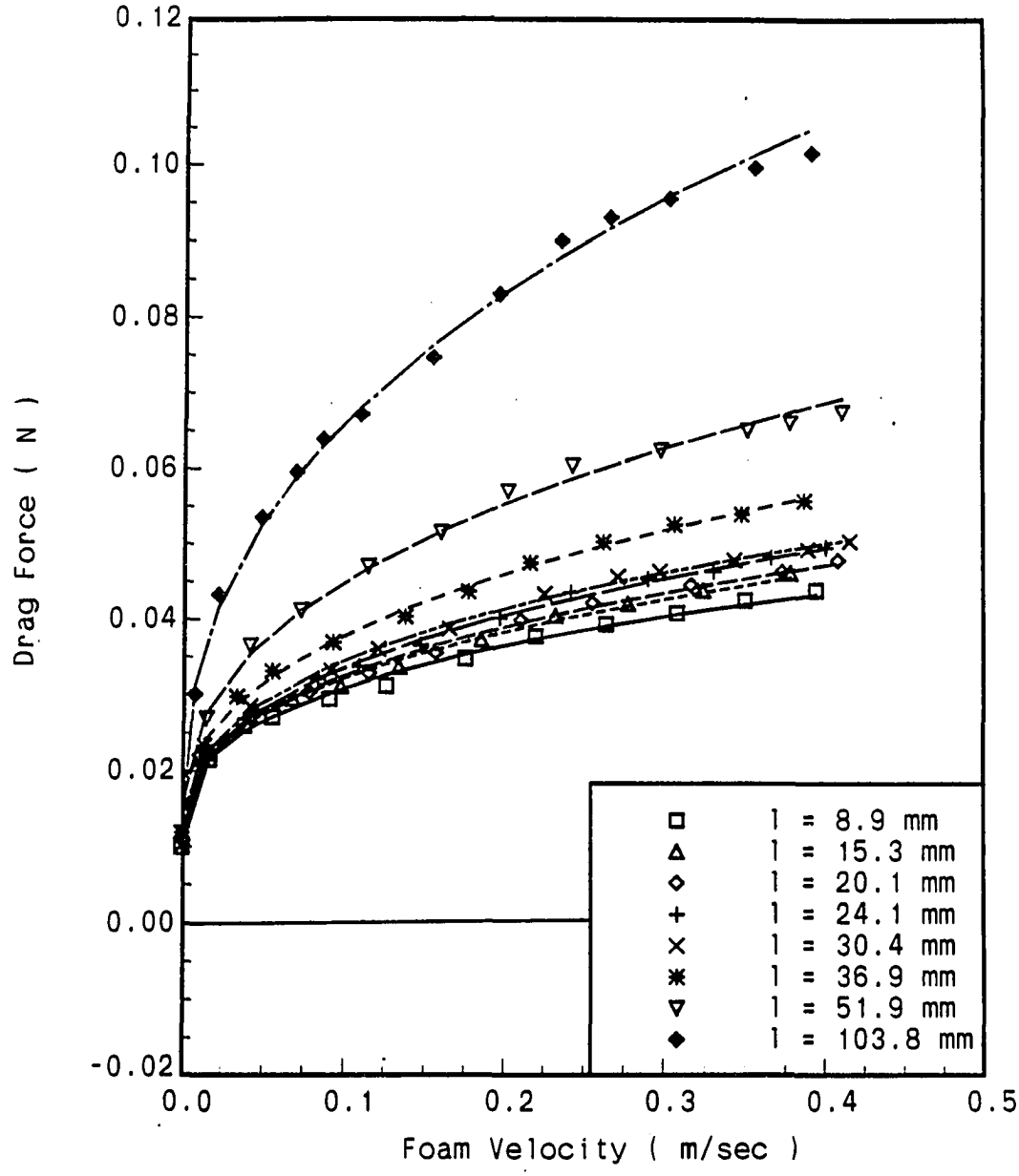

Figure 6.9: Drag force on ellipsoids for foam ID = SCFC

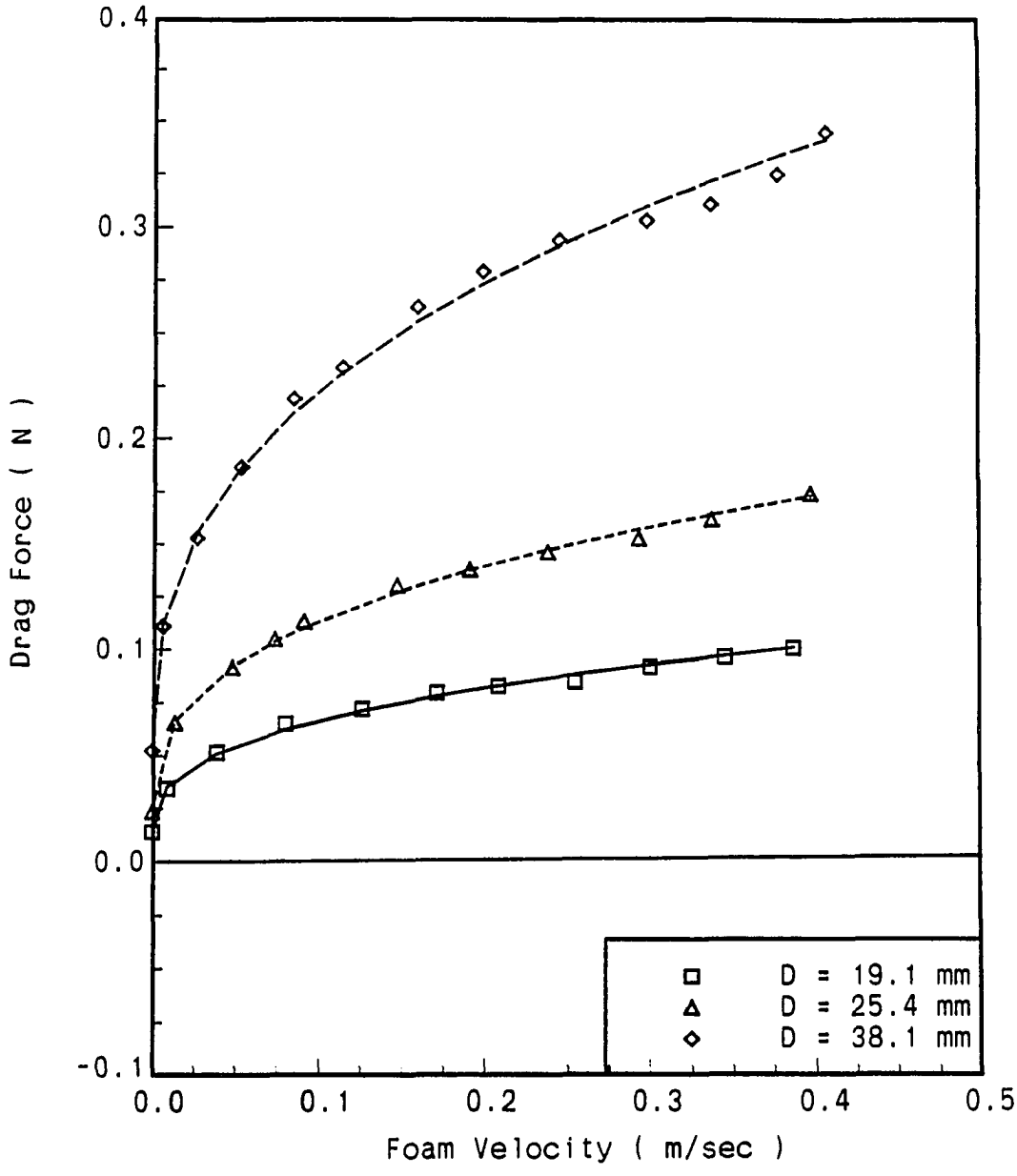

Figure 6.10: Drag force on spheres for foam ID = SCFD

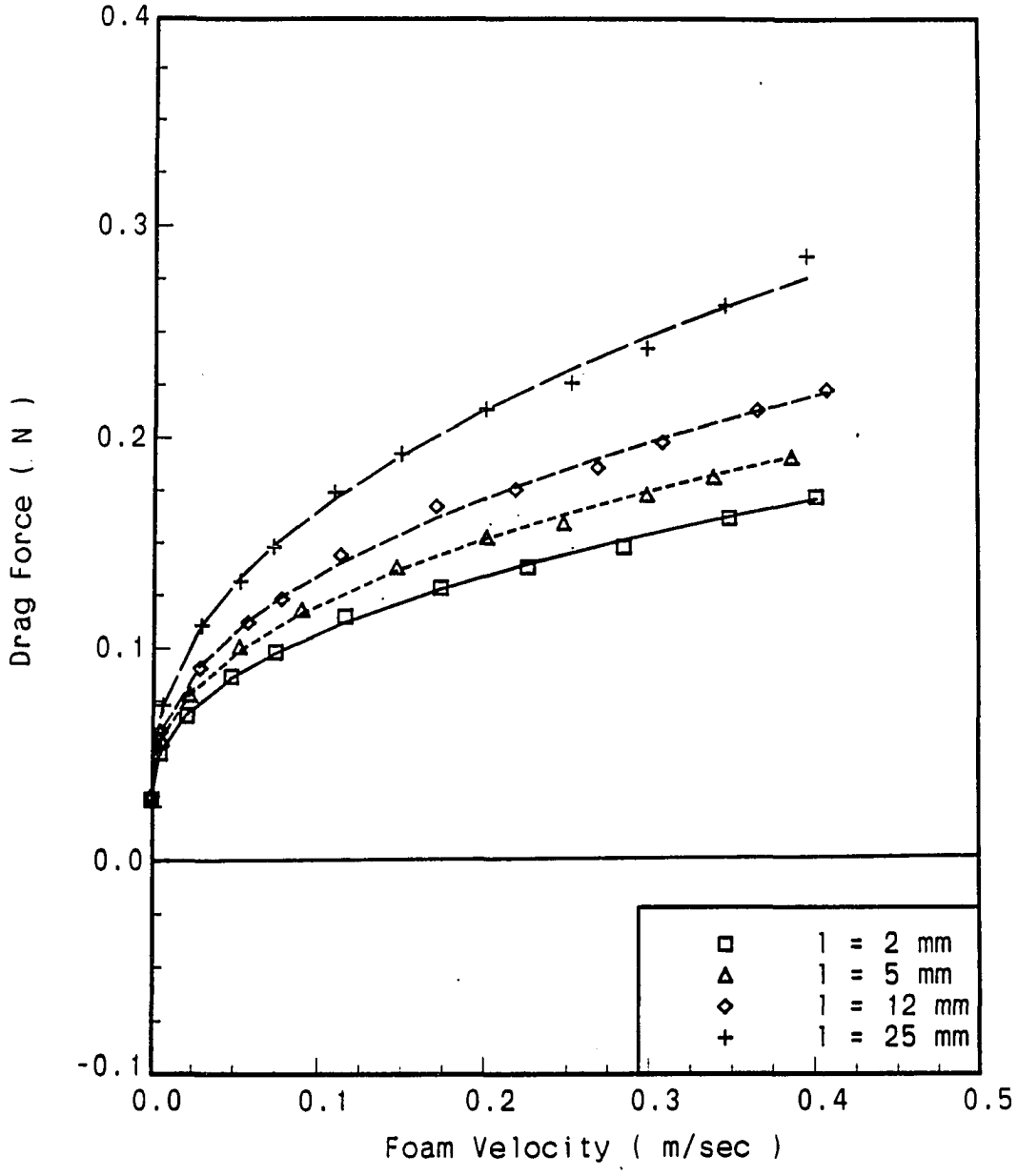

Figure 6.11: Drag force on disks for foam ID = SCFD

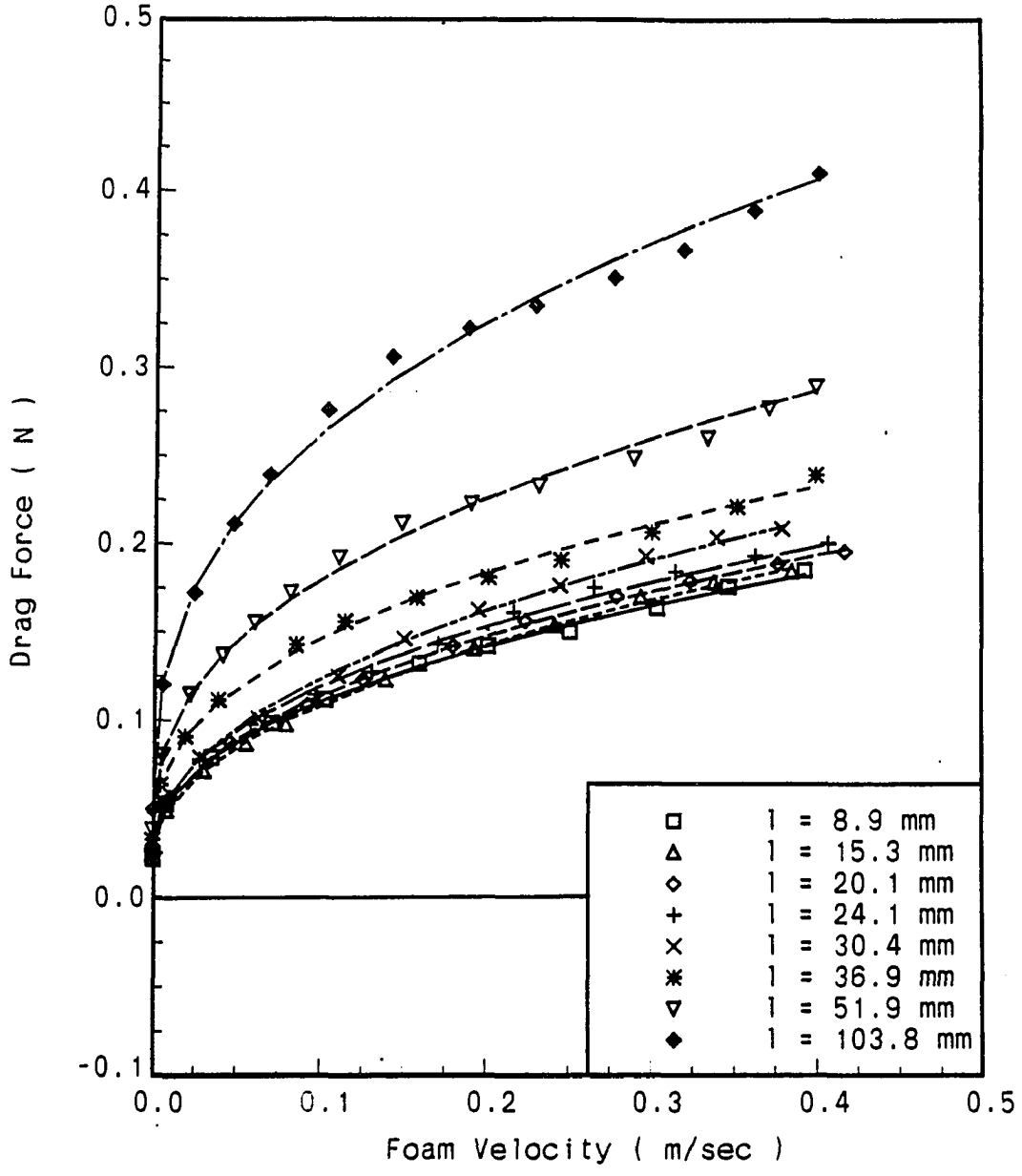

Figure 6.12: Drag force on ellipsoids for foam ID = SCFD

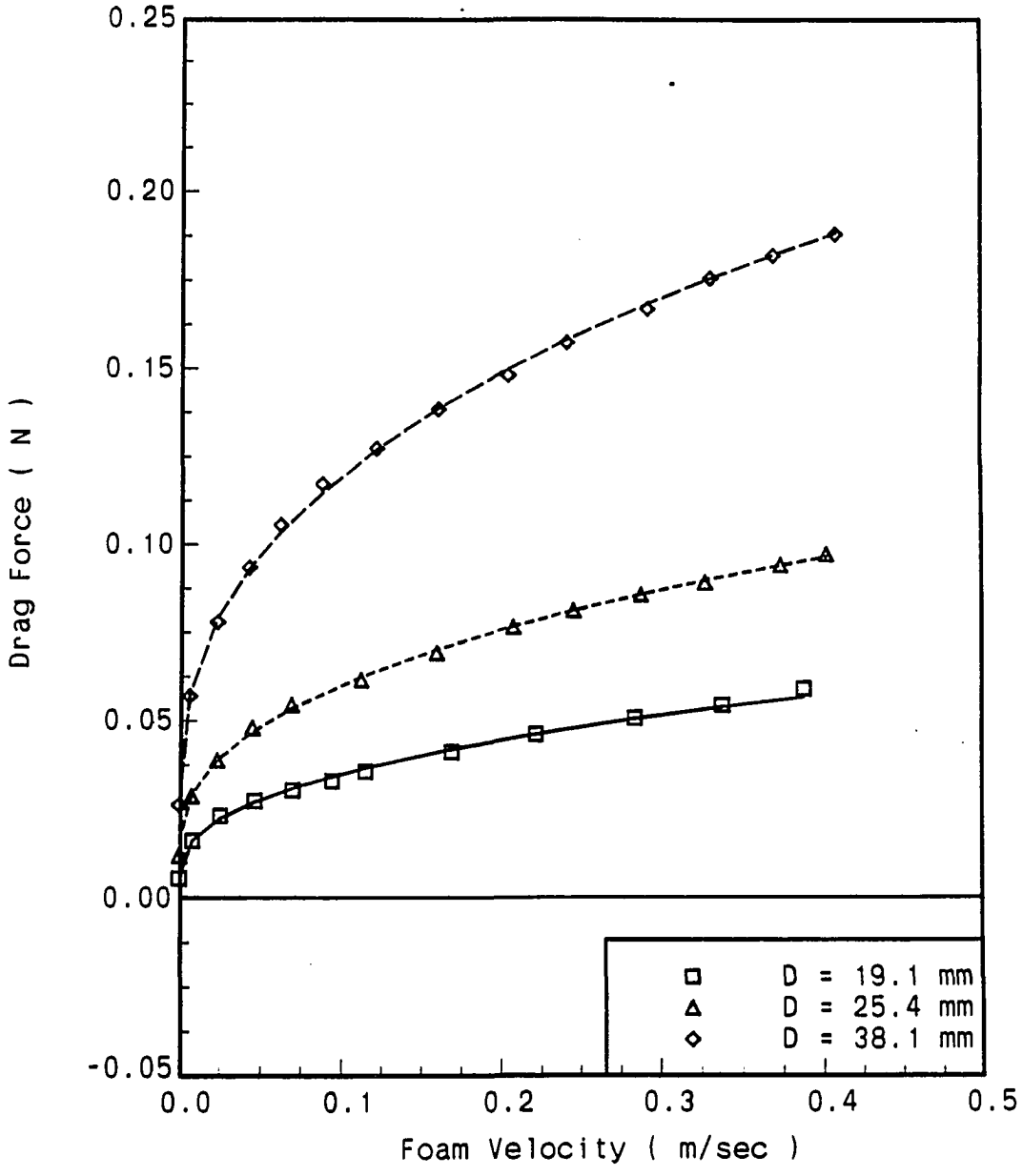

Figure 6.13: Drag force on spheres for foam ID = SCFE

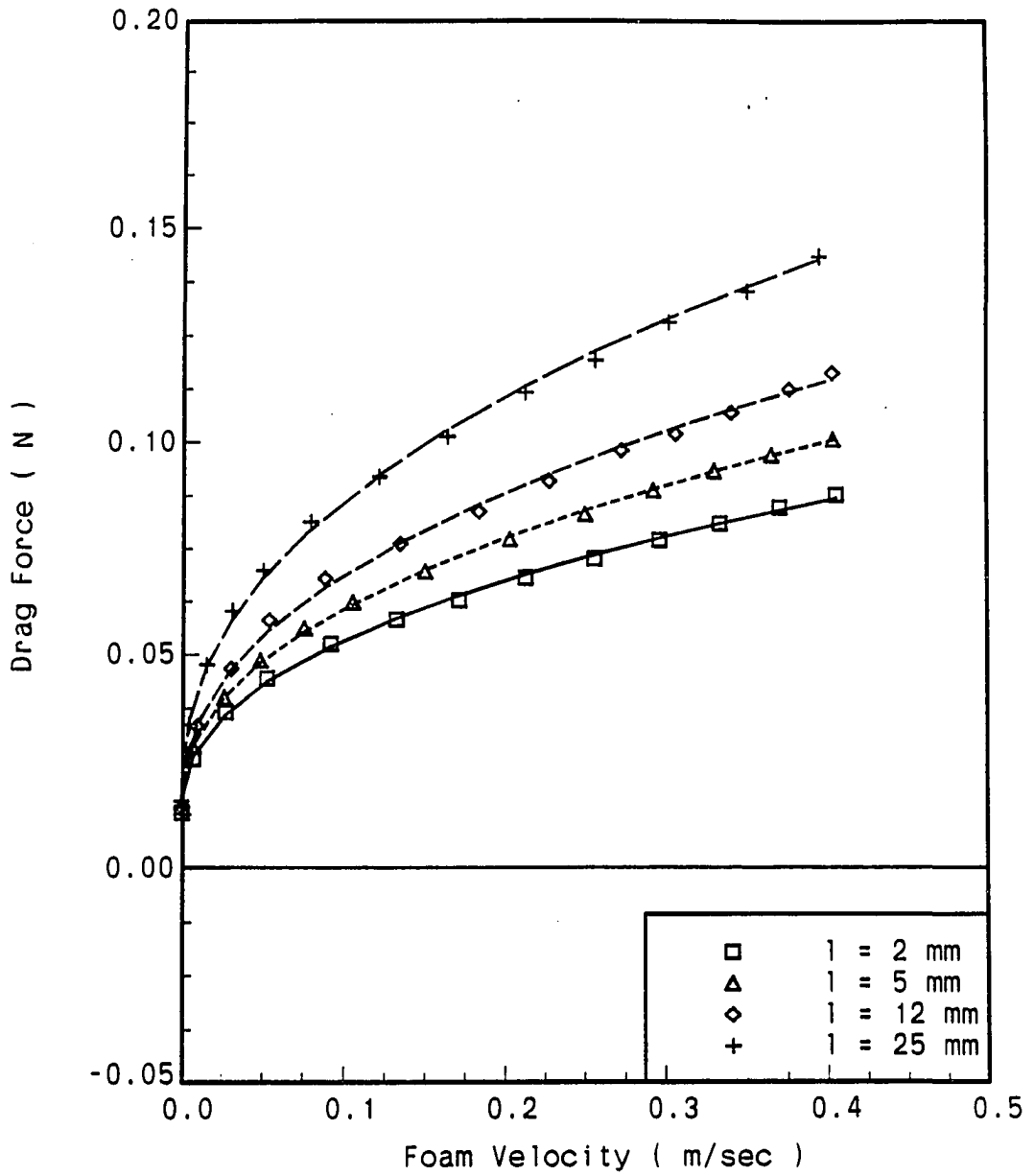

Figure 6.14: Drag force on disks for foam ID = SCFE

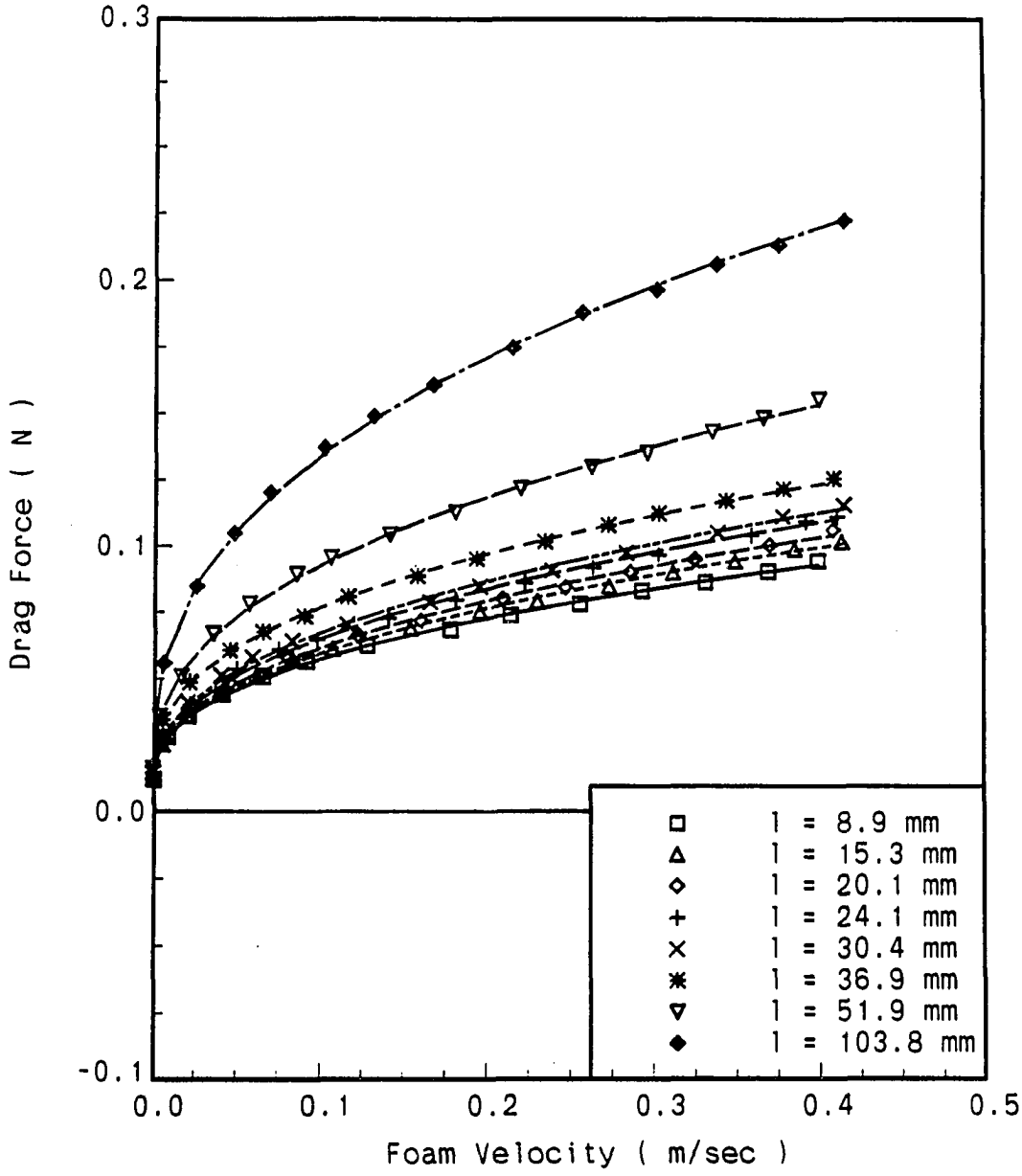

Figure 6.15: Drag force on ellipsoids for foam ID = SCFE

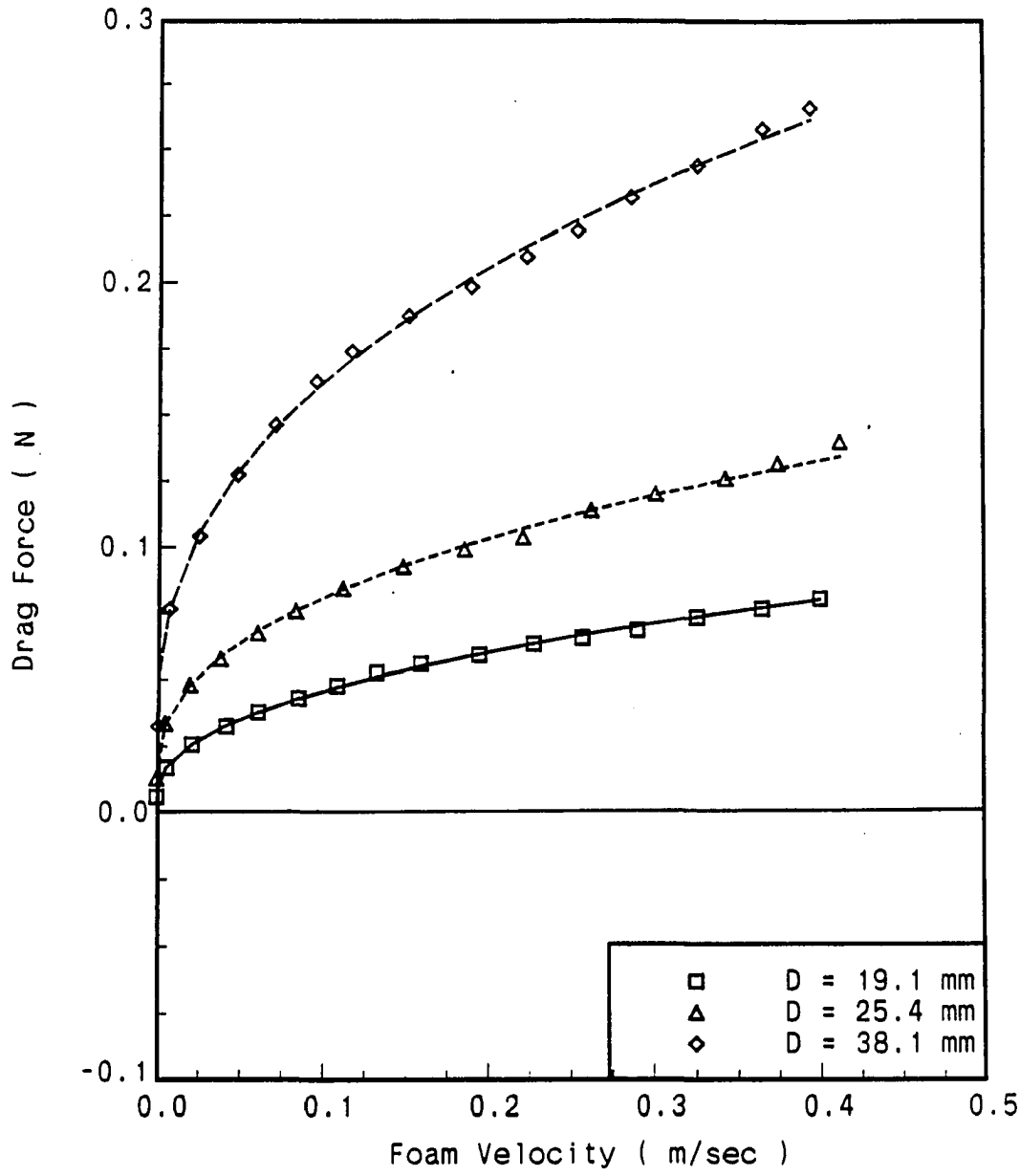

Figure 6.16: Drag force on spheres for foam ID = SCFF

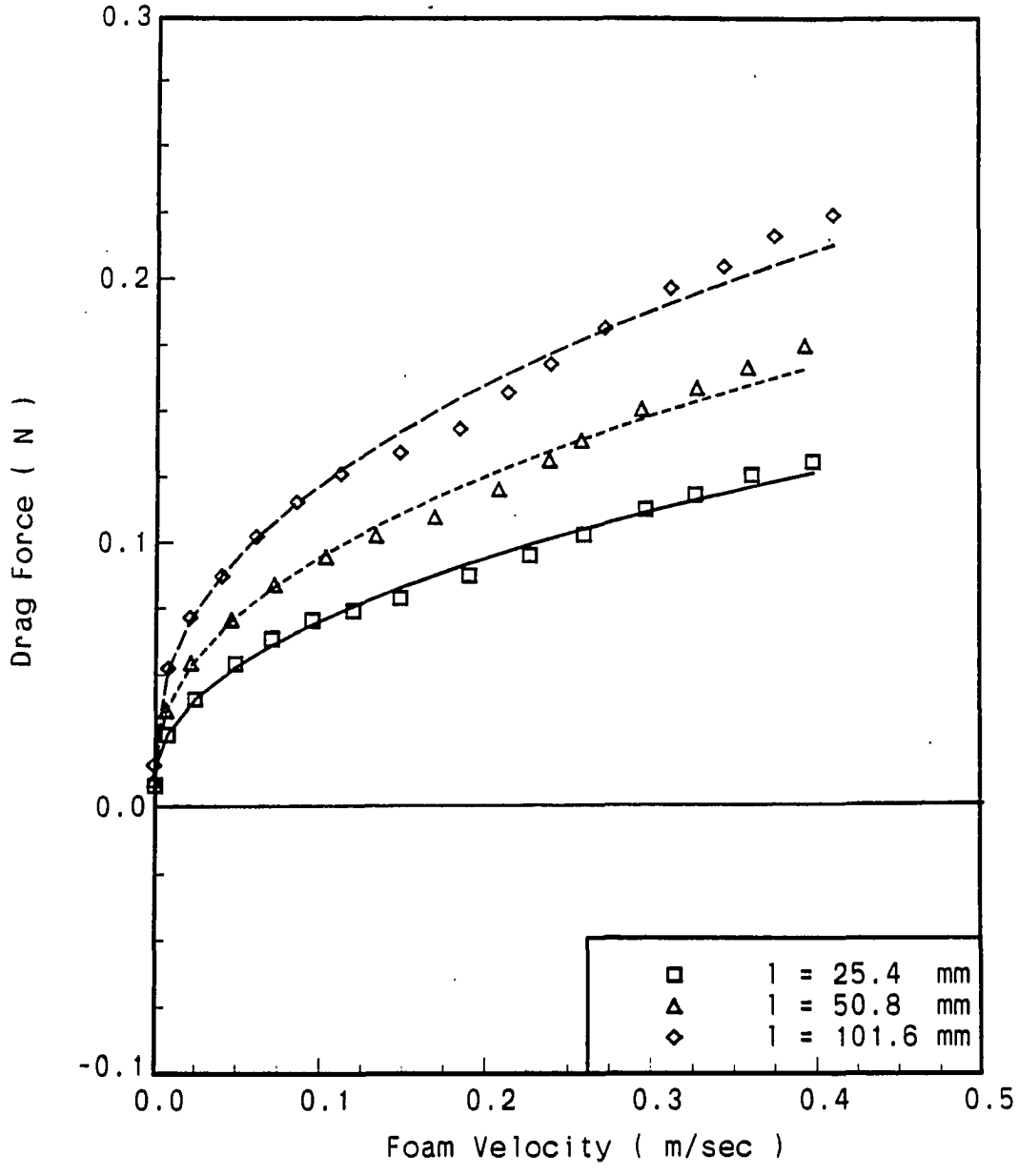

Figure 6.17: Drag force on flat plates for foam ID = SCFF

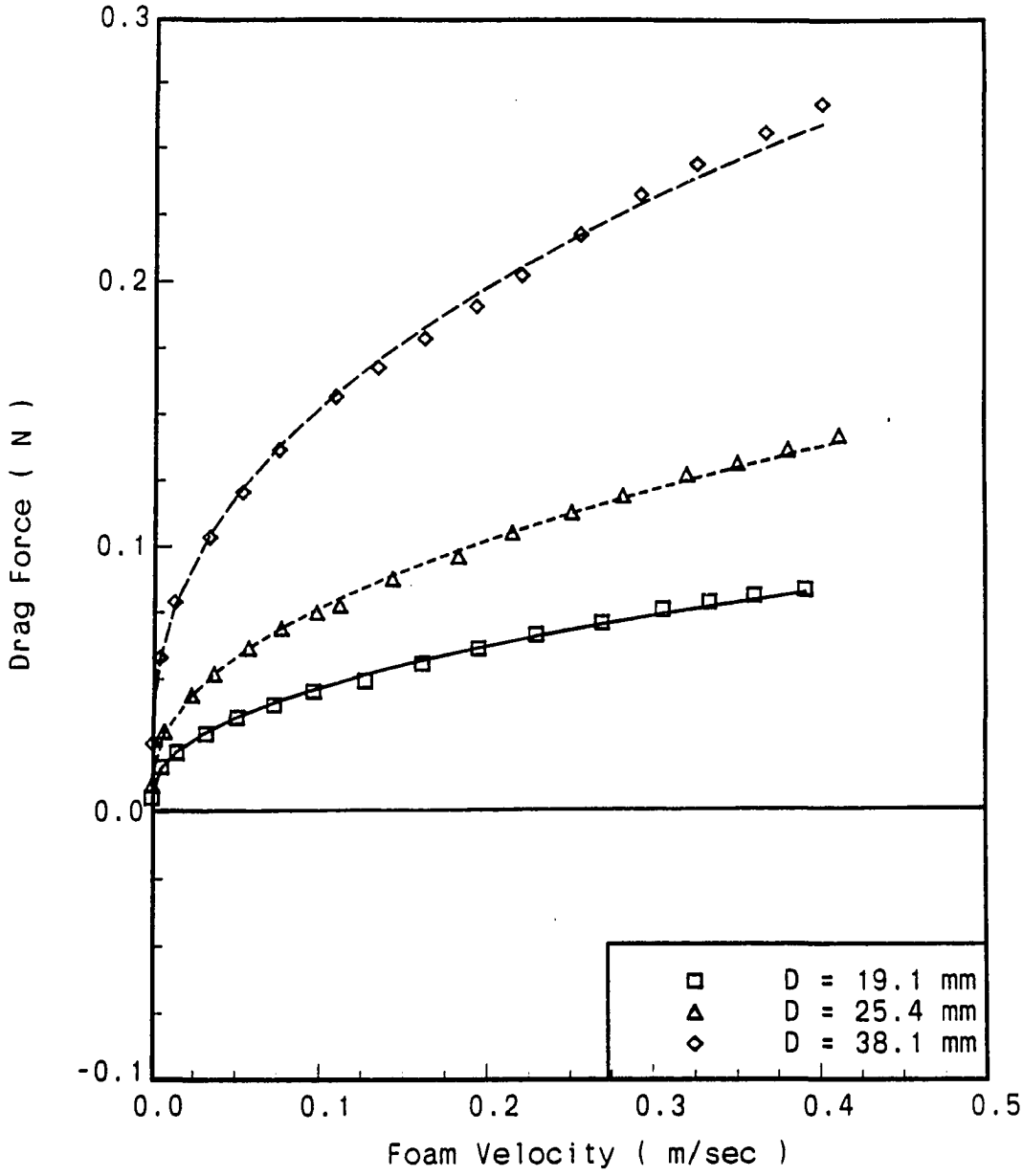

Figure 6.18: Drag force on smooth spheres for foam ID = SCFG

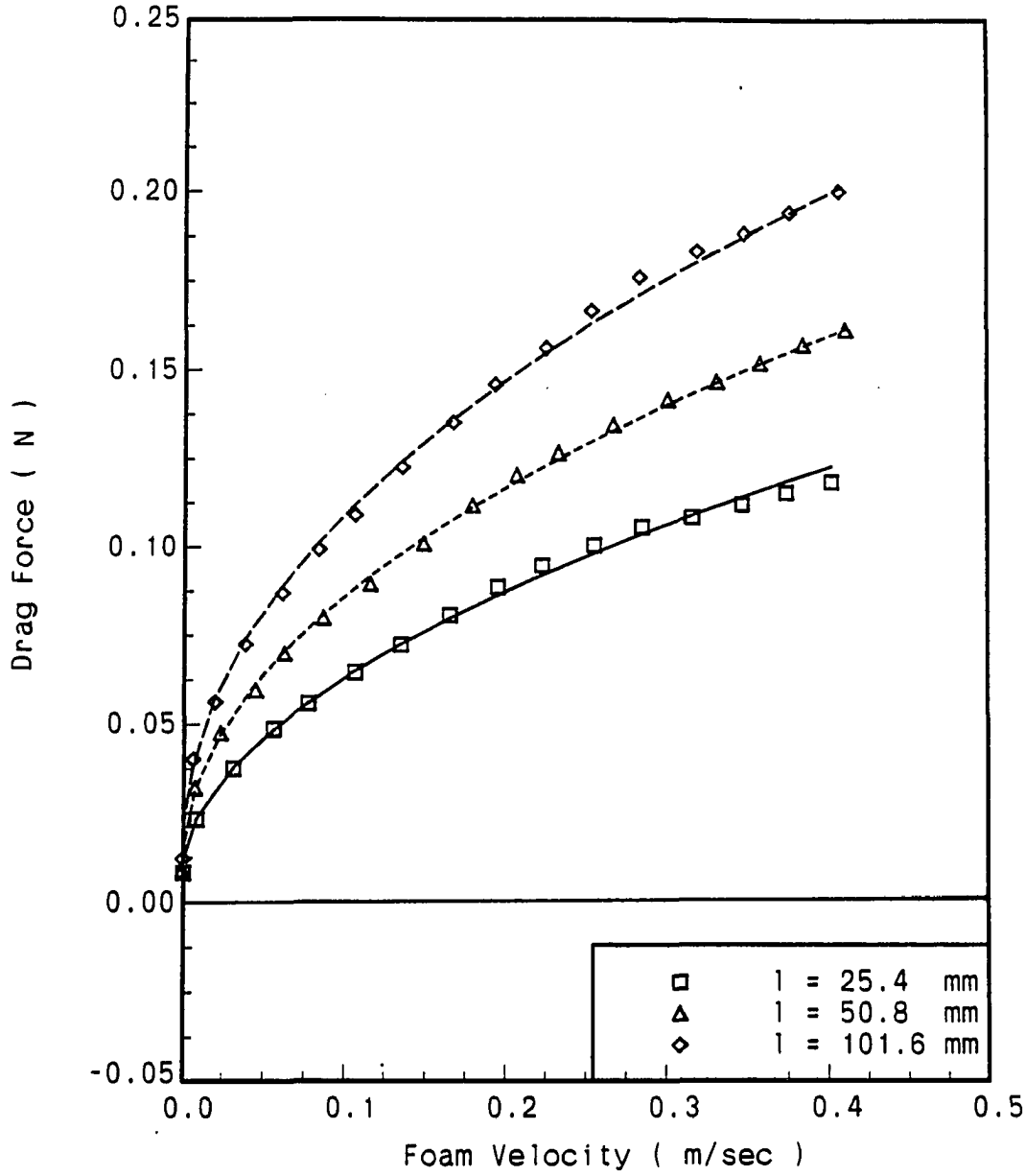

Figure 6.19: Drag force on flat plates for foam ID = SCFG

Table 6.2: Constants for the curve fit equation for foam $ID = SCFA$

Model no.	a	b	c
2	0.0427	0.3522	0.0048
3	0.0738	0.3904	0.0109
4	0.1469	0.3689	0.0210
5	0.0625	0.3582	0.0150
6	0.0719	0.3058	0.0173
7	0.0891	0.3894	0.0178
8	0.1182	0.4016	0.0182
9	0.0721	0.3572	0.0162
10	0.0804	0.3831	0.0164
11	0.0847	0.3837	0.0165
12	0.0906	0.3953	0.0165
13	0.0935	0.3879	0.0164
14	0.1052	0.3967	0.0146
15	0.1299	0.4002	0.0116
16	0.1973	0.4009	0.0122

The drag-velocity data were fit to a general equation of the power law type

$$F_D = aU^b + c \tag{6.1}$$

where a, b, and c are constants dependent upon the specimen and foam properties. With the given values of a, b, and c, the unit on F_D is in N when U is in m/sec. To fit the curve, a least squares regression analysis was applied to the data points.

Tables 6.2 through 6.8 show the tabulated coefficients after modifying for the stem effect. That is, the drag on the bare stem supporting the model was subtracted from the measured drag that was generated by both the model and the stem. Recall that the specimen size and shape are related to the model no. as given in Table 3.1 and Figure 3.5.

The results indicate Bingham plastic-type charateristics for the drag-velocity

Table 6.3: Constants for the curve fit equation for foam $ID = SCFB$

Model no.	a	b	c
2	0.0327	0.3738	0.0054
3	0.0563	0.3914	0.0104
4	0.1103	0.3889	0.0247
5	0.0510	0.3888	0.0140
6	0.0609	0.3818	0.0128
7	0.0689	0.3771	0.0139
8	0.0882	0.3728	0.0142
9	0.0551	0.3730	0.0128
10	0.0594	0.3833	0.0125
11	0.0627	0.3784	0.0115
12	0.0685	0.4047	0.0125
13	0.0705	0.3877	0.0111
14	0.0848	0.4066	0.0103
15	0.0977	0.4018	0.0121
16	0.1651	0.4336	0.0127

Table 6.4: Constants for the curve fit equation for foam $ID = SCFC$

Model no.	a	b	c
2	0.0330	0.4119	0.0046
3	0.0516	0.3841	0.0090
4	0.1066	0.4039	0.0190
5	0.0427	0.3904	0.0116
6	0.0468	0.3898	0.0136
7	0.0575	0.3997	0.0133
8	0.0738	0.3792	0.0131
9	0.0456	0.3365	0.0099
10	0.0485	0.3762	0.0118
11	0.0508	0.3708	0.0109
12	0.0545	0.3812	0.0109
13	0.0551	0.3533	0.0101
14	0.0642	0.3925	0.0118
15	0.0813	0.3897	0.0118
16	0.1357	0.3936	0.0111

Table 6.5: Constants for the curve fit equation for foam $ID = SCFD$

Model no.	a	b	c
2	0.1234	0.3716	0.0140
3	0.2090	0.3672	0.0235
4	0.4067	0.3787	0.0523
5	0.2104	0.4227	0.0284
6	0.2415	0.4251	0.0296
7	0.2807	0.4293	0.0301
8	0.3653	0.4364	0.0317
9	0.2390	0.4460	0.0251
10	0.2581	0.4732	0.0220
11	0.2585	0.4586	0.0240
12	0.2609	0.4376	0.0240
13	0.2928	0.4658	0.0236
14	0.2917	0.4094	0.0325
15	0.3624	0.4095	0.0382
16	0.5045	0.3754	0.0496

Table 6.6: Constants for the curve fit equation for foam $ID = SCFE$

Model no.	a	b	c
2	0.0752	0.4105	0.0056
3	0.1219	0.4031	0.0119
4	0.2308	0.3941	0.0262
5	0.1090	0.4326	0.0130
6	0.1288	0.4426	0.0142
7	0.1498	0.4379	0.0140
8	0.1903	0.4323	0.0157
9	0.1181	0.4170	0.0121
10	0.1306	0.4449	0.0125
11	0.1361	0.4418	0.0123
12	0.1444	0.4343	0.0118
13	0.1491	0.4349	0.0124
14	0.1571	0.4035	0.0147
15	0.2009	0.4221	0.0165
16	0.2918	0.3986	0.0173

Table 6.7: Constants for the curve equation for foam $ID = SCFF$

Model no.	a	b	c
2	0.1122	0.4512	0.0060
3	0.1747	0.4099	0.0129
4	0.3376	0.4150	0.0325
5	0.1660	0.4258	0.0135
9	0.1841	0.4087	0.0142
16	0.4223	0.4281	0.0304
17	0.1819	0.4669	0.0082
18	0.2356	0.4458	0.0102
19	0.2910	0.4380	0.0159

Table 6.8: Constants for the curve equation for foam $ID = SCFG$

Model no.	a	b	c
2	0.1192	0.4592	0.0054
3	0.1960	0.4677	0.0100
4	0.3488	0.4396	0.0258
5	0.1649	0.4444	0.0111
9	0.1847	0.4637	0.0110
16	0.4432	0.4597	0.0249
17	0.1857	0.5316	0.0083
18	0.2345	0.4842	0.0090
19	0.2903	0.4776	0.0122

relationship for various kinds of models. There is an apparent yield force (represented by the value of c) which must be reached before the specimen moves. Since it is very difficult to obtain precise measurements at very low velocities, the precise character of the drag-velocity relationship near zero velocity is not clear from the data obtained. In the lower velocity region, the drag is strongly dependent on the velocity. A slight decrease in velocity produces a large decrease in drag. This phenomenon might have happened due to the slip condition at the wall under effective yield stress of a foam. This could be explained as a strain recovery and can be seen as an elastic material that is one of foam's characteristics. When the velocity decreases to the limit where the shear stress does not exceed the foam yield stress, the deformed foam matrices suddenly release their residual stress. This strain recovery process could be possible due to the slip condition of foam at the wall.

As mentioned earlier, this limit value of shear stress is considered to be an effective (true) yield stress of foam, and the yield stress on the plot of drag at zero velocity is an apparent yield stress, whose value is lower than effective yield stress. In other words, the effective yield stress is the theoretically defined yield stress that could be measured experimentally by correcting for the slip velocity. The apparent yield stress is the experimentally measured yield stress. There is evidence [46] that the experimentally measured yield stress is lower than the true foam field yield stress.

In any case, the data, when plotted over the velocity range indicated, show that the existence of yield force and shear thinning characteristics represent a reasonable approximation of the observed characteristics. The fact that the parameter b is less than one for each case indicates a shear thinning characteristic. An increase in size of the sphere produces a corresponding increase in drag force (e.g., Figure 6.1), with

Table 6.9: The drag force on different sizes of spheres and the drag force ratios for foam $ID = SCFC$ and SCFD

Foam ID	Foam vel. (m/sec)	Drag force (N)			Drag ratio	
		F_{D_1}	F_{D_2}	F_{D_3}	F_{D_2}/F_{D_1}	F_{D_3}/F_{D_1}
SCFC	0.1	0.0174	0.0303	0.0611	1.74	3.51
	0.2	0.0216	0.0368	0.0746	1.70	3.43
	0.3	0.0247	0.0415	0.0845	1.68	3.42
SCFD	0.1	0.066	0.113	0.222	1.71	3.36
	0.2	0.082	0.139	0.273	1.70	3.33
	0.3	0.093	0.158	0.310	1.70	3.33

similar velocity dependence.

Figures 6.20 and 6.21 show the relationship on drag force versus sphere diameter. In the case with foam $ID = SCFC$ (see Table 6.1 for correspond foam properties), the drag for sphere of diameter $D_1 = 19.1mm$ is 0.0174 N at foam velocity 0.1 m/sec. Similarly, the drag for diameter $D_2 = 25.4mm$ and $D_3 = 38.1mm$ spheres are 0.0303 N and 0.0611 N, respectively, at foam velocity 0.1 m/sec. Table 6.9 shows the tabulated calculated results and drag force ratios between different sizes of spheres.

As can be seen in Table 6.9, the ratios of the drag force at a constant speed for the different diameters, F_{D_2}/F_{D_1} and F_{D_3}/F_{D_1}, are approximately constant. It is recalled that for Stoke's flow of a Newtonian fluid past a sphere the drag is proportional to the sphere diameter. Hence if foam were a Newtonian fluid the drag ratios would be $F_{D_2}/F_{D_1} = D_2/D_1 = 25.4/19.1 = 1.33$ and $F_{D_3}/F_{D_1} = D_3/D_1 = 38.1/19.1 = 2.0$ rather than the actual value given in Table 6.9.

In the sense that under constant agitation the bubble diameter is specified as a unique function of the given liquid viscosity and the foam quality, and the bubble

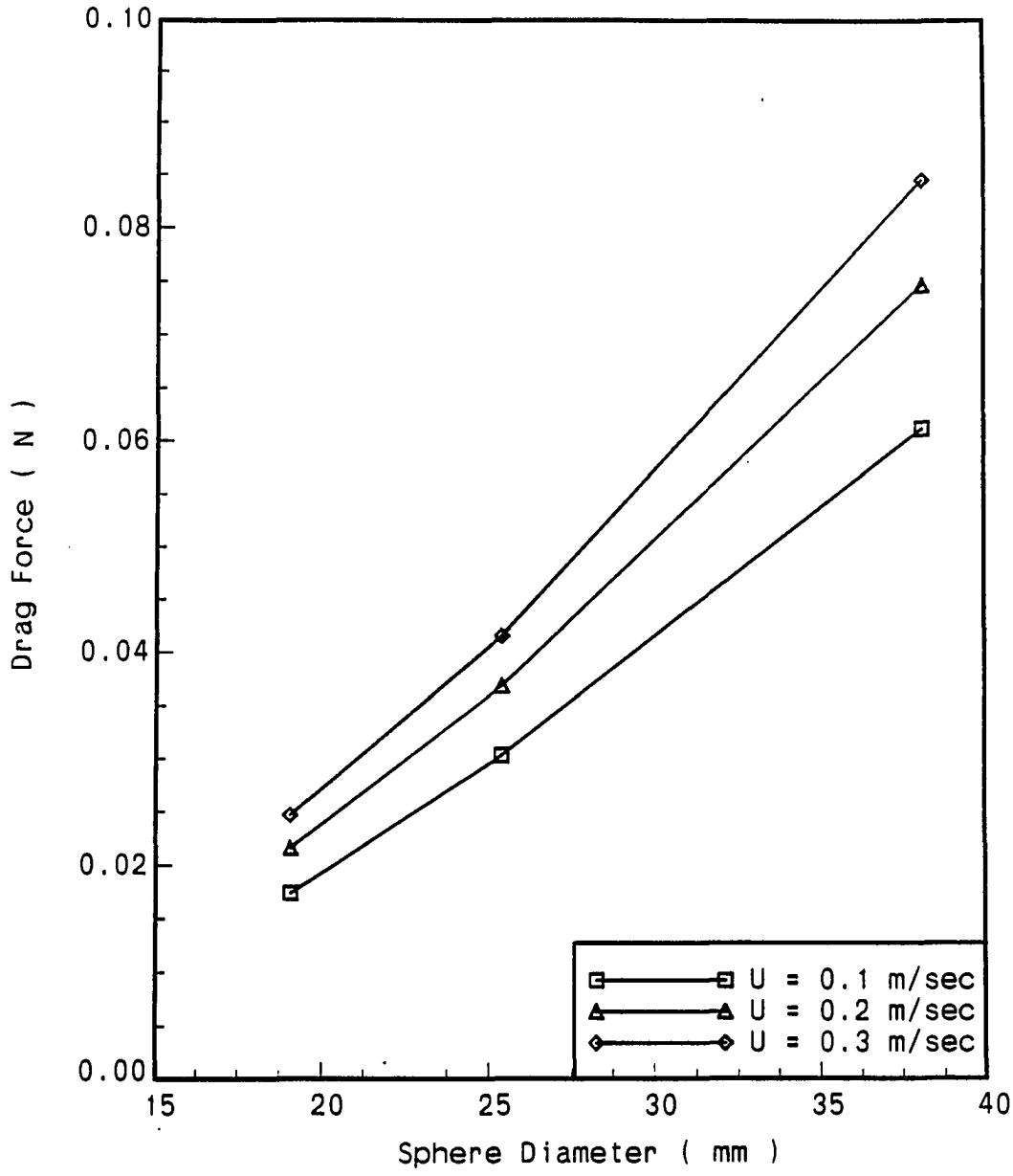

Figure 6.20: Drag force as a function of sphere diameter on foam ID = SCFC

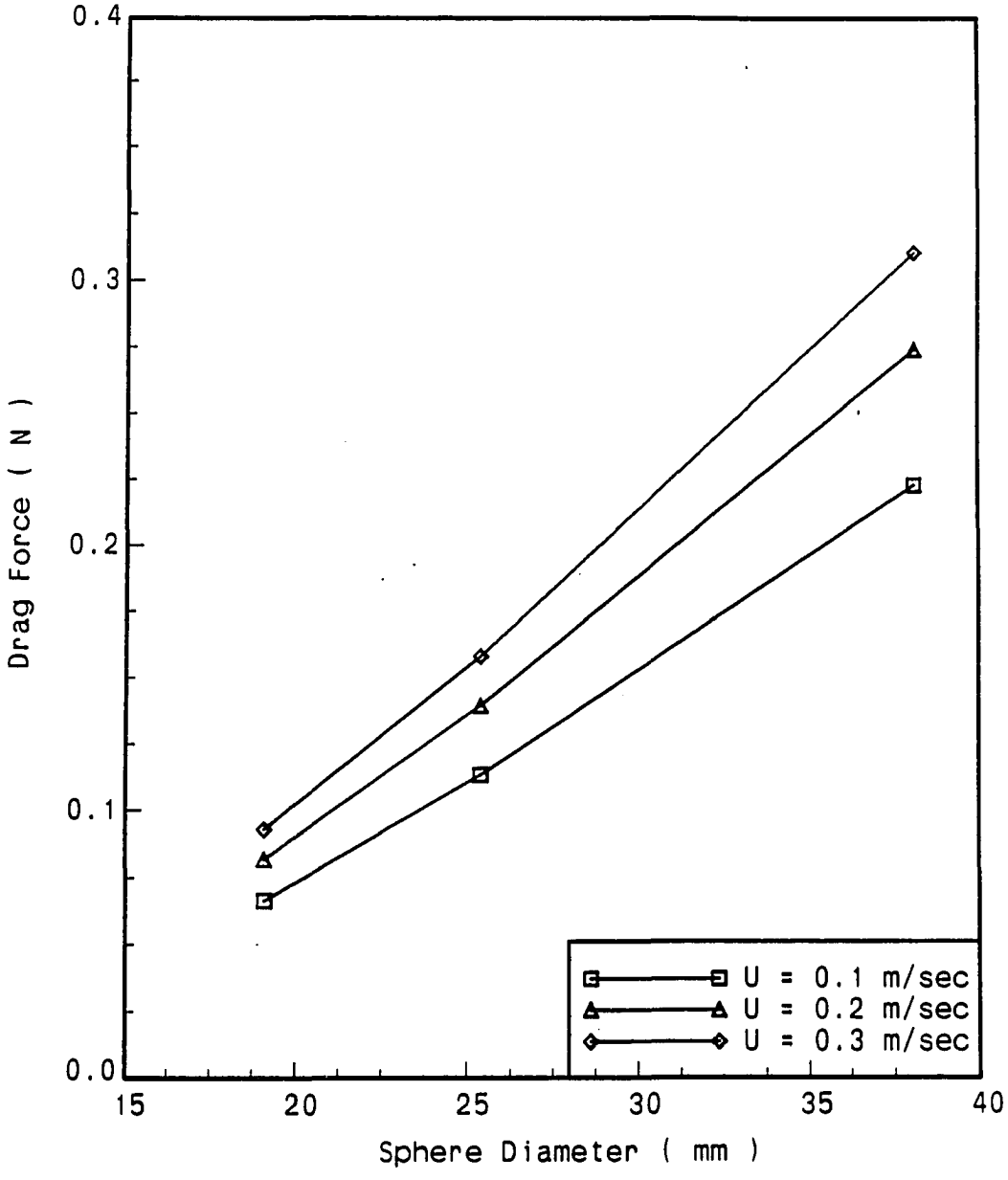

Figure 6.21: Drag force as a function of sphere diameter on foam ID = SCFD

diameter is taken to be an implicit function of the liquid viscosity and the foam quality at steady-state. It should be emphasized here once again that, in general, the effect of bubble diameter must be investigated. Since the actual measurement of average bubble diameter is not easy in a dynamic situation, development of another parametric method is desirable. We considered the foam drainage rate as an index of bubble size. Some thoughtful suggestions with our attempt regarding the foam decaying rate follow in Section 6.2.

Under the assumption that the surface tension and average bubble size are implicit functions of liquid viscosity and foam quality for our case, the drag force is now a function of liquid viscosity and quality. The dependence of the drag force on the viscosity and quality are shown in Figure 6.22 for the 38.1-mm diameter sphere at a velocity of 0.3 m/s. The results of the two types of experiments are represented on this three-dimensional graph. The solid dots are the results of the experiments run for arbitrary combinations of viscosity and the foam quality. The triangles and pluses are the results of experiments performed at different qualities, but with constant viscosities of 12.9×10^{-3} and $4.68 \times 10^{-3} Ns/m^2$, respectively. By observing the drag force-quality plane, we can notice that the data sets are consistent in giving drag a unique function of quality and viscosity, and form a surface in three-dimensional space.

As shown in Figure 6.22, the drag force increases with increasing viscosity or increasing quality. When viewed from the microscale on the order of the size of the foam bubbles, it is clear that the viscosity of the liquid making up the films between bubbles should play a role in the drag force [14]. The larger the viscosity, the larger the drag force. Similarly, as the quality is increased, the average liquid film thickness

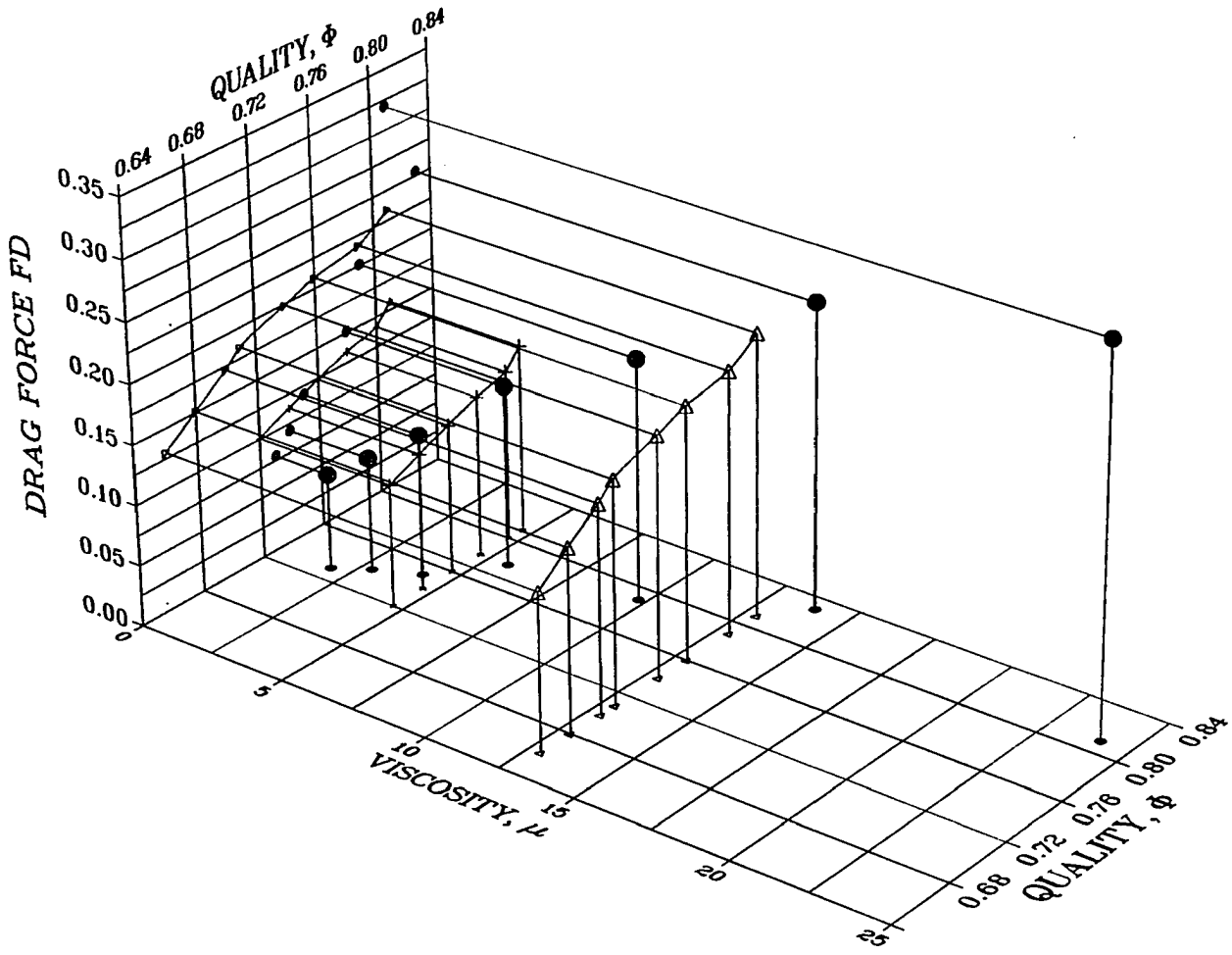

Figure 6.22: Relationship for drag force–viscosity–quality for 38.1 mm sphere at foam velocity 0.3 m/sec

is decreased and the shear force is increased. That is, for a given velocity difference across the liquid film, drier foams (high quality foam) have a larger velocity gradient, and therefore a larger viscous stress.

Figure 6.23 shows the projection of drag force at the constant viscosity onto the drag force–quality plane. The general curvature of the data points show that the power function relationship between drag force and foam quality. However for each viscosity, the drag data at the largest quality do not appear to lie precisely in line with the remaining data. Although inaccurate data could explain this discrepancy, it is considered that the data are correct since the same phenomena occur for the two different sets of data at approximately same foam quality. Hence, the following concept may explain this unexpected behavior.

From an idealized two dimensional model analysis, the value of the quality for the case of foam where the circular bubbles just touch each other without deformation is 0.9069. This is shown in Figure 6.24. Similarly, the approximate value of ϕ that is of interest for the theorist in the 3-dimensional case is $\phi = 0.7405$. For convenience, the term "high quality foam" can be used to refer the foam quality in the range $0.7405 \leq \phi \leq 1$. In high quality foam, the capillary number, Ca (see Section 2.1), has significant meaning, since the surface dominating factors, such as the surface tension and bubble diameter, are important in bubble interactions.

Consider the fact that an ideally monodisperse system is expected to already develop a finite yield stress at $\phi = 0.6046$, which is the volume fraction beyond the layers of closely packed spheres which can no longer slip past each other, i.e., when these layers are stacked at a repeating distance of less than their diameters, as can be seen in Figure 6.25. Thus, there may be a transition region where the

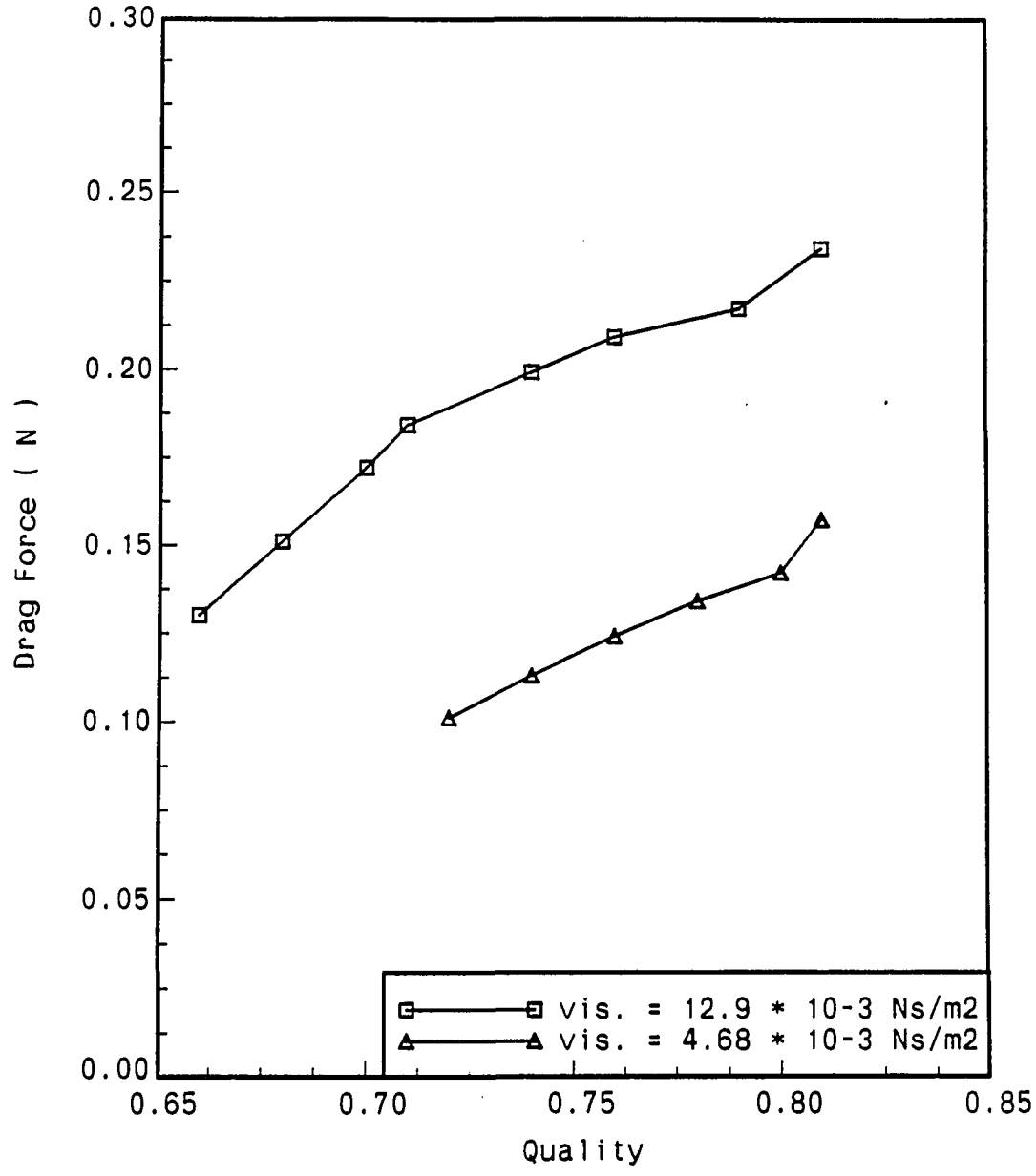

Figure 6.23: Relationship for drag force-quality for 38.1 mm diameter sphere at foam velocity 0.3 m/sec

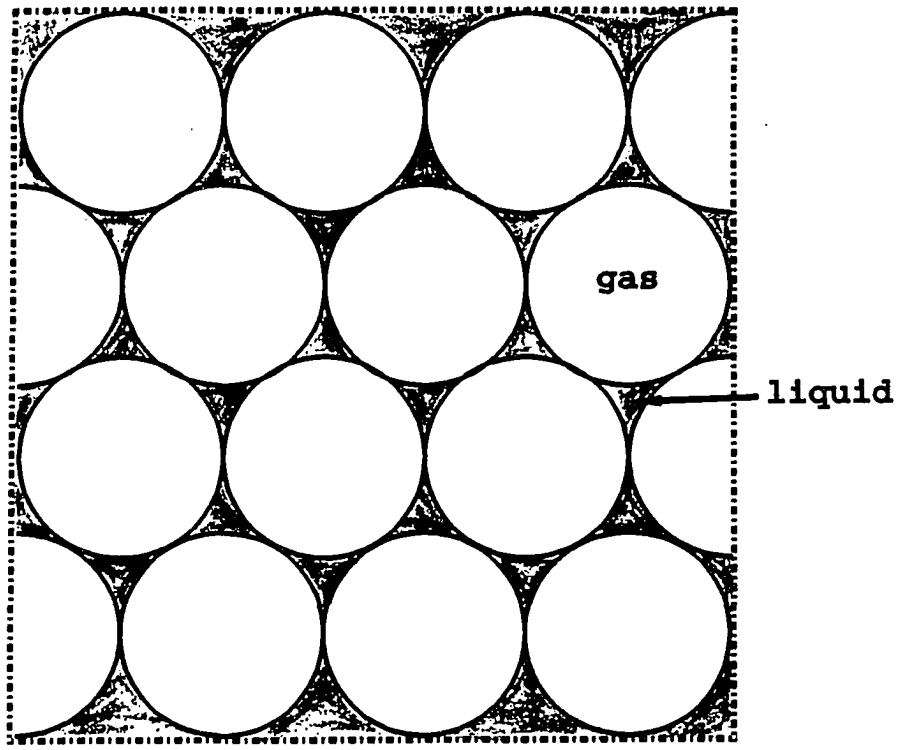

Figure 6.24: The sketch of two-dimensional ideal foam when ϕ=0.9069

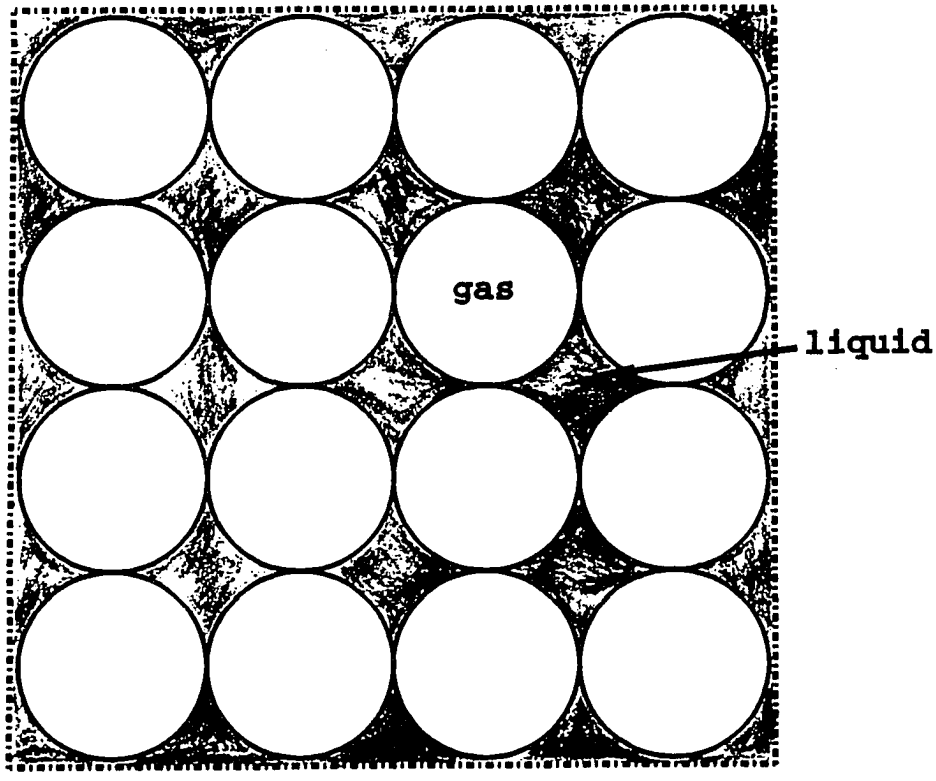

Figure 6.25: The sketch of monodisperse foam when the closely packed spheres just slip past each other

bubble collisions and/or interferences no longer exist. In this ideal case, the bubble interaction relations between the drag and surface functions become less important. In the case of an actual (i.e., not monodispersed) foam, however, the quality limit of this functional transition is uncertain due to the random distribution of bubbles. The largest ϕ data points of Figure 6.38 may be just the beginning of such a functional transition.

6.1.2. Shape dependency

Figures 6.26 and 6.27 show the shape dependency of drag force on flat plates parallel to the flow. By observation, the drag force increases almost linearly with the length of flat plate at a given velocity. Under careful examination, however, a slight slope increase with the increasing plate length can be found. If we calculate the wall shear stress for 50.8 mm-long flat plate in foam type $ID = SCFF$ at a foam velocity 0.3 m/sec, we obtain

$$\tau_A \Big| U=0.3 = \frac{F_D}{2A}\Big|_{U=0.3} = 43.37\ N/m^2 \tag{6.2}$$

where A is the area of one side of the flat plate. The results following the same calculation for foams $ID = SCFF$ and SCFG are shown in Table 6.10.

As can be seen in Table 6.10, the shorter the plate, the higher the wall shear stress. This result indicates the possibility of the boundary layer growing along the plate. However, the theoretical concept of the boundary layer has not been introduced into foam rheology. Indeed the usual concept of boundary layer flow in which inertia effects are dominant is probably not correct for this flow. Because of the relatively small density (foam is mostly air, $\phi \simeq 1$) and large viscosity, foam flow was observed to be more nearly like Stoke's flow (negligible inertia) than like a boundary layer flow.

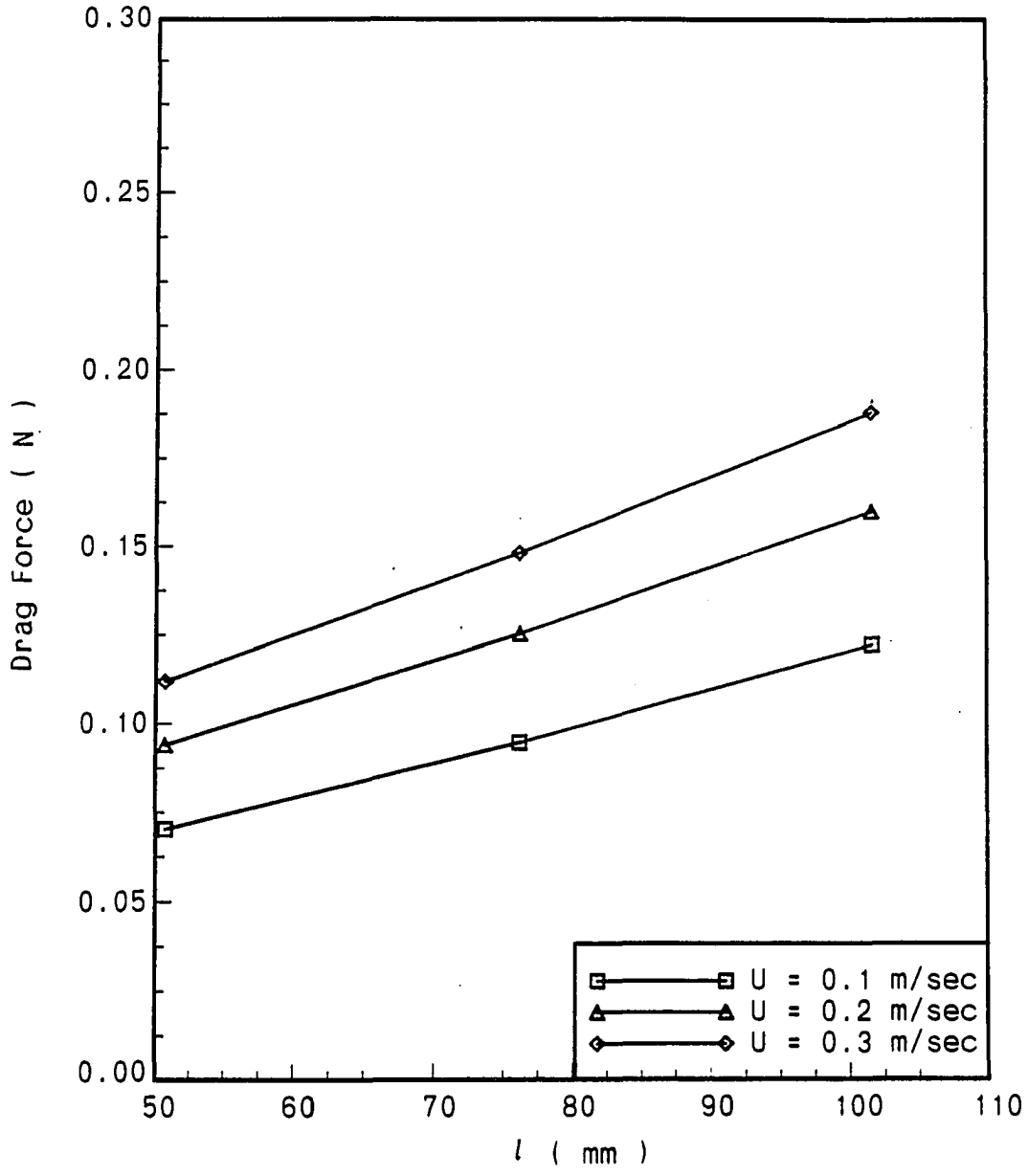

Figure 6.26: Shape dependency of drag force on flat plate for foam ID = SCFF

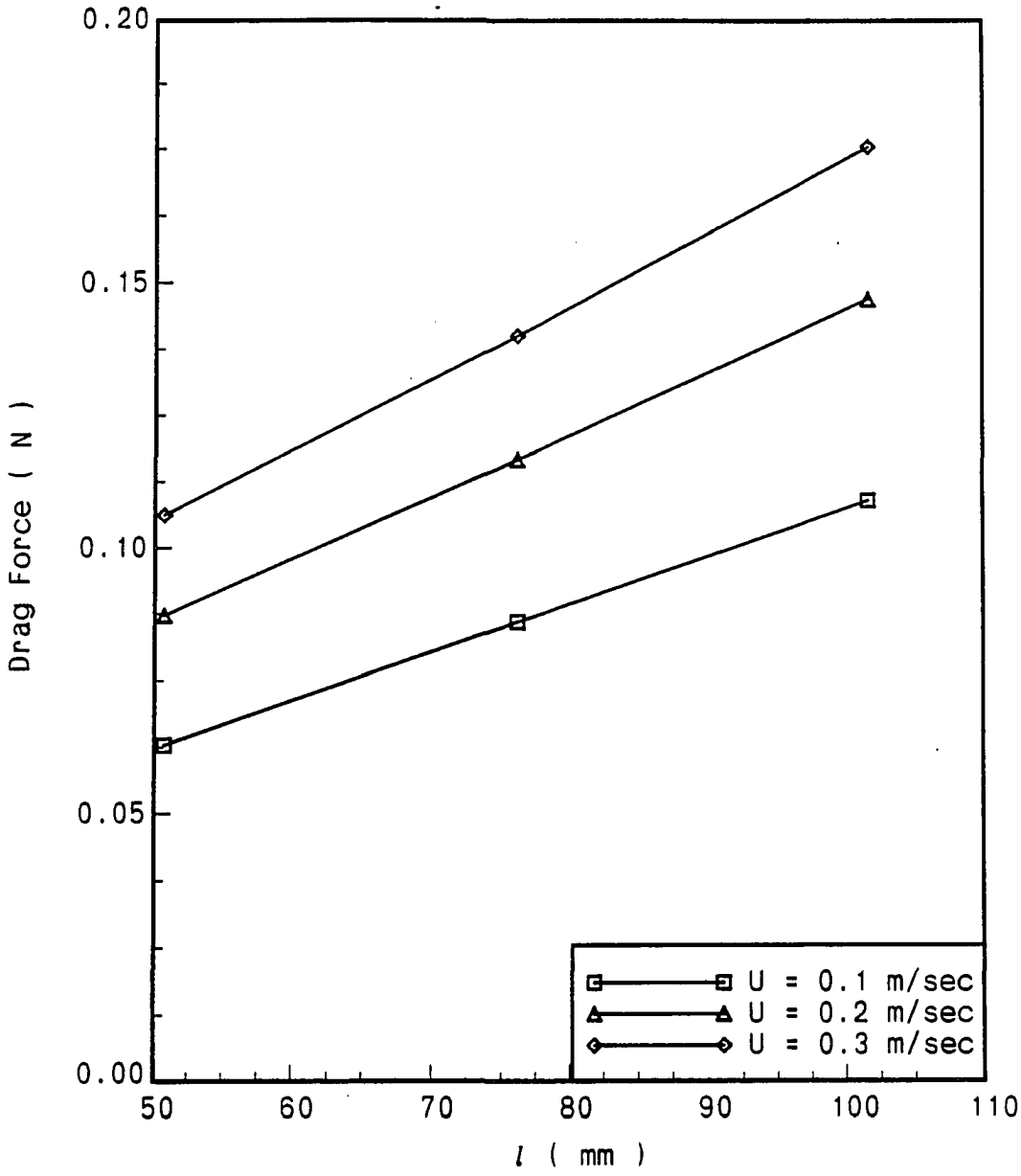

Figure 6.27: Shape dependency of drag force on flat plate for foam ID = SCFG

Table 6.10: The wall shear stress on flat plates for foam $ID = SCFF$ and SCFG at foam velocity U = 0.3 $m/sec.$ (plate length, l, is in mm, F_D is in N, and τ is in N/m^2)

Foam ID		l_1=50.8	l_2=76.2	l_3=101.6	τ_{A1}/τ_{A2}	τ_{A1}/τ_{A3}
SCFF	F_D	1.12	1.479	1.88		
	τ_A	43.37	38.22	36.43	1.05	1.19
SCFG	F_D	1.062	1.399	1.756		
	τ_A	41.16	36.15	34.02	1.06	1.21

That is, once the driving force was stopped (i.e., stop the rotation of the tank), the foam would essentially stop immediately.

Another interesting observation in Figures 6.26 and 6.27 is the slope increase with velocity increase. For example, the relative slope of the case of foam velocity U = 0.3 m/sec is higher than the other cases with smaller foam velocities. No immediate explanation is available for this curious finding.

The shape dependency of drag on disks was similar to the flat plate case (Figures 6.28 and 6.29). Since the disks have the same diameter for oncoming flow, most of the drag differences were assumed to have been produced by the shear forces on the side wall.

Figures 6.30 and 6.31 show the shape effect for different aspect ratios of ellipsoids. As expected, the drag for ellipsoids as l/D approaches zero is the same as the drag for disks when l/D approaches zero. In the case of foam $ID = SCFD$ (Figure 6.30), drag approaches 0.11 N when l/D approaches zero. This is the comparable case of the disks as l/D approaches zero, which shows about the same value in foam $ID = SCFD$ in Figure 6.29. With increasing l/D, the viscous force might become more significant, and therefore the shape of slope becomes similar to that of a flat

plate.

The plot of drag ratio (drag on ellipsoids/drag on sphere) as a function of foam velocity is shown in Figure 6.32. In general observation, the drag ratios are about constant. This result is comparable with low Reynolds number flow in Newtonian fluid case [23].

6.2. Drainage Rate

The drainage rate concept introduced in Section 3.2.1 has been used as an index for determining foam stability by chemists. Bikerman [4] pointed out, however, that stability depends more on the foam rupture process, which differs from the drainage process. Therefore, the significant relationship between the rate of drainage and the rate of foam collapse has not been found.

We propose that the drainage rate would depend on the liquid viscosity (i.e., the viscosity of the liquid portion of the foam), the foam quality, and the average bubble size. If the liquid viscosity and foam quality remain the same, the drainage rate will be a function of the average bubble size, assuming the validity of our hypothesis.

There are two independent mechanisms which contribute to the liquid cumulation in the lower chamber of the drainage rate device (see Figure 3.4). One is the rupture of bubbles and the other is drainage due to gravity. Bubble ruptures are closely related to foam stability. Therefore, one additional assumption might be needed for the drainage rate to be an index of bubble size: the foam should be stable so the liquid cumulation is mostly contributed by the drainage process. During the test, the foamy liquid used in our experiment was very stable, and few ruptures were observed.

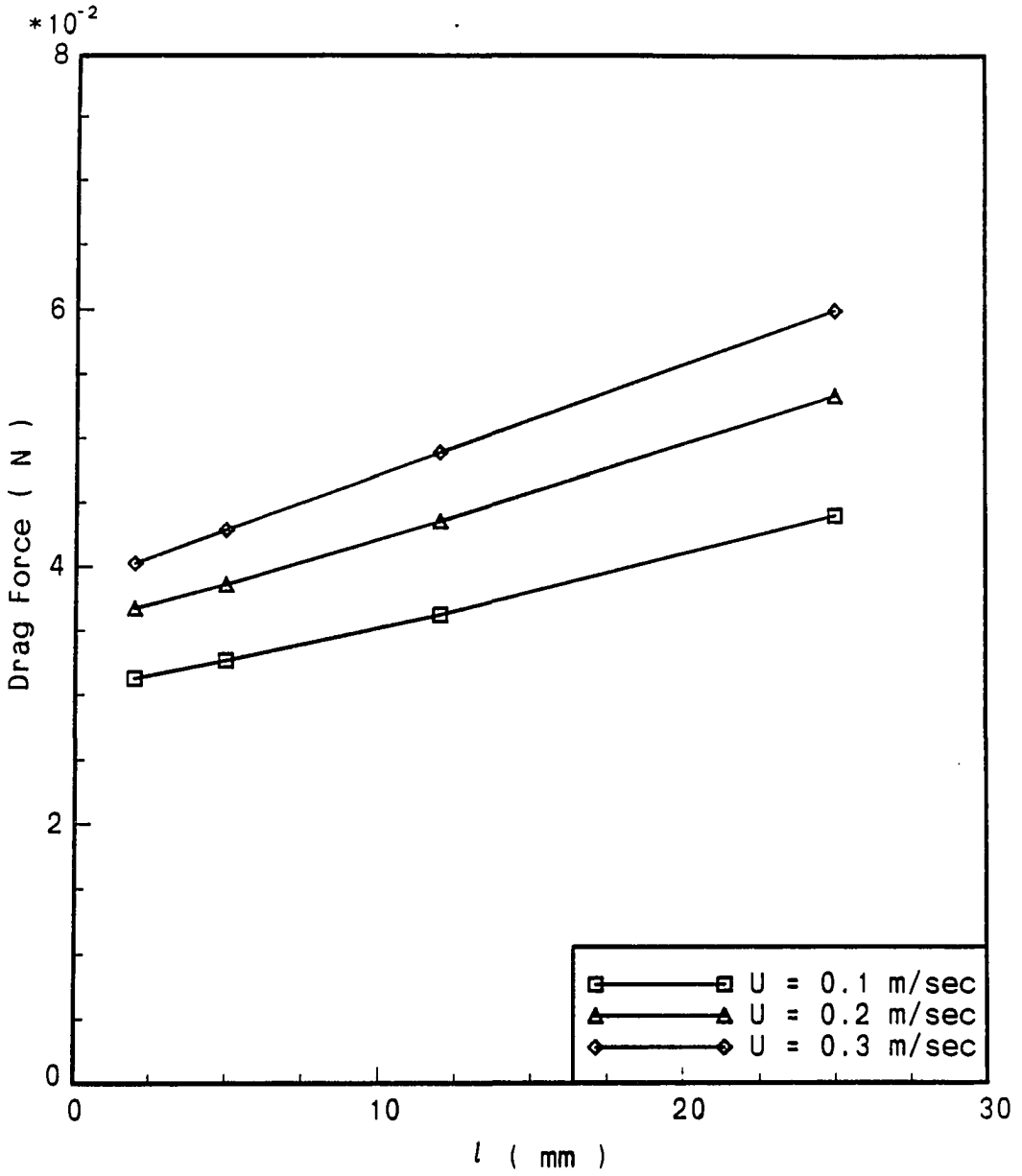

Figure 6.28: Shape dependency of drag force on disks for foam ID = SCFC

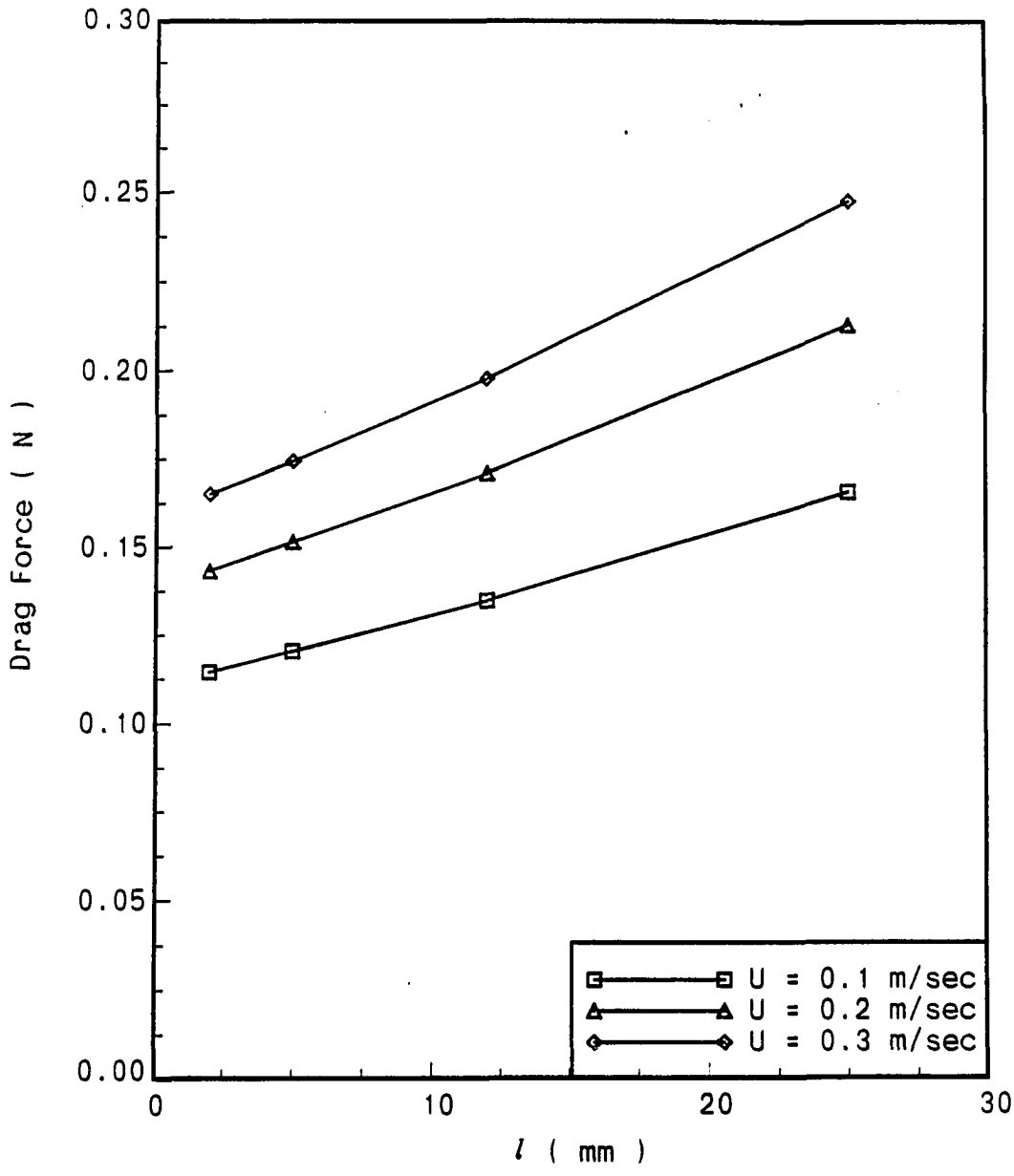

Figure 6.29: Shape dependency of drag force on disks for foam ID = SCFD

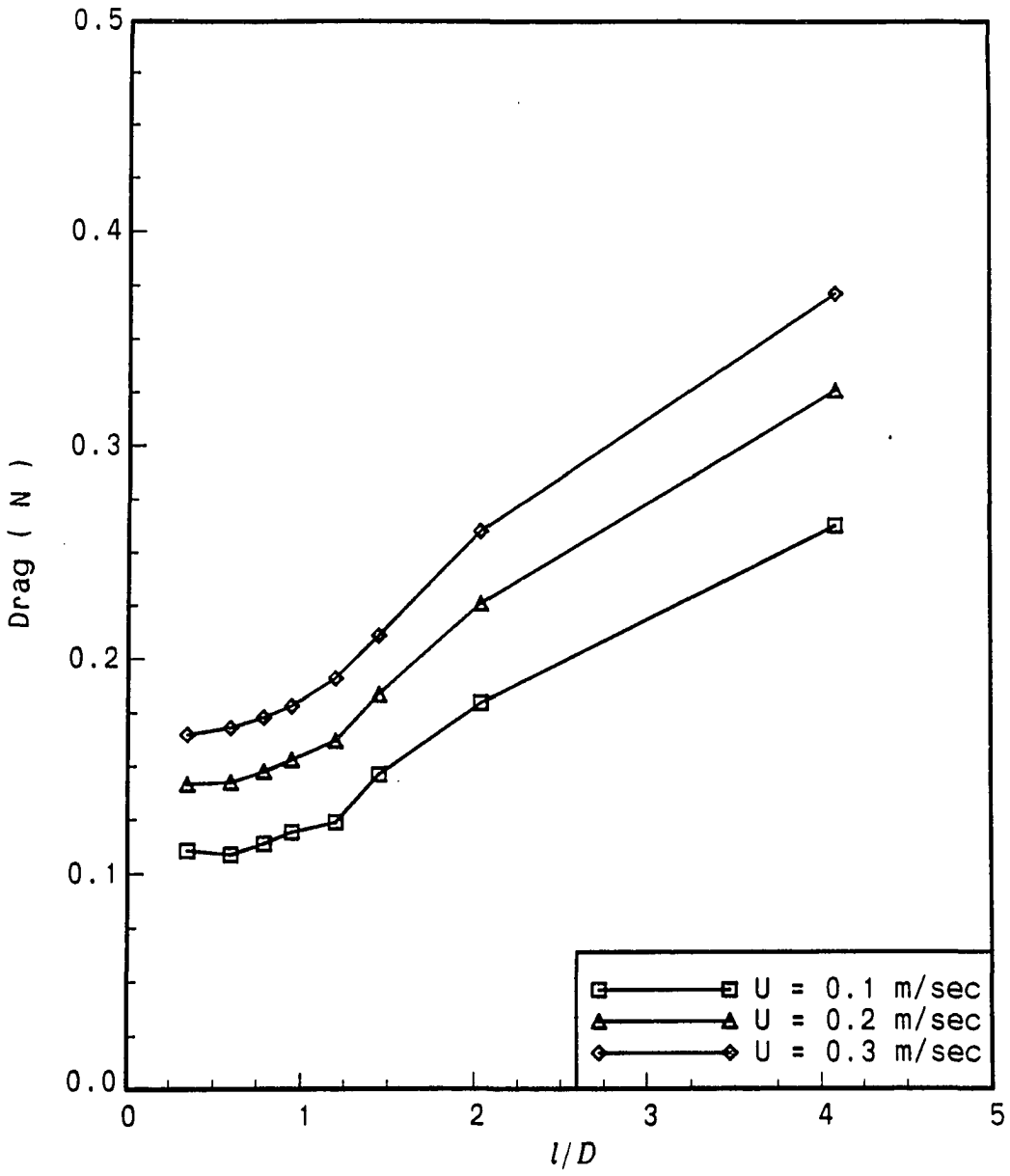

Figure 6.30: Shape dependency of drag force on ellipsoids for foam ID = SCFD

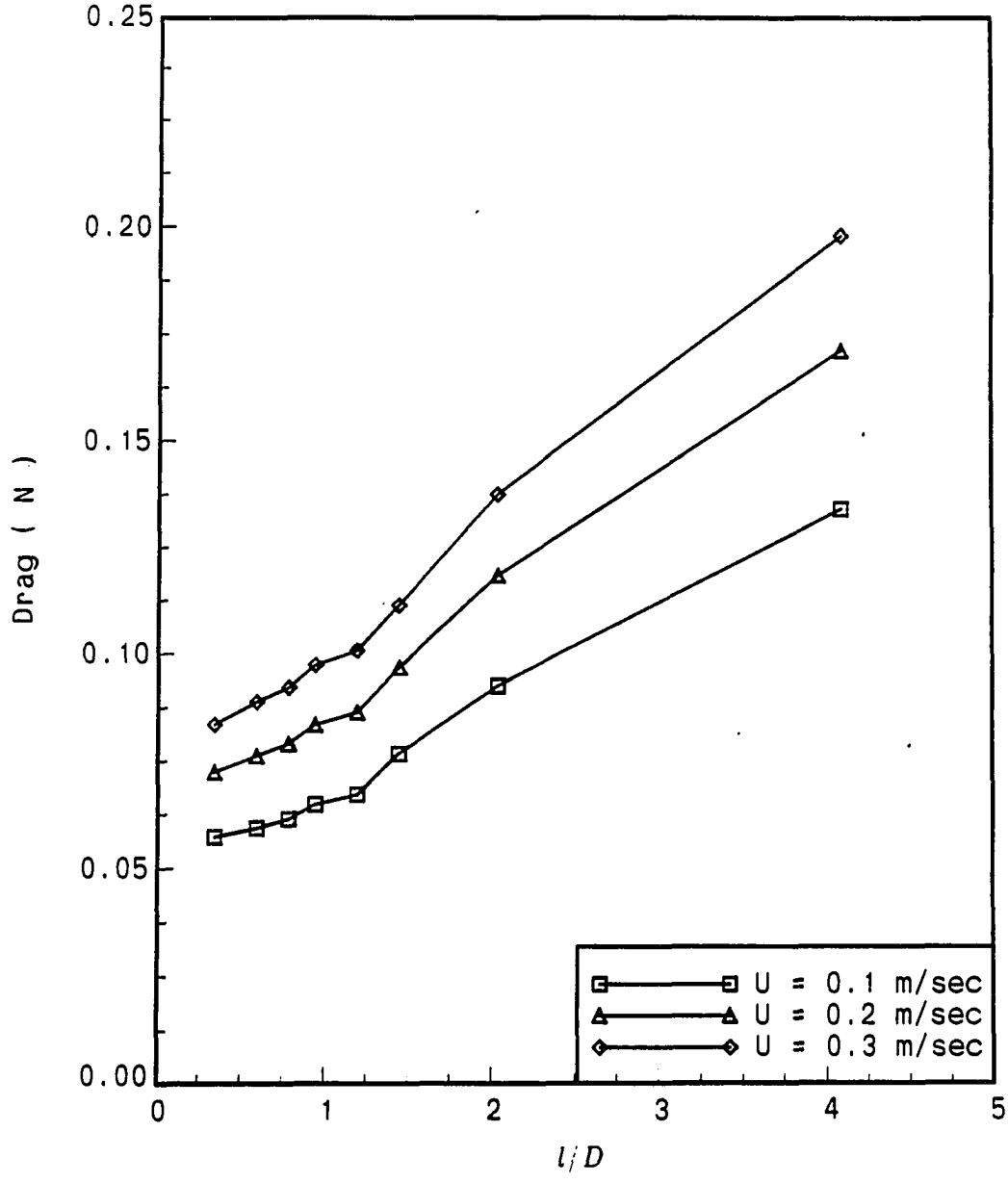

Figure 6.31: Shape dependency of drag force on ellipsoids for foam ID = SCFE

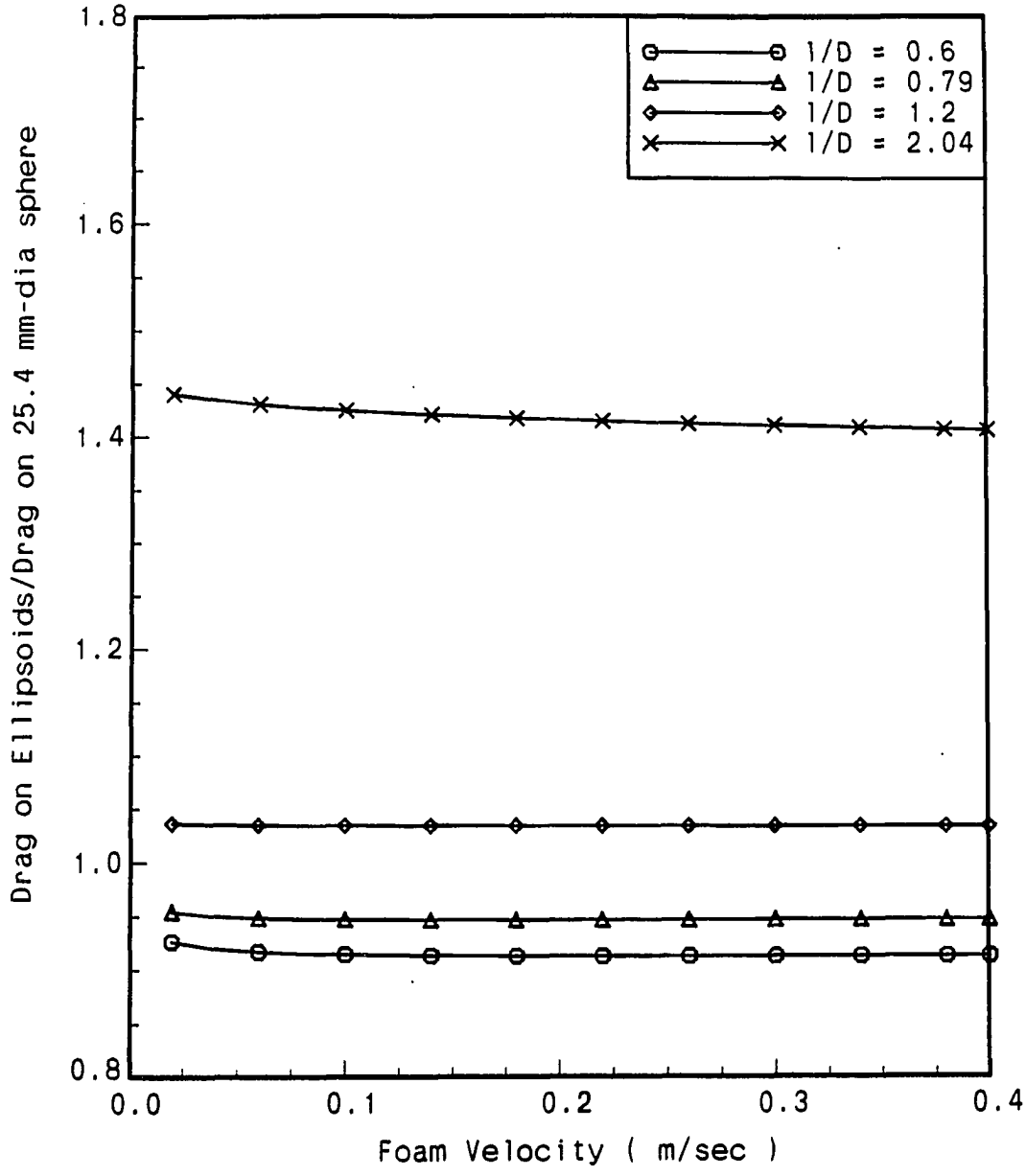

Figure 6.32: $F_{D(ellipsoid)}/F_{D(sphere)}$ as a function of foam velocity for different l/D

As a general observation, the speed of the agitator used to produce the foam in our experiment changed the bubble size, drainage rate, and drag force. Faster stirring produced smaller bubbles and a corresponding higher drag force. The drainage rate was faster for a larger bubble size. The foam with the smaller bubble size has a more complex liquid drain path than does the larger bubble size. Therefore, the drainage rate is slower. Starting agitation of the foam or changing the agitator speed temporarily produced a transient state that existed until the steady-state was obtained. In our experiment, approximately one hour was allowed to ensure steady-state operation. By using a microscope, the approximate magnitude of the average bubble diameter in the steady-state was measured to be about 100 μm. Although this is only an order of magnitude estimate, it does provide an indication of the "fineness" of the foam used.

A general observation of the transient state was a change in bubble size. It was verified that the drainage rates also gradually changed during the transient state and remained the same at the steady-state as shown in Figure 6.33. Figure 6.34 shows the drainage rates for various foams at the steady-state. As was introduced [4] from the typical curvature of drainage rate plot, the curve fit equation has the following expression.

$$V = V_O(1 - e^{-kt}) \tag{6.3}$$

$$\frac{dV}{dt} = kV_O e^{-kt} = k(V_O - V) \tag{6.4}$$

where V is the cumulating drained liquid volume, V_O is the total liquid volume in the foam, and k is the empirical constant.

In our hypothesis, the empirical constant reflects the constant slope in a log-log plot. That is, the constant might be closely related to the complexity of drainage

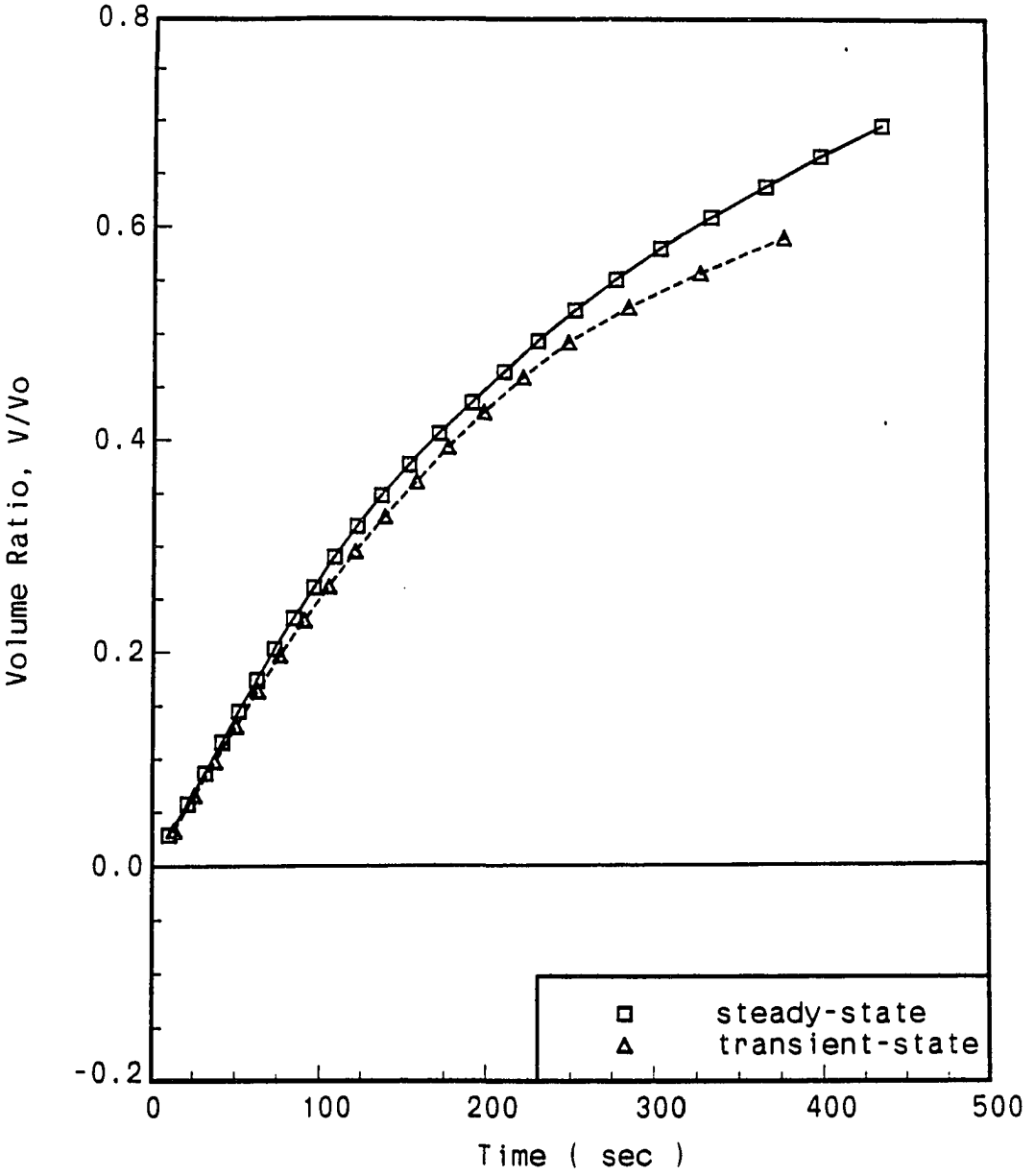

Figure 6.33: Drainage rate on transient state-foam and steady-state foam

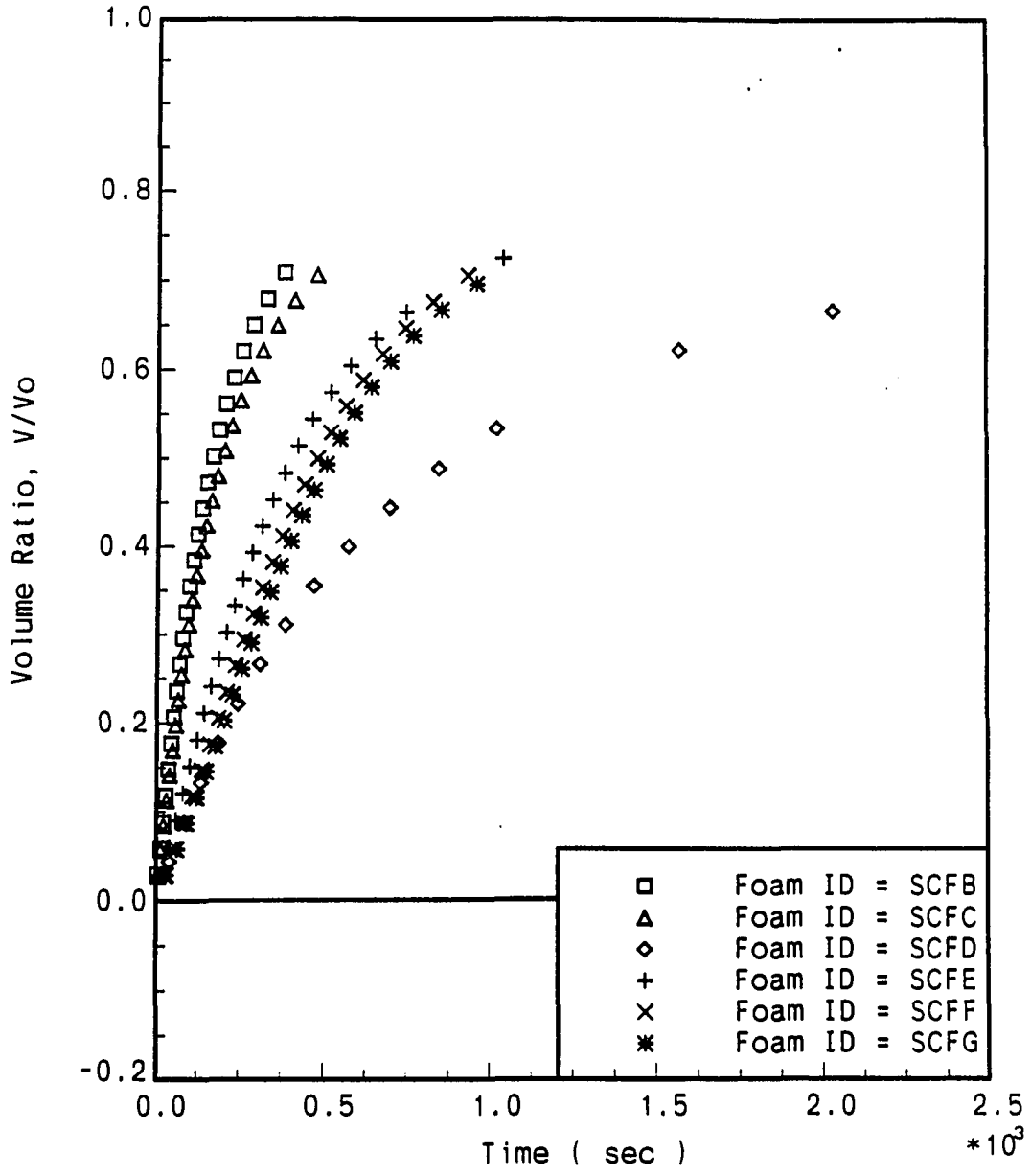

Figure 6.34: Drainage rate for various foams at the steady-state

path, which is again governed by the average bubble size, under constant foam quality and liquid viscosity. In the actual experiment, however, it was not easy to produce different average bubble sizes while the quality and viscosity remain unchanged. This may be because the average bubble size has a close functional relationship with quality. Being acquainted with the above experimental difficulty, one might investigate the functional relationships among the drag force, drainage rate, viscosity, and foam quality by using a statistical scheme such as analysis of variance, if a sufficient amount of experimental foam flow data are accumulated. A more through investigation in this area may provide useful information related to foam properties.

6.3. Wall Effect

The flow around an object located near a wall can be influenced by the wall. The wall effect for drag on a sphere moving through foam near a wall is shown in Figure 6.35. This result is for a 38.1 mm diameter sphere located at various distances from the wall. As discussed in Section 4.5, this was accomplished by locating the sphere at various distances from the wall at the same depth in the foam flow. The data points show there is considerable interaction (i.e., increased drag) when the sphere is close to the wall, while there is no effect away from the wall.

Figure 6.36 shows the comparison of normalized wall effect between the case of foam flow and the case of Newtonian creeping flow case. The Newtonian creeping flow case is a plot of Eq. (5.29). The plot is normalized for the shape comparison purpose by dividing the drag force by each minimum drag force and location by sphere radius. By comparison with the Newtonian creeping flow case, the limited wall effect range is obvious in foam flow case.

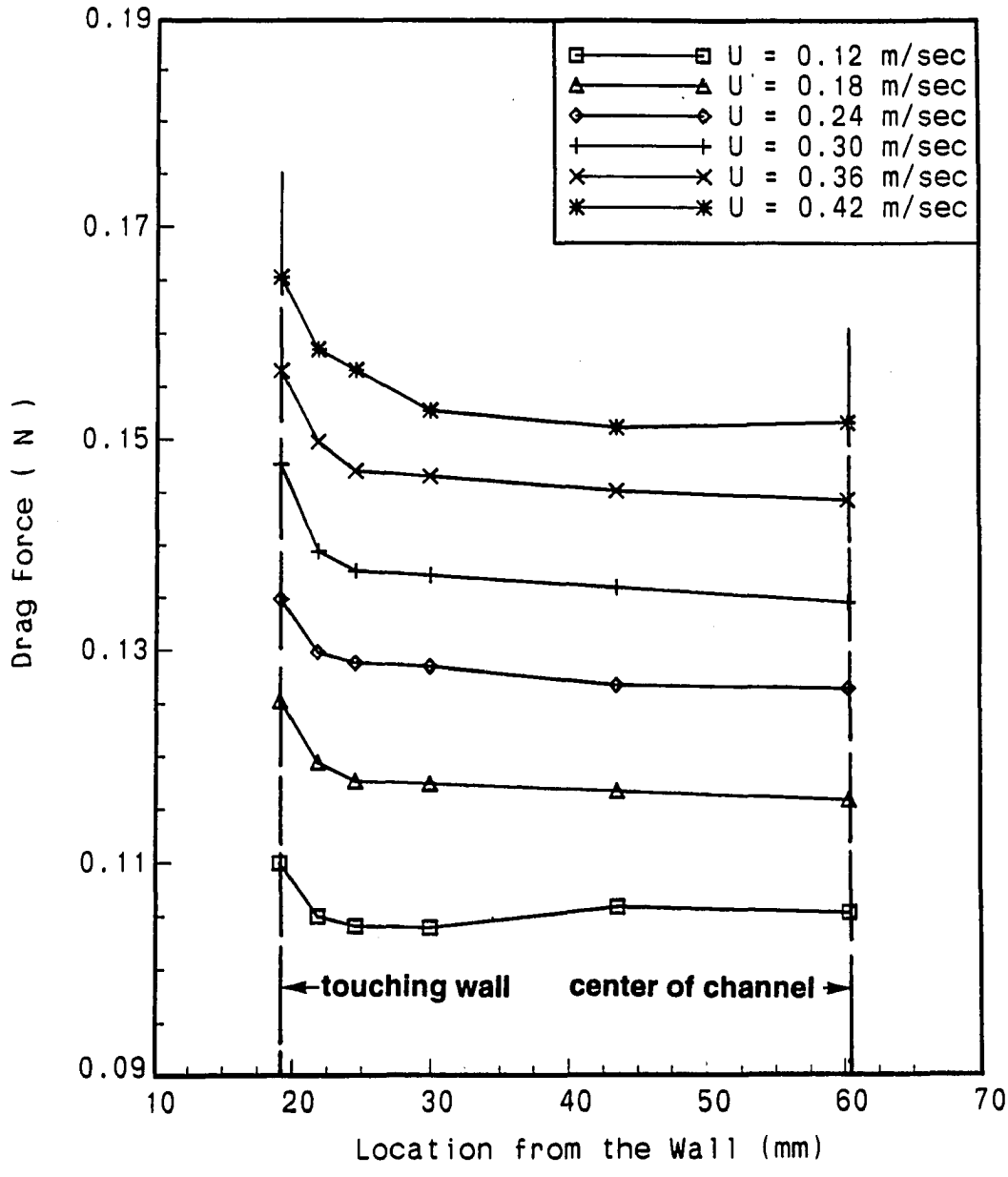

Figure 6.35: Drag variation for the 38.1 mm diameter sphere in the foam flow as a function of distance from near the wall to the center of the test section. Foam viscosity = 2.8 $\times 10^{-3} Ns/m^2$, quality = 0.8

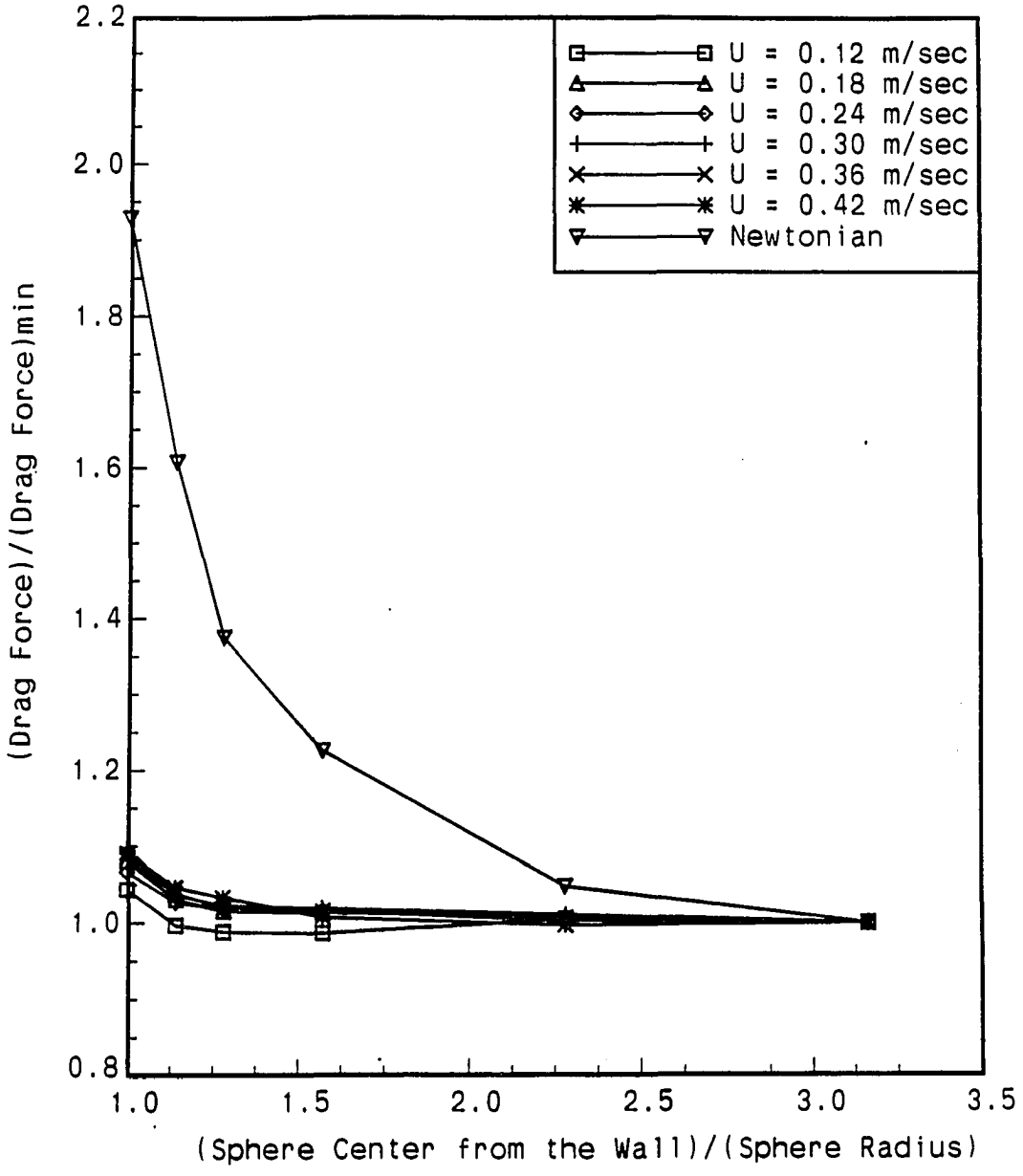

Figure 6.36: Comparison of a normalized wall effect between foam flow and Newtonian creeping flow case

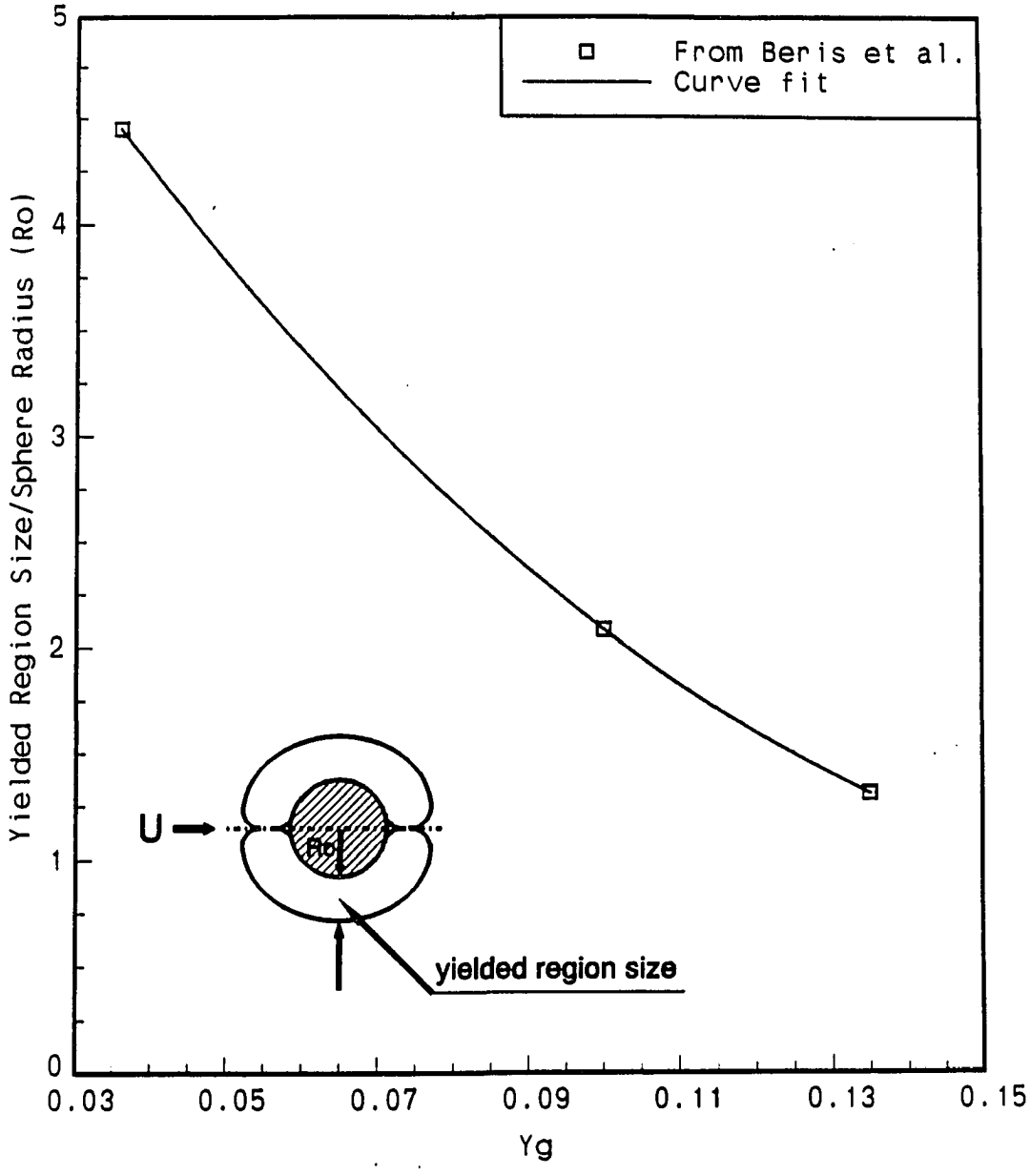

Figure 6.37: Yield region dependency on Y_g for the Bingham material. Calculated from Beris et al. [1]

Since foam can be considered to be a Bingham material, it is of interest to evaluate the expected range of the yield region around the sphere. If the distance between the sphere and the wall is greater than the width of the yielded region, the wall will have no effect on the drag. The range of the yielded region for Bingham material can be predicted by using the theoretical results obtained by Beris et al. [1] for flow of the Bingham material past of a sphere. Following the Bingham theory, the yield region depends on the dimensionless yield stress parameter,

$$Y_g = 2\ \tau_o \pi\ R_o^2 /\ F_D \tag{6.5}$$

As can be seen in Figure 6.35, the wall effect was investigated using several different foam velocities. The foam had a liquid phase viscosity $\mu = 2.8 \times 10^{-3} Ns/m^2$ and a quality $\phi = 0.8$. In this case, $D = 0.0381m$ or $R_o = 0.0191m$, and $F_D\,|_{U=0.3} = 0.135N$. This drag value is comparable with that of foam $ID = SCFA$, which is $F_D\,|_{U=0.3} = 0.138$. Since the shape of foam curve is analogous on same model, choose the value $F_o = 0.021$ from the foam $ID = SCFA$. By using Eq. (5.25).

$$F_D\,\Big|_{U=0} = F_o = 43.4\ \tau_o R_o^2 \tag{6.6}$$

or

$$\tau_o = \frac{0.021N}{(43.4)(0.0191m)^2} = 1.33\ N/m^2 \tag{6.7}$$

From Eq. (6.5), $Y_g = 2(1.33N/m^2)\pi(0.0191m)^2/(0.135N) = 0.0226$

Figure 6.37, obtained from the results of Beris et al., shows how the size of the yield region depends on Y_g. With $Y_g = 0.0226$, the outer yield surface for this yield stress is approximately 5 R_o away from the sphere. From observation of the experimental results in Figure 6.36, however, the yield surface is approximately 0.5

R_0 from the sphere for a foam velocity 0.3 m/sec. That is, the wall effect (i.e., increase in drag) is negligible unless the sphere is closer than one radius from the wall. It should be noted that the apparent yield stress was used in the equation instead of the effective yield stress. Therefore, the Y_g value is evaluated lower than the true value.

6.4. Comparison with Existing Foam Theory

In this section we will compare our experimental results to the approximate foam theory given by Princen et al. [29], which is introduced in Section 5.1. In this section, therefore, an attempt will follow to estimate the average bubble size by the approximate foam theory using available experimental data. For the sample calculation, choose the 101.6 mm flat plate data from the expriment $ID = SCFF$ (see Table 6.7), for which the foam properties are $\phi = 0.81$, $\mu = 17.1 \times 10^{-3} Ns/m^2$ and $\sigma = 0.072 N/m$. The experimentally determined drag (apparent drag) equation is

$$F_D = 0.2910\ U^{0.4380} + 0.0159 \tag{6.8}$$

where U is foam velocity in m/sec and F_D is the drag force in N. The capillary number is defined as

$$Ca = \mu a \dot{\gamma} / \sigma \tag{6.9}$$

We can obtain an approximate value for the shearing ratio as follows. If we assume that the yield region is about 0.01 m at a foam velocity 0.3 m/sec, which is determined from the wall effect analysis in Section 6.3, and assume a linear velocity profile inside

the unyielded region, then the order of the shearing rate is approximately

$$\dot{\gamma} = \frac{0.3\ m/sec}{0.01\ m} = 30\ \text{sec}^{-1} \tag{6.10}$$

Therefore, Eq. (6.9) becomes

$$Ca = (17.1 \times 10^{-3} Ns/m^2)(30 s^{-1})/(0.072 N/m)a = (0.0369/m)a \tag{6.11}$$

where a is in meters.

As mentioned earlier, the direct measurement of the average bubble size is not easy. Although there was no precise measurement of the average bubble size throughout the experiment, one trial was made by observing a sample of the foam (see Section 6.2). By using a microscope to view foam contacting a transparent film, the number of bubbles in a unit length was counted. This conventional method, using a stationary sample of foam and a film contacting the bubbles under a microscope, might result in a larger value of the bubble size than from foam moving in the tank. This attempt determined about 100 μm as the average bubble diameter. With this approximate bubble radius, a = 50 μ m, the capillary number is $Ca = 1.85 \times 10^{-6}$. This is smaller than 10^{-4}, the limit for which the theory used below is valid (see Eq. 5.2). In this case, the yield stress is given by Eq. (5.2).

$$\tau_o = \sigma\ \phi^{1/3} Y(\phi)/\ a \tag{6.12}$$

$$\text{where } Y(\phi) = -0.080 - 0.114\ \log(1-\phi)$$

or with $\phi = 0.81$,

$$Y(\phi) = 2.22 \times 10^{-3} \tag{6.13}$$

Substituting all the values into Eq.(6.12) yields

$$\tau_o = 1.49 \times 10^{-4}/a \tag{6.14}$$

Now, the effective shear expression from Eq. (5.4) is

$$\tau = \tau_O + 32(\phi - 0.73)\frac{\sigma}{a}C'a^{1/2} \tag{6.15}$$

or

$$\tau = \frac{1.49 \times 10^{-4}}{a} + \frac{3.54 \times 10^{-2}}{\sqrt{a}} \tag{6.16}$$

where τ is effective shear stress in N/m^2.

From the experimental results, the apparent drag force at the velocity $U = 0.3\ m/sec$ for the flat plate calculated from Eq. (6.8) is

$$F_D = 1.88 \times 10^{-1} N \tag{6.17}$$

Therefore, the average apparent shear stress, τ_A, is

$$\tau_A = F_D/2A = 36.43\ N/m^2 \tag{6.18}$$

Although the apparent shear stress is lower than the effective shear stress, by assuming that both shear stresses are same order of magnitudes, we can calculate the average bubble size by using Eq. (6.16) That is,

$$36.43 = \frac{1.49 \times 10^{-4}}{a} + \frac{3.54 \times 10^{-2}}{\sqrt{a}} \tag{6.19}$$

By letting $x = \sqrt{a}$, the equation can be transformed to

$$36.43x^2 - 3.54 \times 10^{-2}x - 1.49 \times 10^{-4} = 0 \tag{6.20}$$

The positive value of x is found to be $x = 2.57 \times 10^{-3}$ or $a = 6.58 \times 10^{-6}m$. From this calculation, the approximate average bubble diameter is about 13 μm. This value is smaller by a factor of about 1/8 when compared to the measured average bubble diameter $d = 100\ \mu m$. By considering that the bubble size measured in contact

with the wall may be different than that inside the foam, and the several rough assumptions made for the comparison, this result could be considered comparable to that given by the approximate theory.

6.5. Rough Surfaces

The dependence of drag force, F_D, on the surface roughness, ε, is shown for spheres and flat plates parallel to the flow in Figures 6.38 and 6.39. In each case, it is shown that the rougher the surface, the larger the drag force. Although this behavior is not found for the laminar flow of Newtonian fluids past objects, it is found for turbulent boundary layer flow of a Newtonian flow. For such cases, the surface roughness elements protrude into or through the viscous sublayer and affects the wall shear stress [23]. A related phenomenon is not unexpected for the flow of foam. On the macroscale, foam can be thought of as slipping along a stationary solid surface. That is, the usual non-slip boundary condition valid for viscous fluids is not appropriate for foam. Apparently the amount of slip realized is a function of the surface roughness, as has been shown for the flow of foam in pipes [41]. On the microscale, the surface roughness alters the flow associated with the bubbles (or cells) near the surface and thereby alters the shear stress at the wall.

Note that although the roughness-induced increase in drag is not extremely large, for a given roughness it is the same amount at any velocity. Thus, for example, the drag versus velocity curves of Figures 6.38 and 6.39 are similar in shape, but merely displaced in the vertical (force) direction. To explain this phenomenon, an evaluation of the film thickness at the wall is needed. By using the idealized 3-dimensional foam model, expressions for foam parameters in terms of geometry can be derived [46].

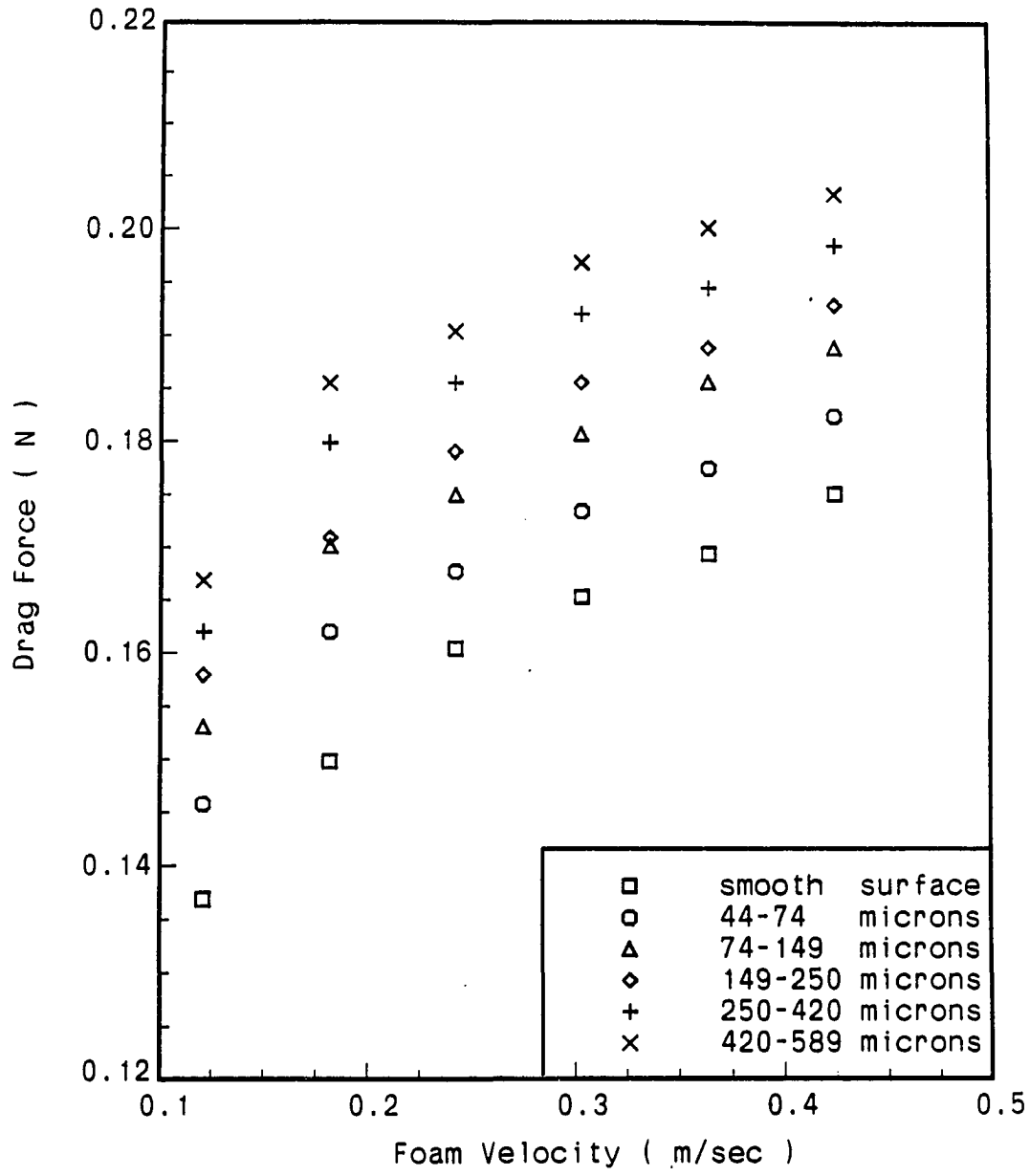

Figure 6.38: Drag for different surface roughnesses on a 38.1 mm diameter sphere. Viscosity = $7.1 \times 10^{-3} Ns/m^2$, quality = 0.8

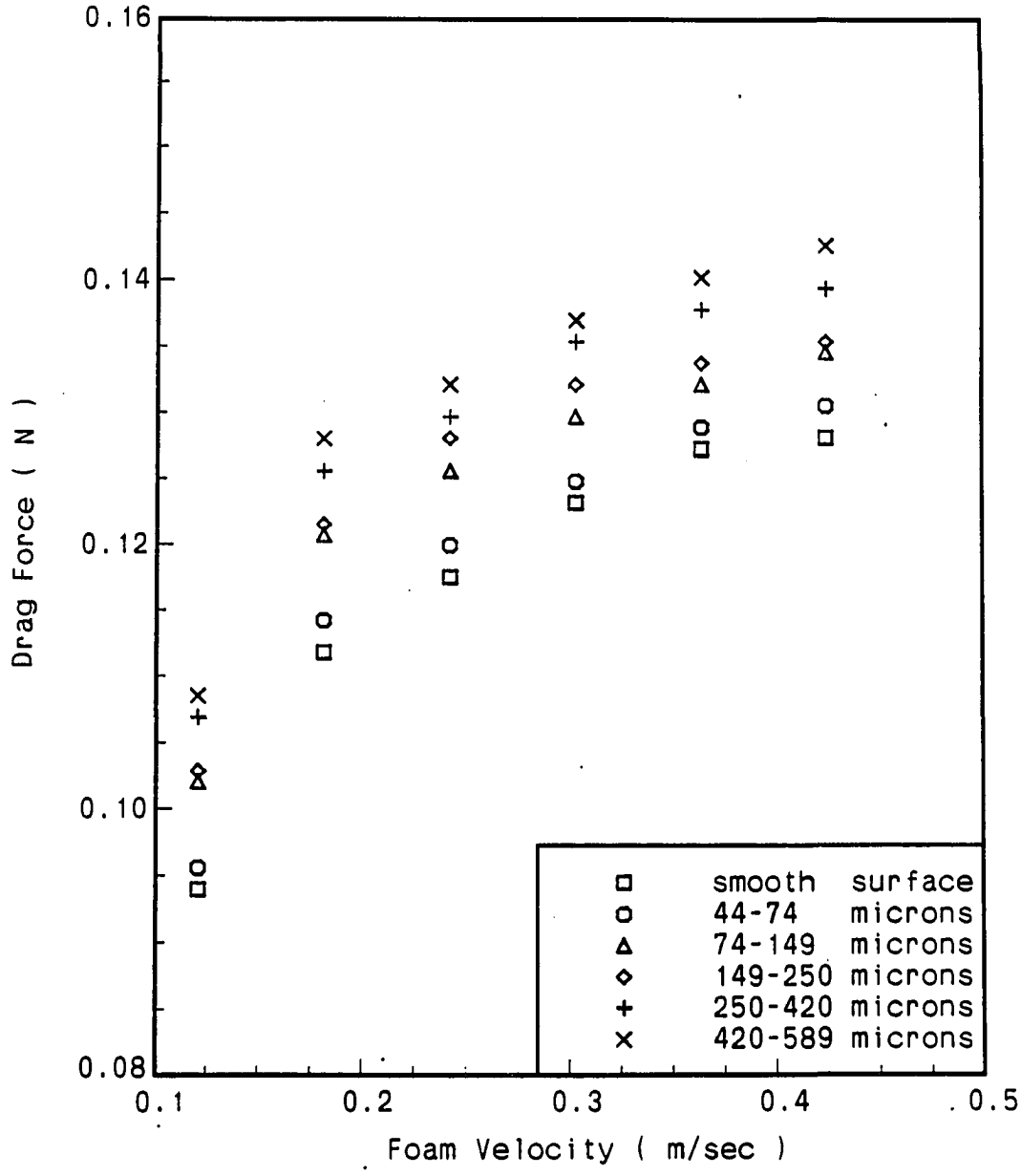

Figure 6.39: Drag for different roughnesses on a 101.6 mm-long flat plate. Viscosity $= 7.1 \times 10^{-3} Ns/m^2$, quality = 0.8

The relationships for expansion factor Ψ is

$$\Psi = \frac{d}{3t}, \text{ and } \Psi \equiv \frac{V_f}{V_l} \tag{6.21}$$

where t is the thickness of a bubble film, d is the bubble diameter, V_f is the volume of the foam, and V_l is the volume of the liquid. The quality of the foam used for rough surface experiment is $\phi = 0.8$ or the expansion factor $\Psi = 1/0.2 = 5$. If we assume that the bubble diameter $d = 100\ \mu m$, then from Eq. (6.21), the thickness of bubble film, t, is about 6.7 μm. Since the foam used in this study (real foam) is not an ideal foam, the film thickness could differ somewhat from the ideal case calculated by Eq. (6.21). In addition, the thickness of the boundary liquid layer may be different than the bubble film thickness. There is experimental evidence [46], however, that the actual liquid layer for a real foam is the same order of magnitude as the thickness of the bubble film calculated.

As can be seen in Figures 6.38 and 6.39, the roughness of the specimens was from 44 μm to 589 μm. That is, the roughness scale is expected to be much bigger than the length scale of the wall liquid boundary layer. On the other hand, the length scale of the actual bubbles, if assume that average bubble diameter $100\mu m$, have the same order of magnitude with the roughness scale. Therefore, from a microscopic point of view, the partial capture of the bubbles in the spaces between intrusions could be imagined. In this case, if the x-component (foam flow direction) of force acting between the bubbles and intrusions exceeds the yield stress of the foam field, deformation and partial relocation of the bubbles will arise. Figure 6.40 describes this conceptual microscopic foam flow at rough surface boundary condition. Since the roughness and bubble sizes are randomly distributed, this partial slip and relocation would not happen at the same time for the entire row of foam cells, as idealized

for foam on a smooth surface. The possibility of cutting the foam matrix, however, will increase in the cases with bigger roughness. Since this static x-component force is dependent on the geometrical distribution between bubbles and intrusions, roughness-induced increase in drag is not a function of foam velocity, and the same amount of drag force increase results for given roughness at any foam velocity.

Figure 6.41 may support this hypothesis. In this figure, the drag on a 38.1 mm-diameter sphere is plotted as a function of surface roughness. Although the supporting data are not extensive, it appears that once the roughness reaches a certain value, the drag force does not greatly increase with a further increase in roughness. From the hypothesis, the maximum variation due to the roughness would be equal to or less than the effective yield force of the foam. The variation of drag force due to roughness is confined to approximately 0.03 N, which is even less than apparent yield force of this foam.

Since surface roughness reduces the amount of slip at the surface, comparison with the Bingham theory introduced in Section 5.2 would be of interest. This theoretical study incorporated the usual no-slip boundary conditions. From the Eq. (5.25),

$$F_D = (3\pi\eta_o D)U + 10.9\tau_o D^2 + 17.6\sqrt{\eta_o \tau_o U D^3} \tag{6.22}$$

if we obtain the yield force, F_o, at zero foam velocity,

$$F_o \equiv F\Big|_{U=0} = 10.9\ \tau_o D^2 \tag{6.23}$$

Then,

$$\frac{F_D}{F_o} = 1 + \frac{3\pi\eta_o U D^3}{10.9\ \tau_o D^2} + \frac{17.6\sqrt{\eta_o \tau_o U D^3}}{10.9\ \tau_o D^2} \tag{6.24}$$

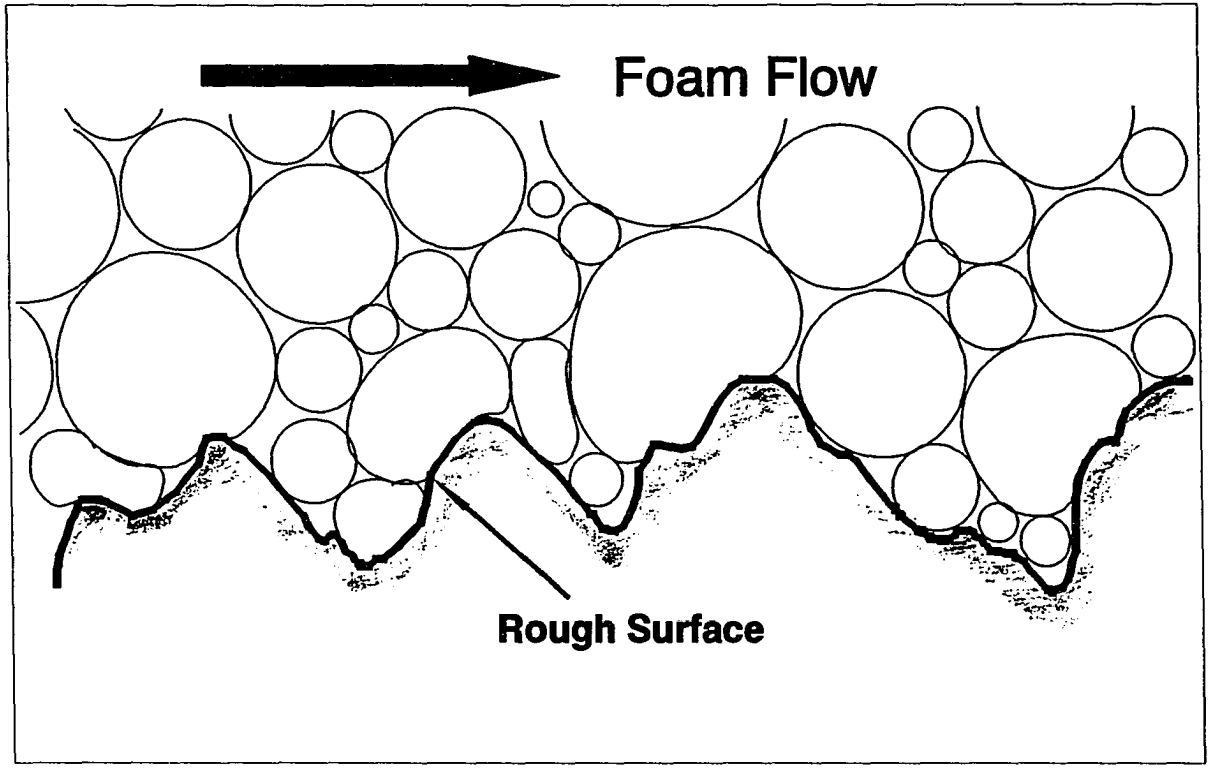

Figure 6.40: Conceptual sketch of microscopic foam flow boundary condition at a rough surfaced wall

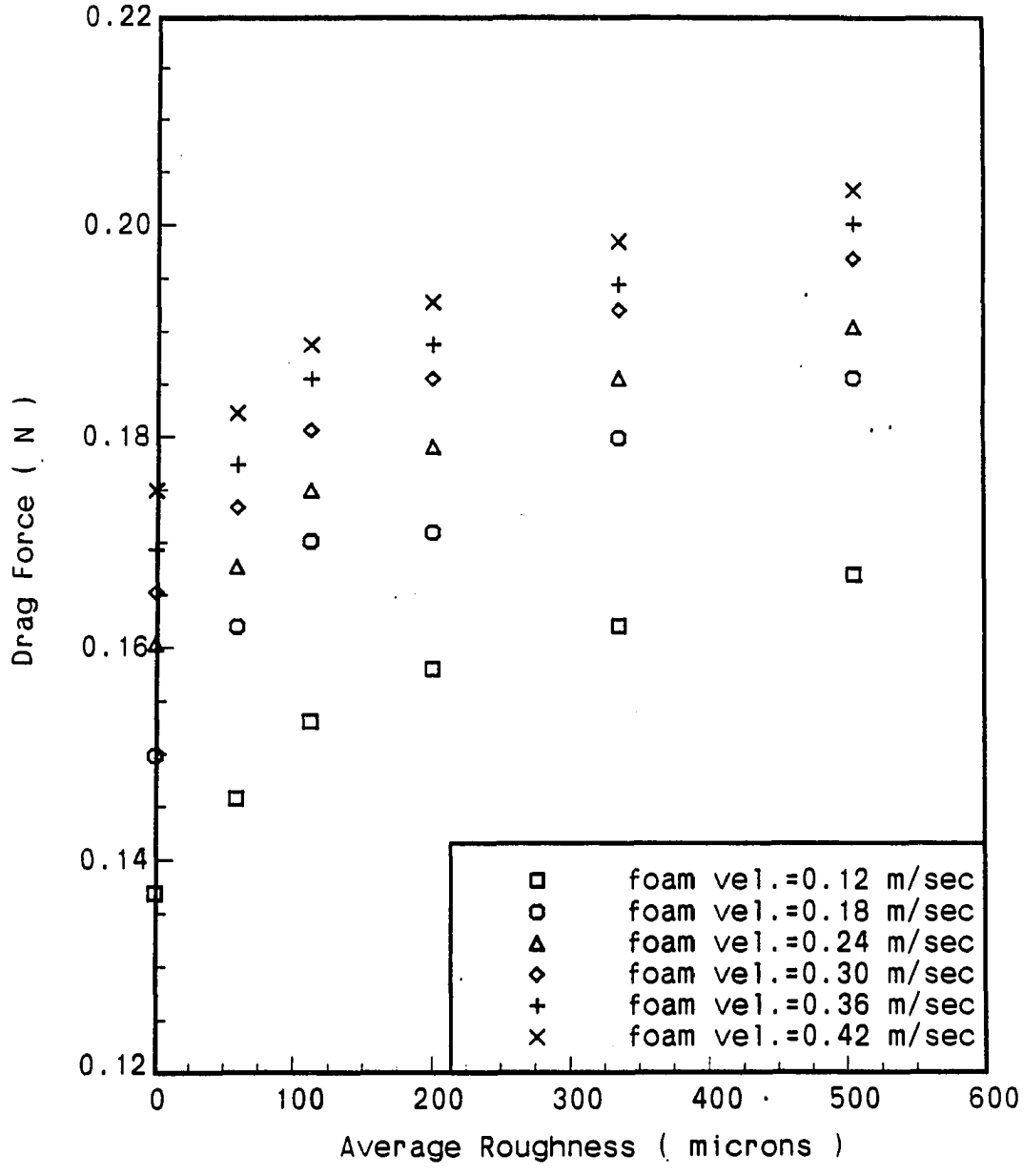

Figure 6.41: Relationship between drags and average roughnesses on 38.1 mm diameter sphere. Viscosity = $7.1 \times 10^{-3} Ns/m^2$, quality = 0.8

or

$$\frac{F_D}{F_o} = 1 + 0.865\frac{\eta_o U}{\tau_o D} + 1.615\sqrt{\frac{\eta_o U}{\tau_o D}} \tag{6.25}$$

or

$$\frac{F_D}{F_o} = 1 + 0.865\frac{U}{U_o} + 1.615\sqrt{\frac{U}{U_o}} \tag{6.26}$$

where $U_o = \tau_o D/\eta_o$.

To plot Eq. (6.26), τ_o and η_o values are needed. These two parameters can be obtained from the sphere drag data, so that the F_o value in Eq. (6.23) is from the experiment. The derivative of Eq. 6.22 is

$$\frac{dF_D}{dU} = 3\pi\eta_o D + 17.6\sqrt{\eta_o\tau_o D^3}(\frac{1}{2}\frac{1}{\sqrt{U}}) \tag{6.27}$$

If U goes to infinity, the curve will be a straight line with a slope of $3\pi\eta_o D$.

This analysis can be applied to the rough surface sphere data, since the rough surface can be considered as having less slip, perhaps even no-slip, on the boundary. The theoretical results from which the above analysis was obtained assumed the no slip boundary conditions. For example, in the case of 38.1 mm sphere with roughness 420–589 μm in foam $ID = SCFG$, we can fit a Bingham plastic F_D versus U curve through two points to evaluate F_o and η. By subsituting the experimental data $F_D = 0.167\ N$ at $0.12\ m/sec$ and $F_D = 0.203\ N$ at $U = 0.424 m/sec$, Eq. 6.22 yields

$$0.167 = 0.01582\ \tau_o + 0.04309\ \eta_o + 0.0453\sqrt{\eta_o}\sqrt{\tau_o} \tag{6.28}$$

$$0.202 = 0.01582\ \tau_o + 0.15261\ \eta_o + 0.0853\sqrt{\eta_o}\sqrt{\tau_o} \tag{6.29}$$

By using a simultaneous non-linear equation solver, subroutine NEQNF in IMSL, from Eqs. (6.27) and (6.28), we obtained for $\tau_o = 8.3619$ and $\eta_o = 0.0602$. With these values,

$$F_o = 10.9\ \tau_o D^2 = 0.132\ N \tag{6.30}$$

and

$$U_o = \tau_o D \ / \ \eta_o = 5.29 \ m/sec \tag{6.31}$$

Substituting values from (6.29) and (6.30) into Eqn. (6.25) provides the curve fit equation using Bingham theory as shown in Figure 6.42. As can be seen in Figure 6.42, the data show more rapid shear thinning curvature than that predicted by Bingham theory. This probably resulted due to the fact that partial slip still occurs on rough surfaces, and therefore the apparent slope of the drag curvature differs from that of non-slip case. If we assume no-slip on a rough surface, the foam material may be a combination of Bingham plastic and pseudoplastic; this has not been clearly explained yet.

6.6. Dispersed Gas Bubble Suspensions

High expansion foam (or dry foam), which is the case when ϕ approaches unity, has been in the spotlight for most of the previous experimental and theoretical work. This was mainly because of the following reasons. In most experimental cases, a conventional air injection type foam generator was used, generating high expansion foam. For the viscometer experiments, leakage and rupture problems, due to the unstable nature of foam, limit the ϕ range for which accurate results can be obtained. In theoretical cases, due to complexity of analyzing the liquid film flow at the microscopic scale in randomly distributed three-dimensional bubbles, current studies have been restricted to the idealized foam structures with a limited range of high expansion foam.

As indicated by the result of this study, high expansion ($\phi \approx 1$) foam behaves as a shear thinning material. On the other hand, a dilute suspension ($\phi \approx 0$) of a

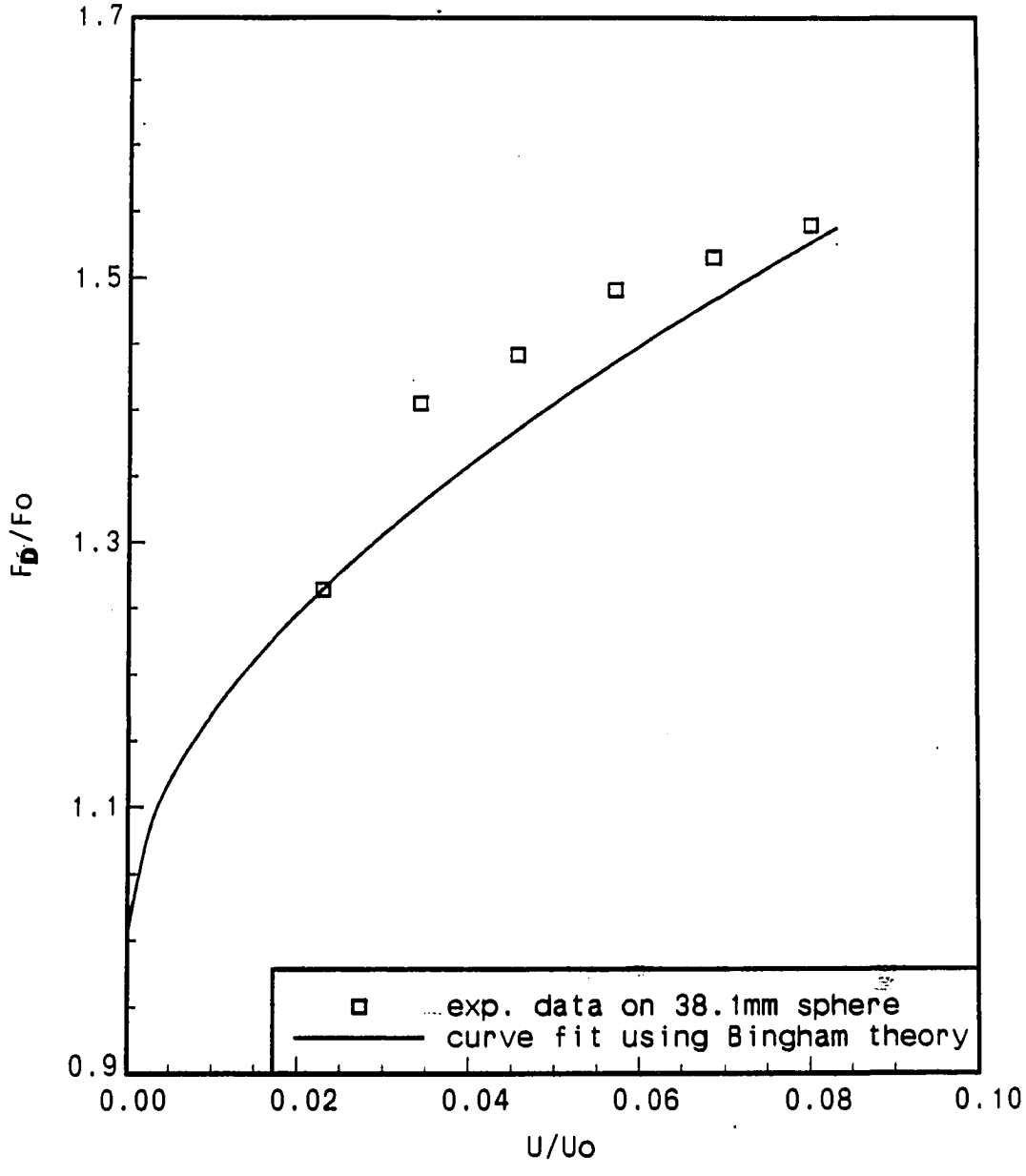

Figure 6.42: Curve fit by using Bingham theory to the 38.1 mm dia. sphere with roughness 420–589 μm

gas in a liquid hehaves as a Newtonian fluid. It is of interest to determine how this transition from a Newtonian to a non-Newtonian character takes place as ϕ varies from 0 to 1. To do this, a simple rotating-cylinder viscometer was used to determine the shear stress versus rate of strain character of low quality foam. The results are presented in this section.

As mentioned earlier, a continuous beating (agitation) method was used to generate foam in the present study. Thus, a wide range of ϕ could be achieved. To achieve sufficiently stable foam at a low quality, a pure Joy solution (not mixed with water) was used because of its high viscosity, measured as $\mu = 210.6 \times 10^{-3} Ns/m^2$ by use of a capillary tube viscometer. In this case, both the air injection and the agitation method were used to produce foam. The foam produced by this combination was found to be stable for a sufficient period of time to run tests in a concentric cylinder viscometer even at low range of ϕ. Figure 6.43 shows the results plotted as drive weight (proportioned to shear stress) versus angular velocity (proportional to rate of strain) from the concentric viscometer tests on foams with various ϕ.

As can be seen in Figure 6.44 (a normalized plot of the data in Figure 6.43) the shear thinning characteristics increase as ϕ increases. The apparent viscosity of different foams was calculated by comparing the slope of each plot in Figure 6.43 with the viscosity of the liquid itself. That is $\mu = \mu_0$ when $\phi = 0$. The slopes were calculated by linear regression analysis. The results are tabulated in Table 6.11.

For the cases of $\phi = 0.0$, 0.17, and 0.27, the data show an almost Newtonian relationship: the shear stress is a linear function of shear rate. The cases of $\phi = 0.5$, 0.56, and 0.63 show apparent non-Newtonian characteristics. That is, shear stress is not a linear function of rate of strain, and a slight shear thinning charateristic is

Table 6.11: The apparent viscosity ratio for different expansion ratios. The viscosity and surface tension of a liquid phase are 210.6 Cst and 0.0627 N/m

ϕ	correlation coeff, r^2	μ/μ_o
0.0	0.999	1.00
0.165	0.998	1.82
0.268	0.9978	2.29
0.505	0.989	5.72
0.564	0.9656	7.72
0.632	0.8329	12.68

observed.

Figure 6.45 shows the relationship between effective viscosity and quality. The effective viscosity parabolically increases with foam quality increase. As an order of magnitude calculation, assume Stoke's flow of a Newtonian fluid to estimate the approximate effective viscosity of the actual foam flow. For example, for the case of a sphere of diameter 25.4 mm in foam ID = SCFE at foam velocity 0.3 m/sec, the Stoke's drag based on the viscosity of the soap-water solution is

$$F_{D(liquid)} = 6\pi U R_o \mu$$

$$= 6\pi(0.3m/sec)(1.27 \times 10^{-2}m)(7.22 \times 10^{-3}Ns/m^2)$$

$$= 5.19 \times 10^{-4}N$$

The actual drag is (see Table 6.6)

$$F_{D(foam)} = aU^b + c = 0.1219(0.3)^{0.4031} + 0.0119$$

$$= 8.69 \times 10^{-2}N$$

Therefore, the viscosity ratio is

$$\frac{F_{D(foam)}}{F_{D(liquid)}} = \frac{(8.69 \times 10^{-2})}{(5.19 \times 10^{-4})} \simeq 170$$

at foam quality $\phi = 0.82$. This approximate value indicate the proper trend of effective viscosity-quality relationship as shown in Figure 6.45.

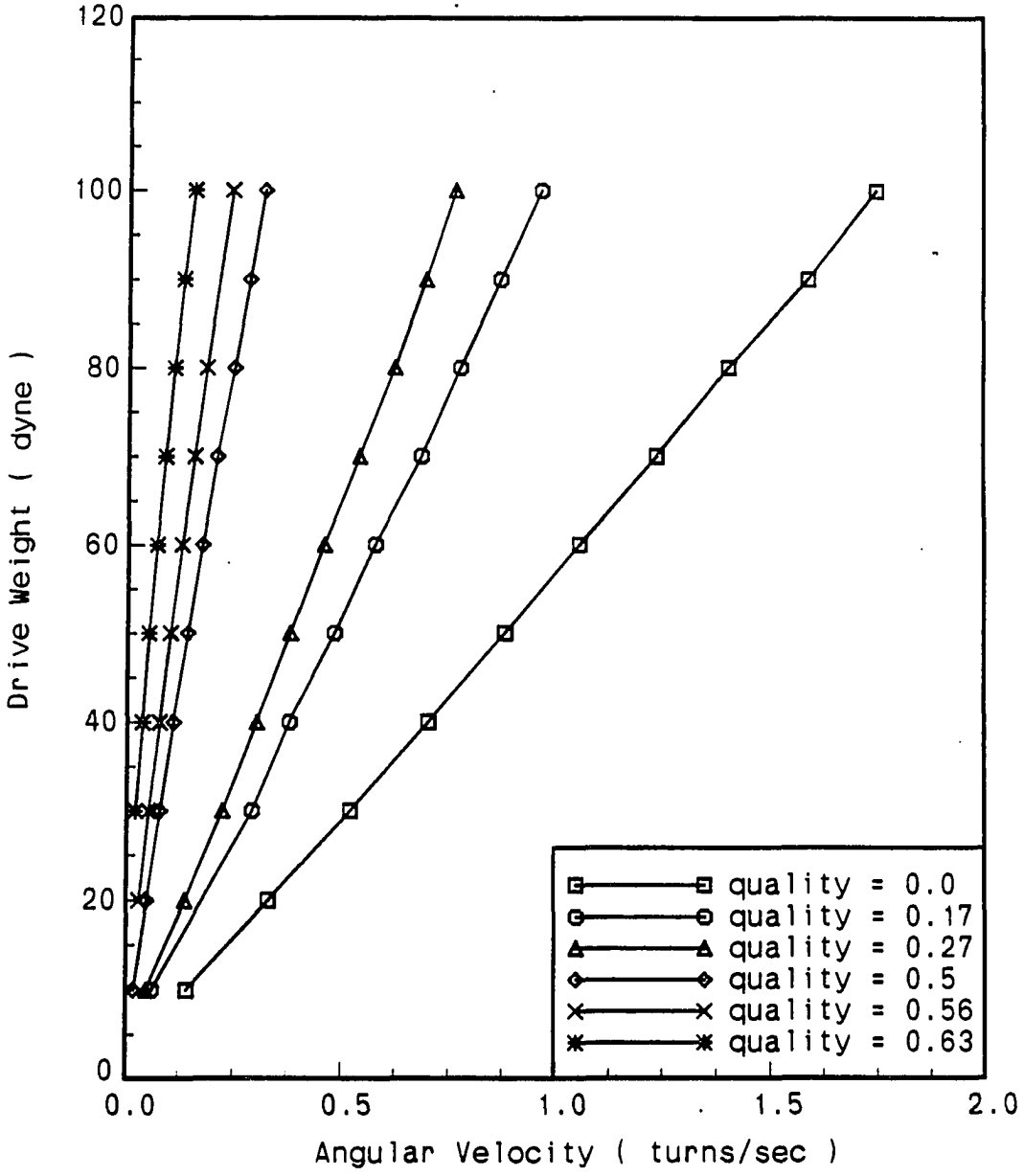

Figure 6.43: Drive weight versus angular velocity from the concentric viscometer test on dilute gas bubble suspensions

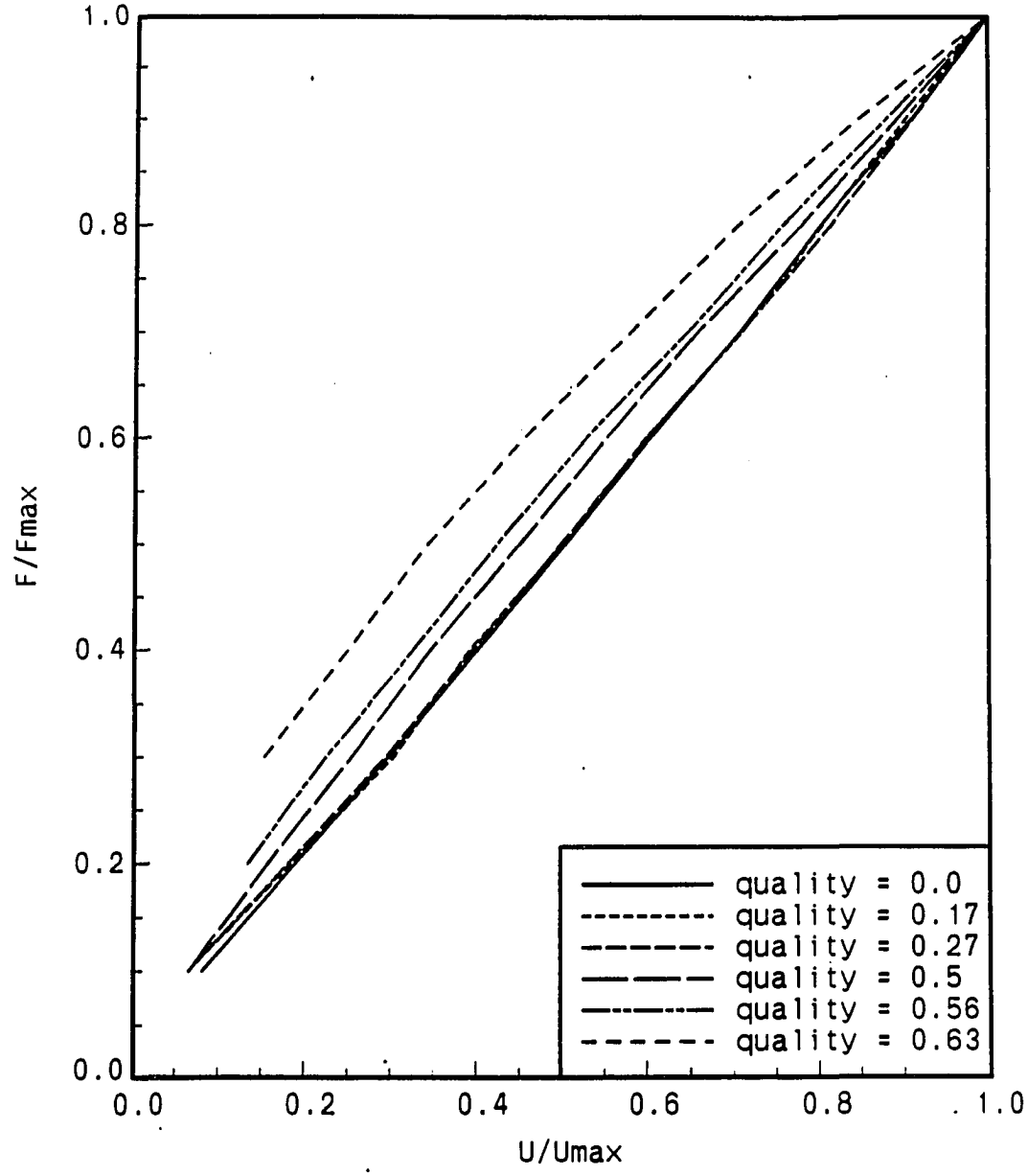

Figure 6.44: Normalized plot for the concentric viscometer test on dilute gas bubble suspensions

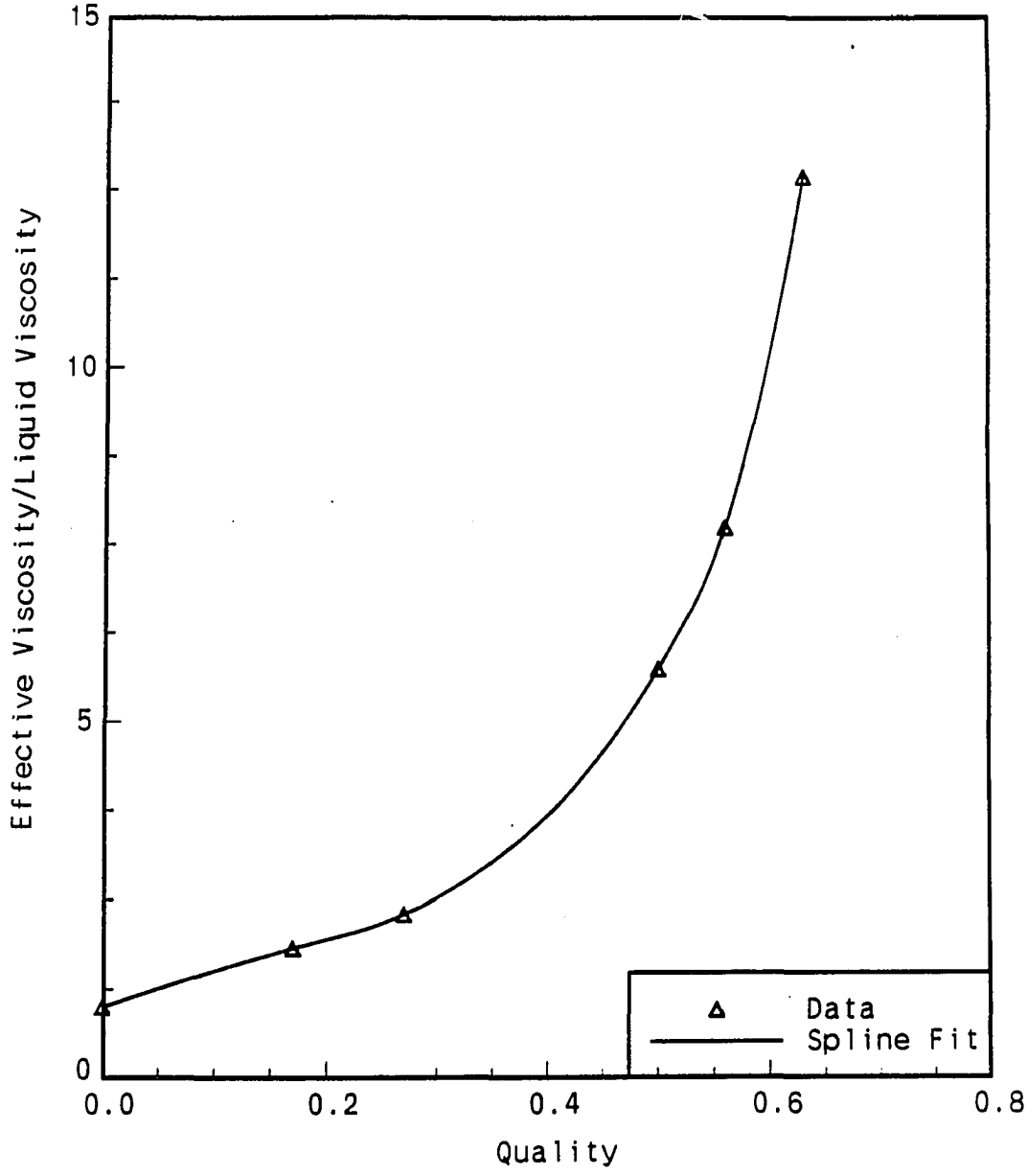

Figure 6.45: Relationship between effective viscosity and quality for dilute gas bubble suspensions

CHAPTER 7. CONCLUSION

Summary

The experimental and theoretical pursuit of the understanding of foam flow has about a half century history. Due to the complex nature of foam itself, however, many of foam flow characteristics are not clearly solved and are still challenging to the people who are engaged in this field. In this experimental study, a new concept of foam making machine was introduced, and drag forces were measured for various types of models moving through foam. A few attempts were made to compare our experimental results with very recent (although still quite simplified) theoretical contributions. It is no hesitation, at this point, to mention the difficulties associated with the experimental investgation of foam flow. Those difficultes mainly arise due to the following reasons.

First, there have been no effective methods to measure the slip velocity on the wall in a dynamic foam flow situation. Second, there is lack of plausible theoretical predictions to guide experimental design and procedures. Very recently, however, a few theoretical studies on two-dimensional ideal foam structure under limited conditions have produced reasonable direction for further research. Third, due to above reasons, most of the previous experimental data were not well defined and omitted one or more important variables. As a result, there has been a lack of dependable

data on foam flow.

In previous theoretical studies, the basic foam model structure, its static and stability charateristics, and the properties of foam making agents were mainly investigated by chemists. Chemical engineers contributed to the understanding of foam's rheological behavior. Nowadays, the attention given to foam is increasing due to the increasing practical demands. Inspite of previous efforts, the current stage of the theoretical development is infant. It remains, for the most part, based on a two-dimensional idealized foam structure. This is mainly because of the challenging complex rheological features of foam or foam flow, such as a yield stress, slip at the wall, and the especially complex real foam structures to simulate.

In this study, experiments were conducted to determine the drag force on an object placed in a uniform stream of foam. The drag force was determined as a function of various model shapes, sizes and surface roughness, foam velocity, and the foam properties. The proposed experiments were successfully accomplished, except for developing a method to determine the average bubble size by using drainage rate measurements. The drainage rate measurement, however, was found to be useful to determine the steady-state of foam flow.

The work and results obtained in this study are summarized as follows:

1. A new device was developed to provide steady-state uniform foam flow. A highly sensitive dual cantilever beam force transducer was designed to detect subtle drag force variation. The experimental set-up produced reliable data.

2. The drag-velocity data for various models tested were fitted to a power function of foam velocity with finite yield force. The results indicate Bingham-plastic like shear thinning characteristics. For a given model the relative drag force ratio was

about same for different foams throughout the velocity range tested, and therefore the curvature was similar for the same model in a scaled frame. The drag force highly depends on and is a unique function of the liquid viscosity and foam quality. The drag force increases with increasing viscosity or increasing quality.

3. The drag force as a function of model shape was investigated by using different lengths of disks, ellipsoids and flat plates. For the cases of flat plates and disks, the drag force essentially linearly increases with length. Wall shear stress calculation shows, however, the shorter the length, the bigger the wall shear. For the case of ellipsoids, if the aspect ratio (l/D) approaches zero, the drag approaches the same value as that of a thin disk. Similarly, with increasing aspect ratio the drag force becomes similar to that of flat plate.

4. The possibility of using the drainage rate as an index of average bubble size was examined. As a general observation, it was found that the bubble size is a function of the speed of the agitator producing the foam. Consequently the agitating speed affected the drainage rate and drag force. Faster stirring produced smaller bubbles and a corresponding higher drag force. The drainage rate was faster for a larger bubble size. In the transient state of producing the foam, the bubble size gradually became smaller, resulting in a slower drainage rate until steady-state was achieved. Upon reaching steady-state, the average bubble size and corresponding drainage rate remained unchanged. Isolation of the drainage rate as a function of only an average bubble size may be possible by either applying statistical method on cumulated data or developing an effective experimental method.

5. Theory predicts the existence of a yield surface around the model moving through a Bingham material. The evidence of the existence of a yield surface in

foam flow was investigated by determining the effect that a near by wall has as the drag force on an object. Compared with the Newtonian creeping flow case, a smaller interference region was detected. This could imply the existence of a yield surface. Outside this region, the drag seemed to be remain constant, independent of the distance between the object and the wall. The size of the interference region was determined to be smaller by a factor of 1/10 than that predicted by approximate use of the Bingham theory. Slip phenomenon and/or lower yield stress (apparent yield stress instead of true yield stress) may contribute to this difference.

6. Highly concentrated emulsion is considered analogous to high quality foam. However, the average bubble size calculated by using a highly concentrated emulsion theory was predicted to be smaller by a factor of 1/8 than the approximate actual bubble size measured. Under the assumption of equal validity of the emulsion theory to foam, the linear velocity distribution approximation used in the calculation may be responsible for the difference. The actual velocity gradient on the model surface may be significantly larger than that of linear approximation. With larger shear rate, the theory will predict larger bubble size. Due to lack of visualization, the actual velocity distribution remains unknown.

7. The drag force dependency on surface roughness was investigated. The rougher the surface, the larger the drag force. For a given roughness, the roughness-induced increase in drag was same amount at any velocity. Thus, the drag velocity curves were similar in shape, merely displaced by a constant force that is a function of surface roughness. Since the bubble sizes were comparable with that of the intrusions (roughness), only some of the bubbles on the object surface may yield when flow occurs. Therefore, it could be imagined that only a fraction of the foam field

yield stress might be delivered to the object. The fact that the drag increase due to roughness was in the range of yield force of the foam might be evidence for this hypothesis.

8. Low quality of foams, namely dilute gas bubble supensions, were investigated to observe the trend of effective viscosity variance with changing quality. Foam with quality less than approximately 0.3 behaves essentially as a Newtonian fluids. Higher quality foams have a shear thinning character. The higher the quality, the more significant the shear thinning charateristics. The effective viscosity parabolically increases with foam quality.

Recommendations

The results of this study represent a first step in measuring drag on objects moving through foam and provide additional information about foam flow in general. The results cover only a portion of the interesting, but complex, phenomena of foam flow. Considerably more experimental and theoretical work is needed. Based on this study, the following are recommended for further experimental study.

1. In almost any branch of fluid mechanics, it is possible to obtain valuable information from flow visualization studies. It is expected that because of the unknown or untested properties of foam (i.e., non-Newtonian characteristics, slip boundary conditions) a systematic, well designed flow visualization study will yield useful information. The implementation of such studies immediately faces the roadblock resulting from the fact that foams are not transparent. Essentially, any foam layer more than a few bubbles thick becomes opaque because of the refractions and reflections of the numerous bubble-film surfaces.

One way to eliminate the problem of the opaqueness of foams is to use a relatively thin two dimensional apparatus, in some ways similar to a very thick gapped Hele-Shaw cell. In such an apparatus, the foam motion can be viewed sufficiently well to extract useful information about the flow. Eventually, an attempt should be made to develop flow visualization techniques appropriate for use in foam flows in general, where the opacity of the foam would normally rule out standard techniques. Although no method currently exists, it may be possible to develop such a technique using a nonstandard method such as X-ray, infrared, or ultrasonic techniques. Such a technique would allow a detailed view of the complex phenomena associated with three-dimensional foam flows.

2. As has been pointed out, the average bubble size is one of important properties of foam. Due to the difficulty of direct measurement of the average bubble size in a dynamic flowing situation, the drainage rate concept was introduced in this study as a possibility of indexing average bubble size. In the actual experiment, however, it was not easy to produce different bubble sizes while the quality and viscosity remain unchanged. This is mainly because the foam quality and average bubble size are also closely related each other. Being acquainted with the above difficulty, one might investigate the functional relationships among the drag force, drainage rate, viscosity, and foam quality by using a statistical scheme such as an analysis of variances, if a sufficient amount of experimental foam flow data are accumulated.

Very recently, one method was reported [10], which provides a direct probe of the average bubble size in bulk foam by using multiple scattering light. Such a technique may be useful for future experimental work on foam flow. With the average bubble size known, generalization of experimental data is possible.

3. As a drag force experiment on objects, the results in this study are valid for tested objects with given surface textures. From a practical point of view, those data sets will be useful for application purposes in spite of the lack of knowledge about the amount of slippage between that foam and the surface of the object. For very rough surfaces it is assumed that there is no slip. On smoother surfaces there is slip. Various types of surface roughnesses could be used to eliminate the slip condition if desired.

Determination of the slip velocity on the moving object, however, is necessary for the genaralization of the foam flow experimental or theoretical results. Such information can be obtained either directly (i.e., actual measurement of the rate of displacement of the bubbles on the surface) or indirectly (i.e., by measurement of some parameters affected in some known way by the slip condition).

The indirect method of determination of the slip velocity by using viscometry has been introduced and proven to be useful for emulsions. For external flow (such as flow past an object), no method to correct for the slip velocity has been attemped yet. Development of either on experimental parametric technique or direct visualization of slip velocity is therefore needed.

BIBLIOGRAPHY

[1] A. N. Beris, J. A. Tsamopoulos, R. C. Armstrong and R. A. Brown. "Creeping Motion of a Sphere through a Bingham Plastic." *Journal of Fluid Mechanics*, 158, (1985): 219-244.

[2] A. H. Beyer, R. S. Millhone and R. W. Foote. "Flow Behavior of Foam as a Well Circulating Fluid." *Society of Petroleum Engineering*, SPE-3986, San Antonio, Texas, 1972.

[3] A. Biesheuvel and L. Wijnggaarden. "Two-phase Flow Equations for a Dilute Dispersion of Gas Bubbles in Liquid." *Journal of Fluid Mechanics*, 148, (1984): 301-318.

[4] J. J. Bikerman. *Foams.* Springer-Verlag: New York, 1973.

[5] R. B. Bird, R. C. Armstrong and O. Hassager. *Dynamics of Polymetric Liquid, Vol. 1: Fluid Mechanics.* New York: Wiley-Interscience, 2nd Ed., 1987.

[6] M. Blackman. "On the Transformation of "Solid" Foam to a "Fluid" Foam under Shear." *Transactions of Faraday Society*, 44, (1948), 205-206.

[7] H. C. Cheng and T . E. Natan. "Measurement and Physical Properties of Foam." *Encyclopedia of Fluid Mechanics*, Ed. N. P. Cheremisinoff, 3, Houston: Gulf, 1986, 3-25.

[8] B. D. Coleman, H. Markovitz and W. Noll. *Viscometric Flows of Non-Newtonian Fluids.* New York: Springer-Verlag, 1966.

[9] G. Dazhi and R. I. Tanner. "The Drag on a Sphere in a Power Law Fluid." *Journal of Non-Newtonian Fluid Mechanics*, 17, (1985), 1-12.

[10] D. J. Durian, D. A. Weitz and D. J. Pine. "Multiple Light-Scattering Probes of Foam Structure and Dynamics." *Science*, Vol. 252, (3 May 1991), 686-688.

[11] D. A. Edwards, "Surface Rheology." Ph.D. Thesis, Illinois Institute of Technology, Chicago, 1987.

[12] H. Faxen, Arkiv. Mat. Astron. Fys. 17, 27, 1923; Dissertation, Uppsala University, 1921.

[13] S. A. Kahn and R. C. Armstrong. "Rheology of Foams: I. Theory for Dry Foams." *Journal of Non-Newtonian Fluid Mechanics*, 22, (1986), 1-22.

[14] S. A. Kahn and R. C. Armstrong. "Rheology of Foams: II. Effects of Polydispersity and Liquid Viscosity for Foams Having Gas Fraction Approaching Unity." *Journal of Non-Newtonian Fluid Mechanics*, 25, (1987), 61-92.

[15] S. A. Kahn, C. A. Schnepper and R. C. Armstrong. "Foam Rheology: III. Measurement of Shear Flow Properties." *Journal of Rheology*, 32(1), (1988), 69-92.

[16] S. A. Kahn and R. C. Armstrong. "Rheology of Foams: IV. Effect of Gas Volume Fraction." *Journal of Rheology*, 33(6), (1989), 881-911.

[17] L. Kelvin. "On the Division of Space with Minimum Partitional Area." *Philosophy Magazine*, 24, (1887), 503-514.

[18] A. M. Kraynik. "Aqueous Foam Rheology." Presented at Annual Meeting of Society of Rheology. Evanston, Ill. 1982.

[19] A. M. Kraynik. "Foam Flows." *Annual Review of Fluid Mechanics*, 20, (1988), 325-357.

[20] R. Matalon. *Foams: In Flow Properties of Disperse System.* Ed. J.J.Hermans, 323-343, New York: Interscience, 1953.

[21] E. B. Metzke. "The Three Dimensional Shape of Bubbles in Foam – An Analysis of the Role of Surface Faces in Three Dimensional Cell Shape Determination." *American Journal of Botany*, 33, (1946), 58-80.

[22] M. Mooney. "Explicit Formulas for Slip and Fluidity." *Journal of Rheology*, 2, (1931), 210-222.

[23] B. R. Munson, D. F. Young and T. H. Okiishi. *Fundamentals of Fluid Mechanics.* John Wiley & Sons, 1990.

[24] C. Oseen. *Neuere Methoden und Ergebnisse in der Hydrodynamik.* Leipzig: Akademische Verlagsgesellschaft, 1927.

[25] J. Plateau. *Statique Experimentale et Theorique des Liquides Soumis aux Seules Forces Moleculaires*, Paris, Gauthier-Villars, 1873.

[26] H. M. Princen. "Rheology of Foams and Highly Concentrated Emulsions: I. Elastic Properties and Yield Stress of a Cylindrical Model System." *Journal of Colloid and Interface Science*, 91, (1 January 1983), 160-175.

[27] H. M. Princen. "Rheology of Foams and Highly Concentrated Emulsions: II. Experimental Study of the Yield Stress and Wall Effects for Concentrated Oil-in-Water Emulsions." *Journal of Colloid and Interface Science*, 105, (1 May 1985), 150-171.

[28] H. M. Princen and A. D. Kiss. "Rheology of Foams and Highly Concentrated Emulsions." *Journal of Colloid and Interface Science*, 112, (2 August 1986), 427-437.

[29] H. M. Princen and A. D. Kiss. "Rheology of Foams and Highly Concentrated Emulsions: IV. An Experimental Study of the Shear Viscosity and Yield Stress of Concentrated Emulsions." *Journal of Colloid and Interface Science*, 128, (1 March 1989), 176-187.

[30] R. K. Prud'homme and R. B. Bird. "The Dilatational Properties of Suspensions of Gas Bubbles in Incompressible Newtonian and Non-Newtonian Fluids." *Journal of Non-Newtonian Fluid Mechanics*, 3, (1978), 261-279.

[31] D. A. Reinelt and A. M. Kraynik. "Viscous Effects in the Rheology of Foams and Concentrated Emulsions." *Journal of Colloid and Interface Science*, 132, (2 October 1989), 491-503.

[32] D. A. Reinelt and A. M. Kraynik. "On the Shearing Flow of Foams and Concentrated Emulsions." *Journal of Fluid Mechanics*, 215, (1990), 431-455.

[33] M. Reiner. "Slippage in a Non-Newtonian Liquid." *Journal of Rheology*, 2, (1931), 337-350.

[34] W. R. Schowalter, C. E. Chaffey and H. Brenner. "Rheological Equation of a Dilute Emulsion." *Journal of Colloid and Interface Science*, 26, (1968), 152-160.

[35] L. W. Schwarts and H. M. Princen. "A theory of Extensional Viscosity for Flowing Foams and Concentrated Emulsions." *Journal of Colloid and Interface Science*, 118, (1 July 1987), 201-211.

[36] A. Siehr. "Zur Kenntnis der Mechanischen Eigenschatfen von Schäumen, III." *Kolloid-Z*, 85, (1938), 70-74.

[37] F. Sugeng and R . I. Tanner. "The Drag on Spheres in Viscoplastic Fluids with Significant Wall Effects." *Journal of Non-Newtonian Fluid Mechanics*, 20, (1986), 281-292.

[38] R. I. Tanner. *Engineering Rheology*. Oxford: Clarendon, 1985.

[39] G. I. Taylor. "The Viscosity of a Fluid Containing Small Drops of Another fluid." *Proceedings of Rheology Society*, London, Serial No. A138, (1932), 41-48.

[40] G. I. Taylor. "The Two Coefficients of Viscosity for an Incompressible Fluid Containing Air Bubbles." *Proceedings of Rheology Society*, London, Serial No. A226, (1954), 34-39.

[41] N. N. Thondavadl and R. Lemlich. "Flow Properties of Foam with and without Solid Particles." *Industrial Engineering & Chemical Process Des. Dev.*, 24, (1985), 748-753.

[42] K. Walters. *Rheometry*. London: Chapman & Hall, 1975.

[43] S. J. Wakiya. Physics Society, Japan, 8, 1953.

[44] D. Weaire and T-L. Fu. "The Mechanical Behavior of Foams and Emulsions." *Journal of Rheology*, 32(3), (1988), 271-283.

[45] H. G. Wenzel, T. E. Stelson and R. J. Brungraber. "Flow of High Expansion Foam in Pipes." *Journal of the Engineering Mechanics Division*, Proceedings of the American Sciety of Civil Engineers, 93, (EM6 December 1967), 153-165.

[46] H. G. Wenzel, R. J. Brungraber and T. E. Stelson. "The Viscosity of High Expansion Foam." *Journal of Materials*, 5, (2 June 1970), 396-412.

[47] A. Yoshimura and R. K. Prud'homme. "Wall Slip Corrections for Couette and Parallel Disk Viscometer." *Journal of Rheology*, 31(1), (1988), 53-67.

APPENDIX A. EXPERIMENTAL DATA

Following tables are the lists of raw data from foam flow experiments stored in VAX (see Section 3.1.4). Drag, F_D, is in N and foam velocity, U, is in m/sec. SCFA2 represents model number 2 in foam ID = SCFA (see Table 3.1 for model numbers and Table 6.1 for foam ID)

Table A.1: Raw drag-velocity data for smooth surfaced models

SCFA2		SCFA3		SCFA4		SCFA5	
U	F_D	U	F_D	U	F_D	U	F_D
0.000	0.005	0.000	0.011	0.000	0.021	0.000	0.015
0.011	0.014	0.009	0.023	0.004	0.040	0.007	0.026
0.027	0.017	0.019	0.026	0.018	0.054	0.020	0.030
0.050	0.020	0.045	0.033	0.028	0.060	0.044	0.035
0.078	0.022	0.077	0.038	0.047	0.069	0.078	0.040
0.113	0.025	0.120	0.043	0.069	0.076	0.113	0.044
0.145	0.026	0.151	0.046	0.109	0.086	0.144	0.046
0.174	0.028	0.179	0.049	0.143	0.093	0.172	0.048
0.208	0.029	0.210	0.051	0.169	0.097	0.206	0.050
0.245	0.031	0.240	0.053	0.194	0.101	0.232	0.052
0.273	0.032	0.276	0.056	0.218	0.105	0.264	0.054
0.301	0.033	0.313	0.058	0.246	0.109	0.293	0.055
0.332	0.034	0.333	0.059	0.275	0.112	0.320	0.056
0.359	0.035	0.358	0.060	0.305	0.116	0.344	0.058
0.382	0.035	0.379	0.061	0.331	0.119	0.378	0.059
0.405	0.036	0.410	0.063	0.355	0.121	0.405	0.060
				0.379	0.124		
				0.402	0.126		

SCFA6		SCFA7		SCFA8		SCFA9	
U	F_D	U	F_D	U	F_D	U	F_D
0.000	0.017	0.000	0.018	0.000	0.018	0.000	0.016
0.001	0.025	0.007	0.031	0.006	0.034	0.010	0.030
0.014	0.037	0.020	0.038	0.013	0.039	0.033	0.038
0.030	0.042	0.049	0.046	0.032	0.048	0.051	0.041
0.064	0.047	0.094	0.054	0.069	0.059	0.080	0.045
0.107	0.052	0.133	0.059	0.105	0.066	0.118	0.050
0.137	0.054	0.169	0.063	0.136	0.071	0.139	0.052
0.175	0.056	0.195	0.065	0.168	0.076	0.175	0.055
0.201	0.058	0.235	0.069	0.196	0.080	0.213	0.058
0.233	0.060	0.270	0.072	0.231	0.084	0.255	0.060
0.263	0.061	0.297	0.074	0.265	0.088	0.280	0.062
0.295	0.062	0.327	0.076	0.291	0.090	0.321	0.064
0.320	0.063	0.357	0.078	0.320	0.093	0.346	0.066
0.346	0.064	0.385	0.079	0.352	0.096	0.379	0.067
0.382	0.066	0.412	0.081	0.376	0.098	0.398	0.068
0.409	0.067			0.403	0.100		

SCFA10		SCFA11		SCFA12		SCFA13	
U	F_D	U	F_D	U	F_D	U	F_D
0.000	0.016	0.000	0.016	0.000	0.016	0.000	0.016
0.008	0.029	0.010	0.031	0.007	0.029	0.007	0.030
0.029	0.037	0.030	0.039	0.023	0.037	0.026	0.039
0.061	0.044	0.071	0.047	0.043	0.043	0.062	0.048
0.090	0.048	0.103	0.052	0.086	0.051	0.096	0.054
0.119	0.052	0.131	0.055	0.126	0.056	0.143	0.060
0.146	0.055	0.168	0.059	0.156	0.060	0.182	0.065
0.192	0.059	0.208	0.063	0.199	0.064	0.222	0.069
0.229	0.062	0.247	0.066	0.236	0.068	0.259	0.072
0.266	0.065	0.291	0.069	0.280	0.071	0.293	0.074
0.302	0.067	0.313	0.071	0.310	0.073	0.317	0.076
0.324	0.069	0.339	0.072	0.330	0.075	0.348	0.078
0.354	0.071	0.371	0.074	0.360	0.077	0.389	0.081
0.382	0.072	0.400	0.076	0.394	0.079		
0.407	0.073			0.418	0.081		

SCFA14		SCFA15		SCFA16	
U	F_D	U	F_D	U	F_D
0.000	0.015	0.000	0.012	0.000	0.012
0.008	0.030	0.005	0.027	0.003	0.030
0.027	0.040	0.014	0.035	0.012	0.045
0.040	0.044	0.029	0.043	0.028	0.059
0.084	0.054	0.056	0.052	0.039	0.066
0.138	0.063	0.084	0.060	0.059	0.076
0.168	0.067	0.124	0.068	0.096	0.089
0.199	0.070	0.152	0.073	0.145	0.103
0.236	0.074	0.173	0.076	0.167	0.108
0.267	0.077	0.196	0.079	0.196	0.115
0.299	0.080	0.221	0.083	0.220	0.120
0.330	0.082	0.244	0.085	0.249	0.125
0.363	0.085	0.279	0.090	0.276	0.130
0.388	0.087	0.311	0.093	0.300	0.134
0.409	0.088	0.333	0.095	0.332	0.139
		0.356	0.097	0.358	0.143
		0.377	0.100	0.377	0.146
		0.395	0.101	0.404	0.149
		0.415	0.103		

SCFB2		SCFB3		SCFB4		SCFB5	
U	F_D	U	F_D	U	F_D	U	F_D
0.000	0.005	0.000	0.010	0.000	0.028	0.000	0.014
0.010	0.011	0.011	0.020	0.007	0.040	0.010	0.022
0.019	0.013	0.030	0.025	0.021	0.049	0.035	0.028
0.033	0.015	0.054	0.028	0.036	0.055	0.066	0.032
0.055	0.016	0.093	0.033	0.060	0.062	0.101	0.035
0.095	0.019	0.132	0.036	0.092	0.068	0.143	0.038
0.132	0.021	0.176	0.039	0.124	0.074	0.171	0.040
0.159	0.022	0.210	0.041	0.156	0.078	0.205	0.041
0.198	0.023	0.238	0.043	0.187	0.082	0.238	0.043
0.226	0.024	0.263	0.044	0.216	0.086	0.268	0.045
0.253	0.025	0.295	0.045	0.250	0.089	0.303	0.046
0.283	0.026	0.328	0.047	0.282	0.092	0.332	0.047
0.304	0.026	0.354	0.048	0.321	0.095	0.366	0.049
0.335	0.027	0.382	0.049	0.350	0.098	0.397	0.050
0.364	0.028	0.403	0.050	0.378	0.100		
0.391	0.028			0.398	0.102		
0.409	0.029			0.413	0.103		

SCFB6		SCFB7		SCFB8		SCFB9	
U	F_D	U	F_D	U	F_D	U	F_D
0.000	0.013	0.000	0.017	0.000	0.014	0.000	0.013
0.008	0.023	0.009	0.026	0.007	0.028	0.013	0.024
0.019	0.026	0.034	0.033	0.031	0.038	0.033	0.028
0.060	0.034	0.064	0.038	0.076	0.048	0.052	0.031
0.087	0.037	0.092	0.042	0.116	0.054	0.087	0.035
0.133	0.041	0.126	0.045	0.156	0.058	0.119	0.038
0.182	0.045	0.166	0.049	0.191	0.062	0.154	0.040
0.213	0.047	0.201	0.052	0.226	0.065	0.189	0.042
0.245	0.048	0.234	0.054	0.262	0.068	0.224	0.044
0.283	0.050	0.274	0.056	0.294	0.070	0.257	0.046
0.310	0.052	0.300	0.058	0.320	0.072	0.295	0.048
0.345	0.053	0.325	0.059	0.357	0.074	0.329	0.049
0.377	0.055	0.363	0.061	0.384	0.076	0.370	0.051
0.393	0.055	0.388	0.062	0.409	0.077	0.398	0.052

SCFB10		SCFB11		SCFB12		SCFB13	
U	F_D	U	F_D	U	F_D	U	F_D
0.000	0.013	0.000	0.012	0.000	0.013	0.000	0.011
0.013	0.024	0.014	0.024	0.009	0.023	0.015	0.025
0.033	0.029	0.044	0.031	0.037	0.031	0.049	0.033
0.059	0.033	0.065	0.034	0.070	0.036	0.083	0.038
0.095	0.037	0.078	0.035	0.102	0.040	0.111	0.041
0.130	0.040	0.115	0.039	0.126	0.042	0.138	0.044
0.165	0.042	0.145	0.042	0.159	0.045	0.171	0.047
0.196	0.044	0.184	0.045	0.176	0.047	0.207	0.049
0.229	0.046	0.218	0.047	0.212	0.049	0.233	0.051
0.264	0.048	0.251	0.049	0.243	0.051	0.284	0.054
0.299	0.050	0.290	0.051	0.278	0.053	0.316	0.056
0.338	0.052	0.320	0.052	0.308	0.055	0.361	0.059
0.377	0.053	0.366	0.054	0.325	0.056	0.393	0.060
0.411	0.055	0.402	0.056	0.354	0.058		
				0.384	0.059		
				0.406	0.060		

SCFB14		SCFB15		SCFB16	
U	F_D	U	F_D	U	F_D
0.000	0.012	0.000	0.012	0.000	0.013
0.010	0.023	0.009	0.027	0.006	0.031
0.030	0.031	0.029	0.036	0.016	0.040
0.069	0.039	0.047	0.041	0.030	0.049
0.079	0.041	0.089	0.049	0.045	0.056
0.105	0.044	0.127	0.055	0.074	0.066
0.147	0.049	0.153	0.058	0.102	0.074
0.177	0.052	0.180	0.061	0.135	0.082
0.219	0.056	0.209	0.064	0.171	0.090
0.254	0.059	0.235	0.067	0.205	0.096
0.286	0.061	0.261	0.069	0.236	0.101
0.314	0.063	0.291	0.072	0.263	0.105
0.338	0.065	0.320	0.074	0.306	0.112
0.374	0.067	0.347	0.076	0.340	0.116
0.403	0.069	0.367	0.077	0.370	0.120
		0.387	0.079	0.396	0.123
		0.408	0.080		

SCFC2		SCFC3		SCFC4		SCFC5	
U	F_D	U	F_D	U	F_D	U	F_D
0.000	0.005	0.000	0.009	0.000	0.022	0.000	0.013
0.014	0.010	0.010	0.018	0.008	0.034	0.009	0.018
0.033	0.013	0.039	0.024	0.027	0.044	0.025	0.022
0.067	0.015	0.068	0.027	0.061	0.054	0.068	0.027
0.100	0.017	0.108	0.031	0.083	0.058	0.096	0.029
0.129	0.019	0.150	0.034	0.127	0.065	0.145	0.032
0.159	0.020	0.193	0.036	0.169	0.071	0.190	0.034
0.193	0.021	0.231	0.038	0.213	0.076	0.230	0.036
0.227	0.023	0.273	0.040	0.244	0.079	0.280	0.038
0.266	0.024	0.319	0.042	0.285	0.083	0.320	0.039
0.305	0.025	0.362	0.044	0.330	0.087	0.357	0.040
0.338	0.026	0.401	0.045	0.373	0.091	0.399	0.041
0.370	0.026			0.404	0.093		
0.400	0.027						

SCFC6		SCFC7		SCFC8		SCFC9	
U	F_D	U	F_D	U	F_D	U	F_D
0.000	0.016	0.000	0.015	0.000	0.017	0.000	0.010
0.012	0.022	0.015	0.024	0.012	0.027	0.017	0.022
0.029	0.025	0.041	0.029	0.038	0.034	0.039	0.025
0.054	0.029	0.060	0.032	0.076	0.041	0.056	0.027
0.086	0.032	0.089	0.035	0.115	0.045	0.091	0.030
0.125	0.034	0.141	0.040	0.161	0.050	0.126	0.033
0.172	0.037	0.182	0.042	0.204	0.054	0.175	0.035
0.214	0.039	0.222	0.045	0.250	0.057	0.220	0.037
0.256	0.041	0.266	0.047	0.295	0.060	0.264	0.039
0.297	0.043	0.312	0.049	0.337	0.062	0.308	0.041
0.346	0.045	0.365	0.052	0.378	0.064	0.350	0.042
0.392	0.046	0.401	0.053	0.414	0.066	0.394	0.043

SCFC10		SCFC11		SCFC12		SCFC13	
U	F_D	U	F_D	U	F_D	U	F_D
0.000	0.012	0.001	0.014	0.000	0.011	0.000	0.010
0.017	0.022	0.013	0.021	0.015	0.022	0.011	0.021
0.042	0.027	0.045	0.027	0.043	0.027	0.042	0.028
0.068	0.030	0.078	0.031	0.084	0.032	0.092	0.034
0.098	0.032	0.115	0.034	0.109	0.034	0.121	0.036
0.134	0.035	0.157	0.036	0.147	0.037	0.165	0.039
0.185	0.038	0.210	0.039	0.197	0.040	0.225	0.043
0.232	0.040	0.255	0.042	0.242	0.043	0.271	0.045
0.277	0.042	0.317	0.044	0.290	0.045	0.297	0.046
0.324	0.043	0.373	0.046	0.331	0.047	0.343	0.048
0.378	0.045	0.408	0.047	0.366	0.048	0.390	0.050
				0.401	0.049	0.416	0.051

SCFC14		SCFC15		SCFC16	
U	F_D	U	F_D	U	F_D
0.000	0.012	0.000	0.016	0.000	0.011
0.014	0.024	0.015	0.028	0.008	0.031
0.034	0.029	0.042	0.035	0.022	0.041
0.056	0.032	0.073	0.041	0.049	0.052
0.093	0.037	0.115	0.047	0.070	0.059
0.138	0.041	0.160	0.052	0.087	0.063
0.177	0.044	0.202	0.055	0.110	0.068
0.216	0.047	0.243	0.059	0.154	0.076
0.262	0.050	0.298	0.063	0.196	0.083
0.306	0.052	0.352	0.066	0.235	0.088
0.348	0.054	0.378	0.067	0.266	0.092
0.387	0.056	0.411	0.069	0.303	0.096
				0.356	0.101
				0.392	0.105

SCFD2		SCFD3		SCFD4		SCFD5	
U	F_D	U	F_D	U	F_D	U	F_D
0.000	0.014	0.000	0.023	0.000	0.052	0.000	0.028
0.009	0.035	0.013	0.066	0.006	0.112	0.005	0.051
0.039	0.051	0.048	0.092	0.027	0.155	0.021	0.069
0.080	0.062	0.073	0.104	0.053	0.186	0.048	0.086
0.126	0.071	0.091	0.110	0.085	0.212	0.075	0.098
0.171	0.078	0.147	0.127	0.114	0.231	0.116	0.112
0.208	0.083	0.191	0.137	0.160	0.255	0.173	0.128
0.255	0.088	0.238	0.147	0.199	0.273	0.226	0.140
0.300	0.093	0.294	0.157	0.245	0.291	0.285	0.151
0.345	0.097	0.337	0.164	0.298	0.310	0.349	0.162
0.386	0.101	0.397	0.172	0.337	0.322	0.401	0.171
				0.377	0.333		
				0.407	0.342		

SCFD6		SCFD7		SCFD8		SCFD9	
U	F_D	U	F_D	U	F_D	U	F_D
0.000	0.030	0.000	0.040	0.000	0.044	0.000	0.025
0.006	0.058	0.006	0.060	0.007	0.073	0.008	0.052
0.023	0.078	0.029	0.092	0.030	0.111	0.035	0.079
0.053	0.099	0.058	0.113	0.053	0.133	0.072	0.099
0.090	0.116	0.078	0.124	0.073	0.149	0.103	0.112
0.147	0.137	0.113	0.140	0.110	0.171	0.160	0.131
0.202	0.152	0.171	0.162	0.150	0.191	0.201	0.142
0.248	0.163	0.219	0.176	0.201	0.213	0.251	0.154
0.299	0.174	0.269	0.190	0.253	0.232	0.303	0.166
0.339	0.182	0.309	0.200	0.299	0.247	0.347	0.174
0.387	0.191	0.366	0.212	0.346	0.262	0.393	0.183
		0.408	0.221	0.395	0.275		

SCFD10		SCFD11		SCFD12		SCFD13	
U	F_D	U	F_D	U	F_D	U	F_D
0.000	0.028	0.000	0.028	0.000	0.024	0.000	0.024
0.008	0.049	0.010	0.056	0.006	0.052	0.007	0.053
0.030	0.071	0.047	0.087	0.028	0.079	0.028	0.079
0.056	0.088	0.093	0.111	0.059	0.100	0.064	0.105
0.080	0.100	0.126	0.124	0.098	0.118	0.111	0.129
0.140	0.124	0.180	0.142	0.131	0.131	0.150	0.145
0.193	0.140	0.224	0.154	0.171	0.145	0.195	0.161
0.242	0.154	0.279	0.168	0.217	0.158	0.245	0.176
0.294	0.167	0.324	0.178	0.266	0.170	0.297	0.190
0.338	0.176	0.377	0.189	0.315	0.181	0.340	0.201
0.385	0.186	0.417	0.197	0.363	0.191	0.379	0.210
				0.407	0.200		

SCFD14		SCFD15		SCFD16	
U	F_D	U	F_D	U	F_D
0.000	0.032	0.000	0.038	0.000	0.050
0.004	0.064	0.006	0.082	0.006	0.122
0.019	0.090	0.022	0.115	0.024	0.175
0.039	0.110	0.042	0.137	0.048	0.211
0.086	0.139	0.061	0.154	0.070	0.235
0.115	0.153	0.082	0.169	0.104	0.265
0.158	0.169	0.111	0.186	0.143	0.293
0.201	0.184	0.149	0.204	0.189	0.320
0.246	0.197	0.191	0.222	0.230	0.340
0.301	0.211	0.232	0.237	0.278	0.361
0.352	0.223	0.290	0.256	0.320	0.379
0.400	0.233	0.334	0.270	0.362	0.394
		0.371	0.280	0.401	0.408
		0.400	0.287		

SCFE6		SCFE7		SCFE8		SCFE9	
U	F_D	U	F_D	U	F_D	U	F_D
0.000	0.014	0.000	0.018	0.000	0.019	0.001	0.018
0.007	0.029	0.010	0.034	0.005	0.035	0.009	0.029
0.026	0.040	0.031	0.047	0.016	0.047	0.022	0.036
0.049	0.048	0.054	0.056	0.031	0.058	0.042	0.043
0.076	0.055	0.089	0.066	0.051	0.068	0.066	0.050
0.105	0.062	0.135	0.076	0.080	0.079	0.092	0.056
0.150	0.070	0.184	0.085	0.122	0.092	0.128	0.062
0.203	0.078	0.227	0.092	0.164	0.103	0.178	0.070
0.250	0.084	0.272	0.099	0.213	0.113	0.215	0.074
0.292	0.089	0.306	0.103	0.256	0.121	0.256	0.079
0.330	0.093	0.340	0.108	0.302	0.129	0.293	0.083
0.365	0.097	0.376	0.112	0.350	0.137	0.331	0.087
0.403	0.100	0.403	0.115	0.395	0.143	0.369	0.090
						0.399	0.093

SCFE6		SCFE7		SCFE8		SCFE9	
U	F_D	U	F_D	U	F_D	U	F_D
0.000	0.014	0.000	0.018	0.000	0.019	0.001	0.018
0.007	0.029	0.010	0.034	0.005	0.035	0.009	0.029
0.026	0.040	0.031	0.047	0.016	0.047	0.022	0.036
0.049	0.048	0.054	0.056	0.031	0.058	0.042	0.043
0.076	0.055	0.089	0.066	0.051	0.068	0.066	0.050
0.105	0.062	0.135	0.076	0.080	0.079	0.092	0.056
0.150	0.070	0.184	0.085	0.122	0.092	0.128	0.062
0.203	0.078	0.227	0.092	0.164	0.103	0.178	0.070
0.250	0.084	0.272	0.099	0.213	0.113	0.215	0.074
0.292	0.089	0.306	0.103	0.256	0.121	0.256	0.079
0.330	0.093	0.340	0.108	0.302	0.129	0.293	0.083
0.365	0.097	0.376	0.112	0.350	0.137	0.331	0.087
0.403	0.100	0.403	0.115	0.395	0.143	0.369	0.090
						0.399	0.093

SCFE10		SCFE11		SCFE12		SCFE13	
U	F_D	U	F_D	U	F_D	U	F_D
0.000	0.015	0.000	0.016	0.001	0.018	0.001	0.018
0.006	0.026	0.007	0.027	0.007	0.028	0.007	0.029
0.021	0.036	0.023	0.038	0.022	0.040	0.021	0.040
0.041	0.044	0.046	0.047	0.050	0.051	0.041	0.049
0.062	0.051	0.081	0.057	0.076	0.059	0.060	0.056
0.084	0.056	0.123	0.066	0.098	0.064	0.084	0.063
0.108	0.061	0.161	0.073	0.142	0.074	0.117	0.071
0.155	0.069	0.210	0.081	0.182	0.081	0.167	0.081
0.196	0.076	0.247	0.086	0.223	0.087	0.196	0.086
0.230	0.080	0.286	0.091	0.264	0.093	0.239	0.092
0.273	0.086	0.325	0.095	0.303	0.098	0.284	0.099
0.312	0.090	0.370	0.100	0.359	0.104	0.339	0.105
0.349	0.094	0.408	0.104	0.392	0.108	0.378	0.110
0.385	0.098			0.411	0.110	0.415	0.114
0.414	0.101						

SCFE14		SCFE15		SCFE16	
U	F_D	U	F_D	U	F_D
0.000	0.015	0.000	0.016	0.000	0.029
0.006	0.035	0.004	0.036	0.006	0.056
0.022	0.048	0.017	0.052	0.026	0.086
0.046	0.060	0.036	0.066	0.049	0.105
0.066	0.067	0.058	0.077	0.070	0.119
0.091	0.075	0.087	0.088	0.103	0.135
0.117	0.081	0.107	0.095	0.133	0.148
0.159	0.090	0.142	0.105	0.169	0.161
0.194	0.096	0.182	0.114	0.216	0.176
0.235	0.102	0.221	0.123	0.257	0.187
0.273	0.108	0.263	0.131	0.302	0.198
0.303	0.112	0.296	0.137	0.338	0.207
0.344	0.117	0.336	0.143	0.375	0.215
0.379	0.121	0.367	0.148	0.415	0.223
0.409	0.124	0.400	0.153		

SCFF2		SCFF3		SCFF4		SCFF5	
U	F_D	U	F_D	U	F_D	U	F_D
0.000	0.008	0.000	0.013	0.001	0.052	0.001	0.020
0.006	0.017	0.005	0.033	0.007	0.076	0.008	0.034
0.021	0.026	0.020	0.048	0.025	0.105	0.028	0.049
0.042	0.033	0.038	0.059	0.048	0.128	0.051	0.060
0.061	0.038	0.060	0.068	0.071	0.145	0.075	0.068
0.085	0.043	0.083	0.076	0.096	0.160	0.102	0.076
0.108	0.047	0.112	0.084	0.117	0.171	0.123	0.081
0.132	0.051	0.148	0.093	0.151	0.187	0.138	0.085
0.159	0.055	0.185	0.101	0.189	0.202	0.178	0.093
0.194	0.060	0.221	0.107	0.223	0.214	0.210	0.099
0.227	0.064	0.262	0.114	0.254	0.224	0.250	0.105
0.257	0.067	0.301	0.120	0.286	0.233	0.285	0.111
0.290	0.070	0.342	0.126	0.326	0.244	0.321	0.116
0.325	0.074	0.374	0.130	0.365	0.255	0.360	0.121
0.364	0.077	0.412	0.134	0.394	0.262	0.393	0.125
0.399	0.080					0.417	0.128

SCFF16		SCFF17		SCFF18		SCFF19	
U	F_D	U	F_D	U	F_D	U	F_D
0.000	0.041	0.001	0.014	0.000	0.015	0.000	0.016
0.007	0.080	0.008	0.027	0.007	0.036	0.008	0.052
0.019	0.108	0.025	0.041	0.022	0.053	0.022	0.070
0.035	0.132	0.049	0.053	0.047	0.070	0.041	0.087
0.053	0.151	0.071	0.061	0.073	0.083	0.062	0.102
0.080	0.175	0.095	0.069	0.103	0.096	0.086	0.115
0.114	0.198	0.120	0.076	0.133	0.106	0.112	0.127
0.136	0.211	0.148	0.083	0.169	0.117	0.148	0.142
0.174	0.231	0.190	0.092	0.208	0.127	0.185	0.155
0.203	0.245	0.227	0.099	0.239	0.135	0.214	0.164
0.240	0.261	0.260	0.105	0.259	0.139	0.240	0.171
0.276	0.275	0.297	0.111	0.295	0.147	0.272	0.181
0.306	0.286	0.327	0.116	0.328	0.154	0.312	0.191
0.342	0.298	0.361	0.121	0.359	0.159	0.344	0.198
0.371	0.308	0.398	0.126	0.393	0.166	0.375	0.205
0.395	0.315					0.411	0.213

SCFG2		SCFG3		SCFG4		SCFG5	
U	F_D	U	F_D	U	F_D	U	F_D
0.000	0.006	0.000	0.014	0.000	0.037	0.000	0.012
0.005	0.016	0.007	0.030	0.004	0.057	0.009	0.032
0.015	0.023	0.023	0.044	0.013	0.078	0.025	0.043
0.032	0.030	0.037	0.052	0.034	0.105	0.039	0.050
0.051	0.036	0.058	0.062	0.054	0.122	0.064	0.060
0.073	0.041	0.077	0.069	0.075	0.138	0.088	0.067
0.096	0.046	0.098	0.076	0.109	0.158	0.126	0.077
0.127	0.052	0.112	0.080	0.135	0.170	0.170	0.086
0.161	0.057	0.143	0.089	0.162	0.183	0.204	0.093
0.194	0.062	0.183	0.098	0.193	0.195	0.240	0.099
0.229	0.066	0.215	0.105	0.221	0.205	0.270	0.103
0.269	0.071	0.251	0.113	0.256	0.218	0.301	0.108
0.306	0.075	0.282	0.118	0.293	0.229	0.336	0.113
0.333	0.077	0.320	0.125	0.326	0.239	0.368	0.117
0.360	0.080	0.350	0.130	0.368	0.250	0.387	0.119
0.391	0.083	0.381	0.135	0.402	0.259	0.416	0.123
		0.412	0.139				

SCFG16		SCFG17		SCFG18		SCFG19	
U	F_D	U	F_D	U	F_D	U	F_D
0.000	0.025	0.001	0.012	0.000	0.014	0.001	0.020
0.005	0.063	0.009	0.023	0.008	0.032	0.007	0.039
0.018	0.094	0.031	0.038	0.023	0.047	0.020	0.057
0.039	0.124	0.056	0.049	0.046	0.062	0.039	0.074
0.061	0.148	0.078	0.056	0.063	0.070	0.062	0.089
0.084	0.167	0.107	0.065	0.087	0.081	0.084	0.101
0.107	0.184	0.135	0.072	0.116	0.092	0.107	0.112
0.139	0.204	0.166	0.080	0.149	0.102	0.136	0.124
0.170	0.221	0.195	0.086	0.179	0.111	0.168	0.136
0.191	0.232	0.223	0.092	0.207	0.118	0.193	0.145
0.224	0.248	0.255	0.098	0.233	0.125	0.225	0.155
0.249	0.259	0.285	0.104	0.267	0.133	0.254	0.163
0.279	0.271	0.316	0.109	0.301	0.140	0.283	0.171
0.309	0.283	0.346	0.114	0.331	0.146	0.319	0.180
0.332	0.292	0.374	0.118	0.357	0.151	0.347	0.187
0.359	0.302	0.402	0.123	0.384	0.156	0.376	0.194
0.386	0.311			0.411	0.161	0.407	0.201
0.417	0.321						

Folling tables are the raw data from wall effect experiment with 38.1 mm diameter sphere. Location is the distance from the wall to the center of the sphere in mm, and F_D is the drag in N.

Table A.2: Experimental data for wall effect for 38.1 mm diameter sphere. ($\mu = 2.8\times10^{-3}Ns/m^2$, $\phi = 0.8$)

U = 0.12		U = 0.18		U = 0.24	
Location	F_D	Location	F_D	Location	F_D
19.100	0.110	19.100	0.125	19.100	0.135
21.812	0.105	21.812	0.119	21.812	0.130
24.524	0.104	24.524	0.118	24.524	0.129
29.948	0.104	29.948	0.117	29.948	0.128
43.508	0.106	43.508	0.117	43.508	0.127
60.322	0.105	60.322	0.116	60.322	0.126

U = 0.30		U = 0.36		U = 0.42	
Location	F_D	Location	F_D	Location	F_D
19.100	0.148	19.100	0.156	19.100	0.165
21.812	0.139	21.812	0.150	21.812	0.158
24.524	0.137	24.524	0.147	24.524	0.157
29.948	0.137	29.948	0.146	29.948	0.153
43.508	0.136	43.508	0.145	43.508	0.151
60.322	0.134	60.322	0.144	60.322	0.151

Following tables are the experimental data for the drag-velocity relationship on rough surfaced 38.1 mm diameter sphere and 101 mm-long flat plate. U is in m/sec, F_D is in N, and ε is roughness in μm.

Table A.3: Experimental data for rough surfaced 38.1 mm diameter sphere. (μ = 7.1 $\times 10^{-3} Ns/m^2$, ϕ = 0.8)

smooth		$44 \leq \varepsilon \leq 74$		$74 \leq \varepsilon \leq 149$	
U	F_D	U	F_D	U	F_D
0.121	0.137	0.121	0.146	0.121	0.153
0.182	0.150	0.182	0.162	0.182	0.170
0.242	0.160	0.242	0.168	0.242	0.175
0.303	0.165	0.303	0.173	0.303	0.181
0.364	0.169	0.364	0.177	0.364	0.185
0.424	0.175	0.424	0.182	0.424	0.189

$149 \leq \varepsilon \leq 250$		$250 \leq \varepsilon \leq 420$		$420 \leq \varepsilon \leq 589$	
U	F_D	U	F_D	U	F_D
0.121	0.158	0.121	0.162	0.121	0.167
0.182	0.171	0.182	0.180	0.182	0.185
0.242	0.179	0.242	0.185	0.242	0.190
0.303	0.185	0.303	0.192	0.303	0.197
0.364	0.189	0.364	0.194	0.364	0.200
0.424	0.193	0.424	0.198	0.424	0.203

Table A.4: Experimental data for rough surfaced 101.6 mm-long flat plate. (μ = 7.1 $\times 10^{-3} Ns/m^2$, $\phi = 0.8$)

smooth		$44 \leq \varepsilon \leq 74$		$74 \leq \varepsilon \leq 149$	
U	F_D	U	F_D	U	F_D
0.121	0.094	0.121	0.096	0.121	0.102
0.182	0.112	0.182	0.114	0.182	0.121
0.242	0.117	0.242	0.120	0.242	0.126
0.303	0.123	0.303	0.125	0.303	0.130
0.364	0.127	0.364	0.129	0.364	0.132
0.424	0.128	0.424	0.130	0.424	0.134

$149 \leq \varepsilon \leq 250$		$250 \leq \varepsilon \leq 420$		$420 \leq \varepsilon \leq 589$	
U	F_D	U	F_D	U	F_D
0.121	0.103	0.121	0.107	0.121	0.109
0.182	0.121	0.182	0.126	0.182	0.128
0.242	0.128	0.242	0.130	0.242	0.132
0.303	0.132	0.303	0.135	0.303	0.137
0.364	0.134	0.364	0.138	0.364	0.140
0.424	0.135	0.424	0.139	0.424	0.143

Following tables are the raw data from the experiment for dilute gas bubble suspensions by using concentric cylinder viscometer. U is angular velocity in turns/sec. and W is driving weight in dyne.

Table A.5: Experimental data for dilute gas bubble suspensions. ($\mu = 210.6 \times 10^{-3} Ns/m^2$)

$\phi = 0.0$		$\phi = 0.17$		$\phi = 0.27$	
U	W	U	W	U	W
0.144	10.00	0.064	10.00	0.050	10.00
0.332	20.00	0.293	30.00	0.139	20.00
0.521	30.00	0.380	40.00	0.225	30.00
0.702	40.00	0.483	50.00	0.303	40.00
0.881	50.00	0.578	60.00	0.381	50.00
1.055	60.00	0.685	70.00	0.458	60.00
1.236	70.00	0.775	80.00	0.541	70.00
1.401	80.00	0.870	90.00	0.622	80.00
1.587	90.00	0.964	100.0	0.694	90.00
1.746	100.0			0.763	100.0

$\phi = 0.51$		$\phi = 0.56$		$\phi = 0.63$	
U(turns/sec)	W(dyne)	U(turns/sec)	W(dyne)	U(turns/sec)	W(dyne)
0.021	10.00	0.033	20.00	0.024	30.00
0.050	20.00	0.055	30.00	0.039	40.00
0.081	30.00	0.080	40.00	0.054	50.00
0.111	40.00	0.103	50.00	0.071	60.00
0.144	50.00	0.129	60.00	0.090	70.00
0.176	60.00	0.158	70.00	0.109	80.00
0.210	70.00	0.184	80.00	0.131	90.00
0.248	80.00	0.243	100.0	0.155	100.0
0.284	90.00				
0.318	100.0				